

Development of a photocatalytic reaction system to gain raw materials from lignin derivatives

**Dissertation zur Erlangung des Grades
Doktors der Naturwissenschaften (Dr. rer. nat.)**

des Fachbereiches Biologie und Chemie der Justus-Liebig-
Universität Gießen

vorgelegt von
Colin Awungacha Lekelefac

Gießen, August 2014

Die Untersuchungen zur vorliegenden Arbeit wurden von Oktober 2010 bis August 2014 am Institut für Bioverfahrenstechnik und Pharmazeutische Technologie der Technischen Hochschule Mittelhessen im Rahmen der BMBF Förderlinie ``Ingenieurnachwuchs-Verfahrenstechnik`` durchgeführt.

Gutachter 1: Prof. Dr.-Ing. Peter Czermak
Gutachter 2: Prof. Dr. Bernd Smarsly

Tag der mündlichen Prüfung: 22.10.2014

Lists of Publications

- C. Awungacha Lekelefac, Nadine Busse, M. Herrenbauer, P. Czermak, *Photocatalytic based degradation processes of lignin derivatives*. Accepted for publication in International Journal of Photoenergy, Article ID 137634, 2014, 18 pages, <http://www.hindawi.com/journals/ijp/aa/137634>.
- C. Awungacha Lekelefac, J. Hild, P. czermak, M. Herrenbauer. *Photocatalytic active coatings for lignin degradation in circulating packed bed reactor*. International Journal of Photoenergy, Article ID 502326. 2014, 10 pages, <http://dx.doi.org/10.1155/2014/502326>.
- C. Awungacha Lekelefac, P. Czermak, M. Herrenbauer. *Evaluation of Photocatalytic Active Coatings on Sintered Glass Tubes by Methylene Blue*. International Journal of Photoenergy, Volume 2013, Article ID 614567. 2013, 9 pages, <http://dx.doi.org/10.1155/2013/614567>.

Conference contributions

- Poster: Deutscher Katalytiker Tagung-Weimar 2013, *Photocatalytic reaction system for the degradation of paper waste water lignin derivative*.
- Presentation: Sustainability in the chemical synthesis conference: Kaiserslautern 2012 *Photocatalytic reaction system for the Degradation of paper waste water lignin*.
- Poster: Deutscher Katalytiker Tagung-Weimar 2011, *Photocatalytic reaction system for the degradation of paper waste water lignin derivative*.

1. Summary/ Abstract	1
2. Introduction	2
2.1. Motivation.....	2
2.2. Aim of thesis.....	3
2.3. Scope of the thesis.....	4
3. Lignin as raw material	5
3.1. Chemical structure and sources.....	5
3.2. Biorefinery scheme of lignin.....	7
4. Photocatalysis	9
4.1. Definition.....	9
4.2. On the reaction pathways of lignin photocatalytic degradation.....	9
4.2.1. Formation of radical species for photocatalysis.....	9
4.2.2. Adsorption mechanism of photocatalysis.....	11
4.2.3. Structural representation of some proposed lignin degradation pathway.....	13
4.3. Conclusion.....	15
5. Photocatalysis of lignin derivatives: state of the art	16
5.1. Influence of process parameters.....	16
5.1.1. Influence of catalyst.....	21
5.1.2. Influence of metal ion (doping) and additives.....	22
5.1.3. Influence of lignin concentration.....	23
5.1.4. Influence of pH.....	24
5.1.5. Influence of Illumination.....	25
5.2. Process analytical methods.....	25
6. Material	30
6.1. Laboratory apparatus.....	30
6.2. Work material.....	31
6.3. Chemicals.....	32
7. Analytical methods	35
7.1. UV-Visible spectroscopy.....	35
7.2. High performance liquid chromatography (HPLC, HP1090).....	36
7.3. Programmable fluorescence detector attached to HPLC (HP1040A).....	36
7.4. Gas chromatography (GC).....	36
8. Experimental	37
8.1. Description of reaction systems.....	37
8.2. Reactor characterization.....	38
8.2.1. Brunauer-Emmett-Teller (BET) surface area.....	39
8.2.2. Flow measurements.....	39

8.3.	Photonic efficiency of reactor	40
8.4.	Discussion	42
8.5.	Conclusion	43
9.	Catalyst preparation and characterization.....	44
9.1.	Introduction.....	44
9.2.	Categories of catalytic coatings, mode of catalyst selection	44
9.3.	Catalyst synthesis.....	45
9.3.1.	Preparation of TEOS solution	45
9.3.2.	Preparation of TiOSO ₄ _30.6wt% gel	45
9.3.3.	Preparation of TiO ₂ -P25 suspension	46
9.3.4.	Preparation of ZnO suspension	46
9.3.5.	Preparation of ZnO +TiO ₂ -P25-SiO ₂ suspension	46
9.3.6.	Preparation of TiOSO ₄ _30.6wt%+PEG gel	46
9.3.7.	Preparation of doped TiO ₂ catalyst.....	47
9.3.8.	Preparation of TiOSO ₄ _30.6wt% + TiO ₂ -P25 suspension	47
9.3.9.	Preparation of TTIP gel.....	47
9.3.10.	Coating procedure of TEOS on glass	47
9.3.11.	Coating procedure of gels and suspensions on glass	47
9.4.	Results and discussion	48
9.4.1.	Morphology of coatings	49
9.5.	Conclusion	50
10.	Evaluation of photocatalytic active coating by methylene blue	51
10.1.	Introduction	51
10.2.	Degradation pathway of MB	52
10.3.	Photocatalytic experiments	52
10.4.	Results	53
10.5.	Conclusion.....	60
11.	Photocatalysis of lignin in circulating packed bed reactor	61
11.1.	Introduction	61
11.2.	Experimental	61
11.3.	Analytics.....	62
11.4.	Results	63
11.4.1.	Degradation experiments.....	63
12.	Comparative catalyst study in an optimized work up procedure involving simultaneous reaction-extraction of waste water lignin sulfonate	68
12.1.	Introduction	68
12.2.	Experimental	68

12.3.	Results	69
12.4.	Conclusion.....	73
13.	A photocatalytic study of lignin standard (model) compounds.....	74
13.1.	Introduction	74
13.2.	Selection of sample molecules	77
13.2.1.	Phenyl alkyl ether.....	78
13.2.2.	Aryl-Aryl ether bond.....	79
13.3.	Experimental	80
13.3.1.	Phenyl propane methoxy unit.....	81
13.3.2.	C(aryl)-C(alkyl) bonds in lignin subunit	83
13.3.3.	Aryl-aryl ether bonds	85
13.3.4.	Aryl-Alkyl ether bond	87
13.3.5.	Phenyl-phenyl bond	88
13.4.	Discussion	89
13.5.	Conclusion.....	89
14.	Summarizing conclusion and outlook.....	90
14.1.	Summarizing conclusion	90
14.2.	Outlook.....	92
15.	References.....	93
16.	Acknowledgement.....	101
17.	List of figures	103
18.	List of tables	106

Abbreviations

ADMI	American dye manufacture institute value
APCI	Atmospheric pressure chemical ionization
Ag	Silver
Au	Gold
Approx.	Approximately
~	Approximately
AOP	Advanced oxidation process
B	Barrel (158.98L)
BOC	Biochemical oxygen demand
¹³ C-NMR	Carbon-13-nuclear magnetic resonance
COD	Chemical oxygen demand
CO ₂	Carbondioxide
CO	Carbon monoxide
Conc.	Concentration
DOC	Dissolved organic carbon
DC	Dissolved carbon
e.g.	For example
E	Irradiance
Ep	Energy quanta of a photon
ESI	Electrospray ionization
EI	Electron ionization
Ex	Excitation
Em	Emission
FLD	Fluorescence detector
GC	Gas chromatography
g	Grams
GC-MS	Gas chromatography-mass spectrometry
GPC	Gel permeation chromatography
¹ H NMR	Hydrogen(proton)-1-nuclear magnetic resonance
HPLC	High performance liquid chromatography
HRP	highly porous polystyrene divinylbenzene adsorbent resin
FTIR	Fourier transform infrared spectroscopy
J. s	Joules-seconds
L	Liters
LS	Lignin sulfonate
Lac	Laccasse
LDP	lignin degradation product
m	metres
MB	Methylene blue
mAU	Milli absorbance unit
MS	Mass Spectrum/ Mass Spectrometry
m/z	Mass/charge
MSQ	Mass spectrometer quadrupole (mass detector)
m/s	Meters per second
m ² /g	Specific surface area
m ² /g	Meters square per gram
mol	mole

Mt	Million ton
toe	Tons of oil equivalent
NPOC	Non purgeable organic carbon
Norm.	Y-Axis of fluorescence detection chromatogram
N-type	Negative type
N_p	number of photons
PDA	Photo diode array detector
P-type	Positive type
UV-Vis	Ultra violet-visible
RO	Reverse osmosis
SPE	Solid Phase Extraction
SEC	Size exclusion chromatography
PMMA	Polymethylmethacrylate
Pa. s	Pascal-seconds
POX	peroxidases
TLC	Thin layer chromatography
TEOS	Tetraethyl orthosilicate
TiOSO ₄	Titanium(IV) oxide sulfate
TIC	Total ion chromatogram
TOC	Total organic carbon
UV	Ultraviolet
UV-Vis	Ultraviolet-visible (UV-Vis)
UHPLC	Ultra high performance liquid chromatography
W/m ²	Watt per meter square
Pt	Platinum
ZnO	Zinc oxide

List of symbols

A_{tube}	Area of tube [m ²]
D	Diameter [m]
ε	Voidage (dimensionless quantity)
V	superficial velocity [m/s]
Re	Reynolds number (dimensionless quantity)
ρ	Density [kg/m ³]
μ	Dynamic viscosity [Pa.s]
dt	Diameter of tube [m]
dp	Diameter of particle [m]
dr	dt/dp (dimensionless quantity)
ξ	photonic efficiency [mol /Einstein]
$d[c]/dt$	Reaction rate [mol/L.s.]
I^0	Incident photons [Einstein•mol/(L•s)]
h	Planck's constant (6.63•10 ⁻³⁴ Js)
c	speed of light(2.998•10 ⁸ m/s)
f	Frequency[1/m]
λ	Wavelength [m]
N_A	Avogadro number (6.022•10 ²³ mol ⁻¹)

1. Summary/ Abstract

Wood biomass consists of cellulose (40–50%), lignin (16–33%), hemicelluloses (15–30%), and a variety of extractives (1–10%). After cellulose, lignin is the most abundant renewable carbon source on earth. More than 70 million tons of various types of lignin preparations are produced as waste material by the paper industry yearly. Moreover, lignin represents the only viable source to produce aromatic compounds as fossil fuel alternative.

Photocatalysis, belonging to the advanced oxidation processes (AOPs), is a potential new transformation technology for lignin derivatives to value added products such as phenol, benzene, toluene and xylene amongst others.

The goal of this work was to develop a photocatalytic reaction system which could effectively depolymerize lignin into value added chemicals such as phenolic derivatives or thermosets like phenolic resins and thus propose a processing concept for lignin conversion.

This work reports the synthesis of immobilized catalyst via the sol-gel route on porous glass support material. A comparative study is done regarding the morphology of the coatings, degradation rates, reaction rates, dissolved carbon (DC), formation of peaks and fluorescence of product peaks formed from the photocatalytic degradation of lignin sulfonate obtained from a local paper plant. Through simultaneous reaction-extraction pathways applying dialysis filtration and a highly porous polystyrene divinylbenzene adsorbent resin (HR-P) for the solid phase extraction (SPE), an attempt was made to isolate smaller molecules produced from the photocatalytic degradation of lignin sulfonate. Moreover a relatively high concentration of lignin sulfonate (0.5g/L) was used for the experiments. Ultraviolet-visible (UV-Vis) spectroscopy revealed a faster degradation of the aliphatic moiety compared to the aromatic moiety which constitutes lignin. New peaks were observed from High performance liquid chromatography (HPLC) analysis and some of these peaks showed signals when studied under fluorescence detection. This suggested the production of new substances and fluorophores. The catalytic coatings were done through the sol-gel procedure and they could be used many times.

2. Introduction

2.1. Motivation

In October 2014 the price of crude oil was 85 dollars per barrel and the forecast for next year is 98 dollars per barrel [1]. This is a symbolic indicator for the decreasing availability of conventional non-renewable energy sources due to the global economy growth coupled with frequent political instability. According to the World Energy, Technology and Climate Policy Outlook of the European Commission [2], the world total energy consumption levels will rise from 12.1×10^9 tons oil equivalent (toe) (2010) to 14.5×10^9 toe (2020) to 17.1×10^9 toe by 2030. As a result, the world carbon dioxide emission from the combustion of fossil fuels will increase from 29.3×10^9 tons (2010) to 36.7×10^9 tons (2020) to 44.5×10^9 tons (2030). That means the world carbon dioxide emission will be almost doubled by 2030. Also, less than 1% of the 300×10^6 tons of plastic produced per year is natural polymers [3]. Thus, there is a need for the development of bio-based macromolecular materials which would reduce the consumption of fossil resources and hence reduce CO₂ emission.

The major option is the gradual replacement of these fossil resources by renewable alternatives, e.g. wind, sun, water, and biomass. Ligneous biomass also known as lignocellulosic biomass is of great interest for industries (chemistry, biotechnology, and fuel) and biorefineries converting sustainable materials [4]. This is due to the biomass's content of high value-added compounds; cellulose (40-50%), hemicellulose (24-35%), and lignin (18-35%) [5]. Furthermore, biomass is inexpensive, available in large amounts [6] as well as CO₂ neutral [7]. Nevertheless, just 3-3.5% of the yearly produced biomass ($170 - 200 \times 10^9$ tons) is utilized by non-food applications [4] because of reasons related to the lignocellulosic structure per se and its processability.

Commercial lignin is a byproduct of the pulp and paper industries, wood hydrolysis industries and pre-treatment technologies to obtain cellulosic ethanol and bio-diesel. More than 70 million tons of various types of lignin are produced as waste material by the paper industry yearly [8]. However, lignin and its degradation products cannot be completely decomposed by sludge processes and it's a major source of chemical oxygen demand (COD) of waste water from pulp and paper mills [9].

Lignin represents the only viable source to produce aromatic compounds as fossil fuel alternatives. In fact, one of the potential new transformation technologies for the conversion of lignin to value added products is photocatalysis. Photocatalytic transformation of lignin

offers advantages such as the application of mild physical and chemical reaction conditions. In a heterogeneous system, catalyst can be re-used; catalyst leaching and accumulation of particulate matter in the reactor can be minimized. Contrary to a heterogeneous system, in a homogeneous or suspension system, the catalyst particles have to be recovered after reaction through downstream processes such as ultra-filtration which bring along additional process steps and costs. However, the set back of immobilized system (heterogeneous) are the less photonic efficiency values attained compared to suspension systems due to mass transfer limitation [10].

2.2. Aim of thesis

The goal of this work was to develop a photocatalytic reaction system which could effectively depolymerize lignin into value added chemicals such as phenolic derivatives or thermosets like phenolic resins thus proposing a processing concept for lignin conversion. Experimentally this involved the development of stable catalytic coatings on porous glass material through a sol-gel hydrolysis route. The photocatalytic activity of the coatings had to be evaluated by degradation experiments of lignin sulfonate radiated with ultraviolet (UV) light. Furthermore, this work was aimed to present a reaction system which could remediate the pollution problem of waste water discharged from pulp and paper mills on the one hand and on the other hand, give a possibility to further exploit the degradation of lignin sulfonate as an alternative chemical source. It is for this reason why lignin sulfonate used in this study was directly obtained as waste water from a local paper manufacturing plant rather than using already purified lignin from a commercial source.

The reactor used in this study was to be characterized regarding its flow characteristic and photonic efficiency. Also an attempt was to be made applying high concentrations of lignin sulfonate solution for the reactions because such parameters are essential for the rigorous design and scaling-up of a photocatalytic reactor in order to accomplish a commercial application. UV light was the illumination source because of the high amount of solar energy (44%) it contains compared to visible light (3%) [11]. This is also because, it had previously been found out that the amount of light present in either natural sunlight or artificial light was insufficient to process large amounts of organic compounds [12; 13]. Therefore, lignin sulfonate because of its complicated and robust nature was preferentially treated under UV-light.

2.3. Scope of the thesis

The motivation, aim and scope of this thesis are given in chapter 2. Lignin is introduced and an overview of its structure, the various methods of recovery and the different bond types in lignin molecule as well as its potential for fuel and chemical production is treated in chapter 3. Photocatalysis is defined in chapter 4 followed by the reaction principle for the formation of radical species and degradation of lignin while laying emphasis on structural representations proposed by researchers. Chapter 5 outlines the state of the art of the photocatalytic degradation of lignins. This includes process analytical methods and important operating parameters and their impacts. Chapter 6 covers the laboratory materials used while chapter 7 outlines analytical techniques and methods used. This is then followed by chapter 8 that describes and characterizes the reaction design by parameters such as flow, irradiance and photonic efficiency of the reactor. Chapter 9 treats the synthesis and characterization of the catalysts. Chapter 10 covers the effectiveness and photocatalytic activity of the coatings. This is done by studying the degradation of methylene blue (MB) dye under UV light illumination. After that a comparative assessment of the best catalyst obtained from evaluation studies with MB is done with lignin sulfonate (chapter 11). Chapter 13 handles the photocatalytic study of some lignin standard compounds in order to get information about their retention time as a means to identify products arising from the photocatalytic degradation of lignin through peak superimposition. In chapter 12, a comparative study of the different catalysts is done regarding the formation of peaks. High performance liquid chromatography (HPLC) and fluorescence detection results are discussed here. Finally, this reports ends with a conclusion and an outlook.

3. Lignin as raw material

3.1. Chemical structure and sources

Wood biomass consists of cellulose (40–50%), lignin (16–33%), hemicelluloses (15–30%), and a variety of extractives (1–10%) [14]. After cellulose, lignin is the most abundant renewable carbon source on earth [15]. Lignin can be available through various sources and biomass transformation technologies [15]. Commercial lignin is the byproduct of the pulp and paper industry, wood hydrolysis industries and pre-treatment technologies to obtain cellulosic ethanol and bio-diesel.

More than 70 million tons of various types of lignin preparations are produced as waste material by the paper industry yearly [8] mainly from the kraft process as noted by Kamm et al [4]. 98% is burnt for energy recovery in the paper mills [16] while less than 2% is sold, primarily for the formulation of dispersants, adhesives and surfactants [17]. Modified lignin resulting from paper waste water processes are for example liginosulfonate, alkali lignin, sulfate lignin, hydrolytic lignin, steam exploded lignin and organosolv lignin. The sulfite process results in liquor that contains 40-50% of the original wood and having as principal components lignin sulfonate [18]. The kraft and soda pulping processes result in liquors named black liquor containing alkali lignin also called kraft and sulfate lignin [18].

Lignin is the only naturally synthesized aromatic biopolymer [19]. In addition, native lignin is a polydisperse 3D macromolecule with an undefined molecular mass. The biopolymer is made up of randomly arranged phenylpropane units, *p*-coumaryl alcohol, coniferyl alcohol and sinapyl alcohol (Figure 1) contributing to an irregular structure [20].

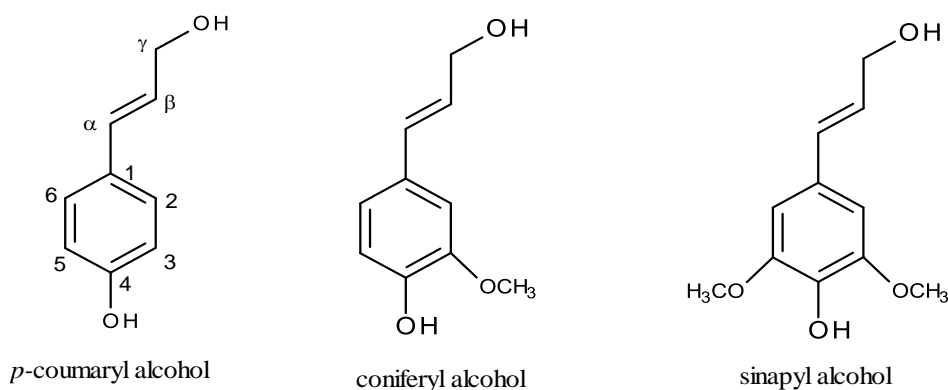


Figure 1: Monomer structures of lignin [21].

The many polymerization sites found in lignin monomer units explain the heterogeneity of the molecule and the complex product distribution which may arise during depolymerization. An overview of the common inter-unit linkages and estimated proportions are shown in Table 1. For a better illustration, Figure 2 shows the structure of a softwood lignin fragment containing all prominent linkage types.

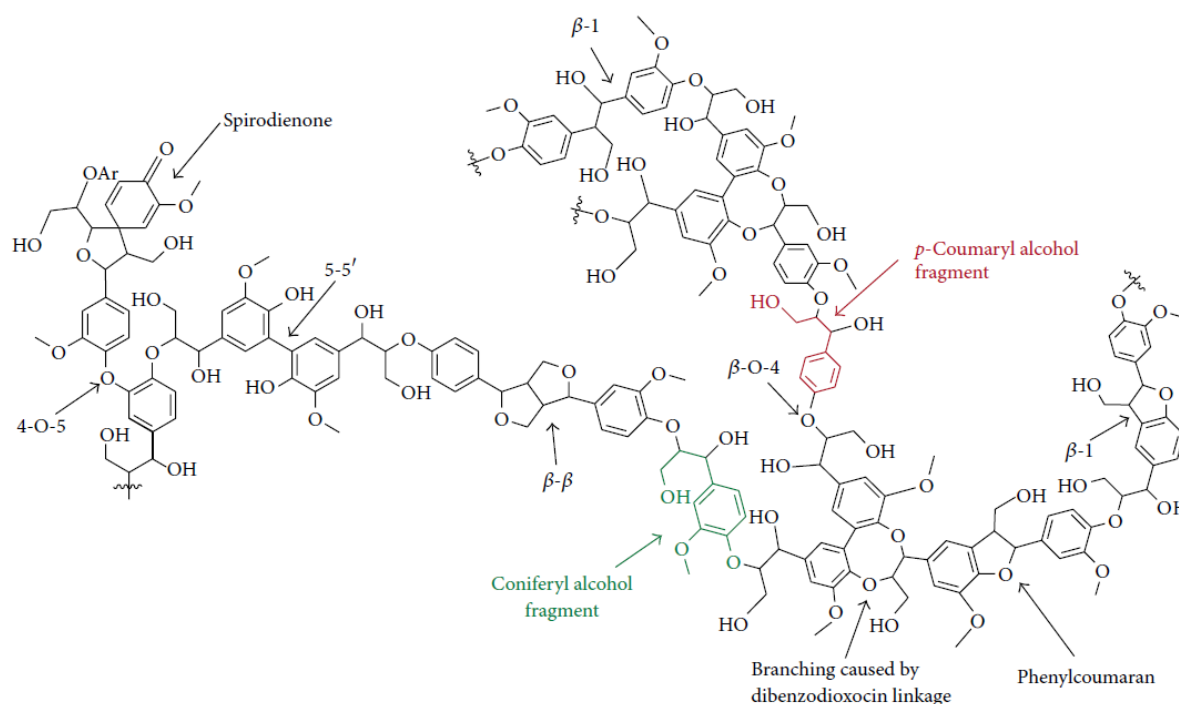


Figure 2: Structure of a softwood lignin fragment showing the prominent linkage types, reprinted with permission from Zakzeski et al.[22] and Evtuguin et al.[23].

Table 1: Overview of most frequent bond types found in lignin

Model linkage ^a	Glasser et al.[24]	Erickson et al. [25]	Nimz[26]
β -carbon-oxygen-4-aromatic carbon	55	49-51	65
α -carbon-oxygen-4-aromatic carbon		6-8	
β -carbon-5-aromatic carbon	16	9-15	6
β -carbon-1-aromatic carbon	9	2	15
5-aromatic-carbon-5-aromatic carbon	9	9.5	2.3
4-aromatic-carbon-5-aromatic carbon	3	3.5	1.5
β -carbon- β -carbon	2	2	5.5
β -carbon- β -carbon forming furanic structure			2
α -carbon- γ -carbon-oxygen- γ -carbon	10		

^a: % of total phenylpropane units.

3.2. Biorefinery scheme of lignin

Lignin is predominantly utilized as secondary fuel, but has the potential to partly replace fossil carbon resources as basis of the chemical industry due to its unique structure comprised of three phenyl propane units.

Figure 3 depicts an exemplary lignocellulosic biorefinery scheme with emphasis on the lignin stream [22]. Lignin has to be removed first before the polysaccharides can be processed, e.g. to 2nd generation biofuels. For separation purposes several pretreatment procedures are currently applied in order to generate lignin derivatives (modification in lignin structure) which can be differentiated on the basis of their isolation method and their origin since as their physical and chemical properties differ [27; 28; 20].

Through photocatalysis, extensive removal of the functional groups present on the lignin monomers yields simple aromatic compounds such as phenol, benzene, toluene, and xylene. These platform chemicals are then reacted in a second step using existing catalytic technology developed for petroleum refineries to produce bulk and fine chemicals. For example, after photocatalytic treatment, biochemical conversion can follow [29]. Alternatively lignin can be converted photo-catalytically directly to valuable chemicals in a one-pot fashion. This requires highly selective catalysts that can disrupt specified functionalities and linkages [30].

Lignin is an aromatic biopolymer of high potential fission products for a wide range of sectors and it is thus gaining attention, e.g. for the production of platform chemicals as depicted in Figure 3. Nonetheless, lignin is still under-utilized and fundamental research and development is needed [4]. This is explained by lignin's complex nature, its recalcitrance to degradation and the difficulty to analyze its numerous degradation products. Therefore, intensive research goes on both sides; process engineering and development (homogeneous, heterogeneous catalysis, thermal, electrochemical and/or hybrid procedures), and process analytics. Besides photocatalysis, lignin derivatives have been described in literature to undergo degradation through other procedures. For example, biochemically through microbial or enzymatic attack [31], thermally [32; 33], or electrochemically through oxidation reactions [34].

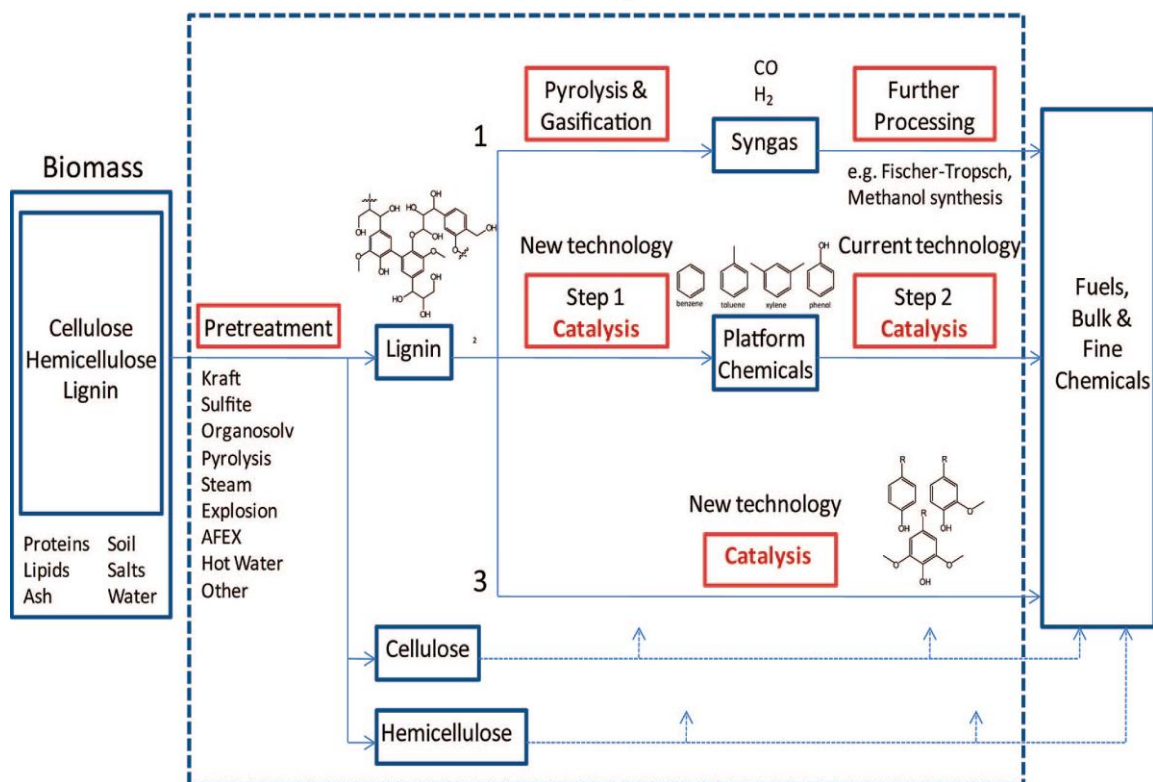


Figure 3: Lignocellulosic biorefinery scheme with particular emphasis on the lignin stream, reprinted with permission from Zakzeski et al. [22]. Copyright (2010). American Chemical Society.

4. Photocatalysis

4.1. Definition

Photocatalysis is the acceleration of a photoreaction in the presence of a catalyst. Photocatalysis, is an advanced oxidation process (AOPs) [35], with the potential to transform lignin to value added products such as phenol, benzene, toluene, and xylene [36]. It can be applicable as stand-alone unit or it can be coupled with other AOPs (e.g. Fenton's reagent, ozone, electrochemical oxidation) as well as biocatalysis [35] (e.g. hydrolysis through ligninolytic enzymes).

4.2. On the reaction pathways of lignin photocatalytic degradation

4.2.1. Formation of radical species for photocatalysis

Photocatalysis is the acceleration of a photoreaction in the presence of a catalyst. In other words, it involves the initial absorption of photons by a molecule or substrate to produce highly reactive electronically excited states.

Lignin degradation is generally in the range of lower energy (between 300 and 400 nm) because of its multifunctional character [37; 38; 39]. This region falls within the UV –light region. TiO₂ is the most applied photocatalyst [40]. In this region TiO₂ has greatest activity because titania being an N-type semiconductor possesses enough energy for electron transfer. The energy band gap of TiO₂ is approximately 3.2e.V. [40]. N-type semiconductors have a larger electron concentration than hole concentration and are thus negative. P-type semiconductors (e.g. silicon doped with boron) possess larger hole concentrations than electron concentrations and are thus positive. An electron hole is referred to the position where an electron could exist in an atom or atomic lattice.

In photogenerated catalysis, the photocatalytic activity depends on the ability of the catalyst to create electron–hole pair which generates free radicals (e.g. hydroxyl radicals: •OH) enabling secondary reactions [41]. Other aspects include, the rate of electron transfer, the rate of charge recombination, crystal structure, surface area of catalyst, porosity and surface hydroxyl group density [11].

In a heterogeneous photocatalytic system, photoinduced molecular transformations or reactions take place at the surface of a catalyst. Depending on where the initial excitation occurs, photocatalysis can generally be divided into two processes [41]. When the initial

photoexcitation occurs in an adsorbate molecule which then interacts with the ground state catalyst substrate, the process is defined as a catalyzed photoreaction. In case the initial photo excitation takes place in the catalyst substrate and the photoexcited catalyst then transfers an electron or energy into a ground state molecule, the process is defined as a sensitized photoreaction. In what follows equations summarizing the formation of radical species under photocatalytic conditions shall be described. S stands for the lignin substrate while TiO_2 (h^+_{VB}) and TiO_2 (e^-_{CB}) represent the electron deficient (valence band) and electron-rich (conduction band) parts in the structure of TiO_2 , respectively.

The initial process for photocatalysis involves the generation of electron - hole pair in the semiconductor particles as a result of UV radiation [42; 43].

Figure 4 shows the excitation of an electron from the valence band to the conduction band initiated by light absorption with energy equal to or greater than the band gap of the semiconductor. This is expressed by equation (1).

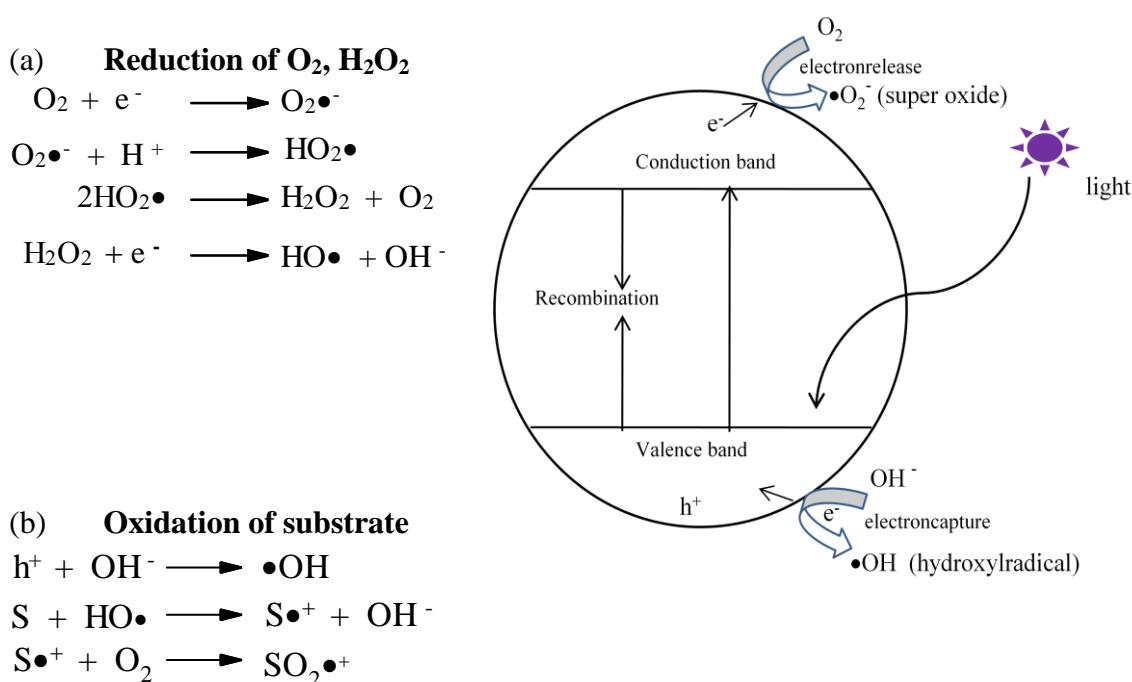


Figure 4: Photocatalysis principle, adapted from Linsebigler et al. [41]

Upon excitation, the fate of the separated electron and hole can follow several pathways. Electron holes can then react with hydroxyl ions (OH^-) or H_2O producing hydroxyl radicals ($\bullet\text{OH}$) as shown in equation 2. Evidence from Jaeger and Bart [44], Matthews [45] and Machado et al. [46] report that the hydroxyl radical ($\bullet\text{OH}$) is the main oxidizing agent in the

photo-catalytic oxidation because of the unpaired electrons. Therefore, it can react fast and unspecifically with almost all organic compounds (S) [47] abstracting an electron with the formation of radical organic species as shown in equation 3 [48].

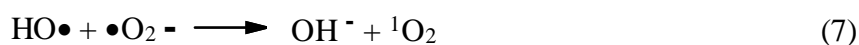
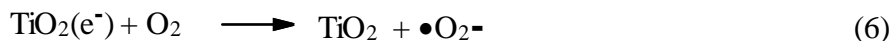
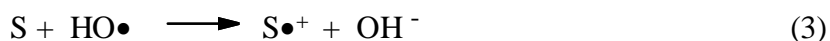
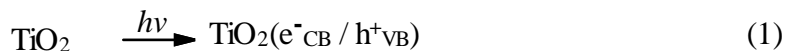


Figure 5: Formation of singlet oxygen, hydroxyl and superoxide radicals as principal reactive species in a photocatalytic process [42; 43].

The organic radicals and radical cations can for example react with molecular oxygen, to form organic peroxy radicals and peroxy radical cations respectively (equation 4). The holes can oxidize organic compounds by electron abstraction to form organic cationic radicals (equation 5) [46]. Superoxides can be formed by the reaction of electrons with electron acceptors such as O_2 (equation 6). Meanwhile the formation of singlet oxygen can be from the reaction of hydroxyl radical and superoxide (equation 7) [46]. Moreover, there is a possibility that electrons and holes recombine if electron acceptors are limited. In this case, recombination can take place in the volume of the semiconductor particle. When recombination takes place, radiation energy is lost or converted into heat (equation 8) [49].

4.2.2. Adsorption mechanism of photocatalysis

The condition for photocatalytic oxidation of organic substances is that they come in contact with the oxidizing species such as hydroxyl and superoxide ($\text{OH}\bullet, \bullet\text{O}_2^-$) radicals. This occurs when they are adsorbed by TiO_2 or if they get close to the TiO_2 surface. Calculations from Turchi and Ollis [50] shows that, for organic substances at a concentration of 1mmol/L suspended in water, the hydroxyl radical ($\text{OH}\bullet$) can diffuse only about 10nm away from its point of origin. This means at lower substrate concentrations the diffusion path for the

hydroxyl radical ($\text{OH}\bullet$) should be greater in order for the reaction to take place. A summary of the process can be described as follows:

- (a) Excitation of the catalyst and the generation of OH radicals.
- (b) Transport of organic substances and O_2 at the surface of the catalyst.
- (c) Adsorption of the organic substances and O_2 to TiO_2 .
- (d) Reaction of organic substances and intermediate oxidation products with radical and reaction of O_2 and electrons (e^-) at the surface of the catalyst. Also, recombination of the charge carrier (h^+ and e^-).
- (e) Desorption of the oxidation products.
- (f) Transportation of products back into solution.

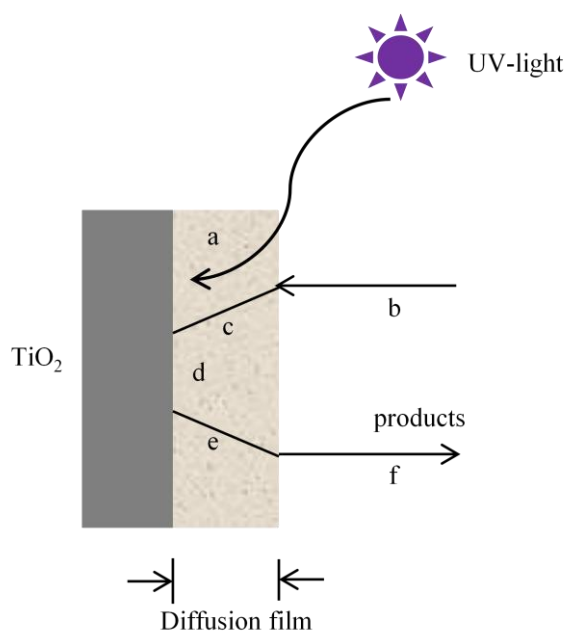


Figure 6: Adsorption–diffusion reaction pathway in photocatalysis. Adapted from Turner [51].

Steps (a) to (f) are depicted in Figure 6. Since as the processes take place one after another, the slowest step determines the rate of degradation [52]. Bahnemann et al. [53] reported that excitation of the catalyst and generation of hydroxyl radicals is very fast. This corresponds to step (a) which can be neglected during the rate equation. However in order to minimize the influence of intermediate oxidation products, the reaction rate should be based on the degradation rates at the beginning of the reaction. This implies steps (e) and step (f) can be neglected as well and thus, the kinetic is determined by mass transport, adsorption and reaction corresponding to step (b), (c) and (d) respectively.

4.2.3. Structural representation of some proposed lignin degradation pathway

From investigations carried out by Mazelier et al.[54](photochemistry of 2,6-dimethylphenol), it was postulated that hydrogen can be abstracted by α -carbonyl groups. In the same context, lignin derivatives having similar functionality can follow a similar pathway. In addition, oxidative chain reactions with the participation of ground-state oxygen can be initiated leading to fragmentation and combination reactions and thus the formation of new dimers or oligomers (Figure 7).

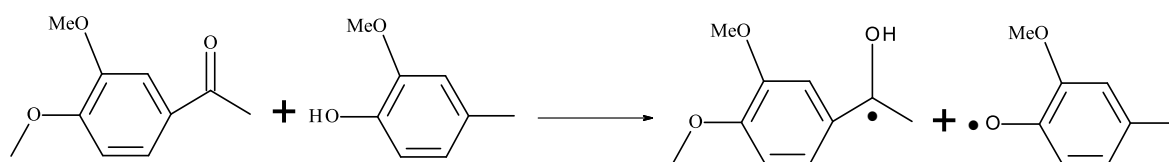


Figure 7: Formation of phenoxyl radicals by intermolecular abstraction of phenolic hydrogen by carbonyl groups [54].

Miyata et al. [55] proposed a cleavage mechanism for the $C\alpha-C\beta$ bonds leading to the formation of small fragments such as vanillin as shown in Figure 8.

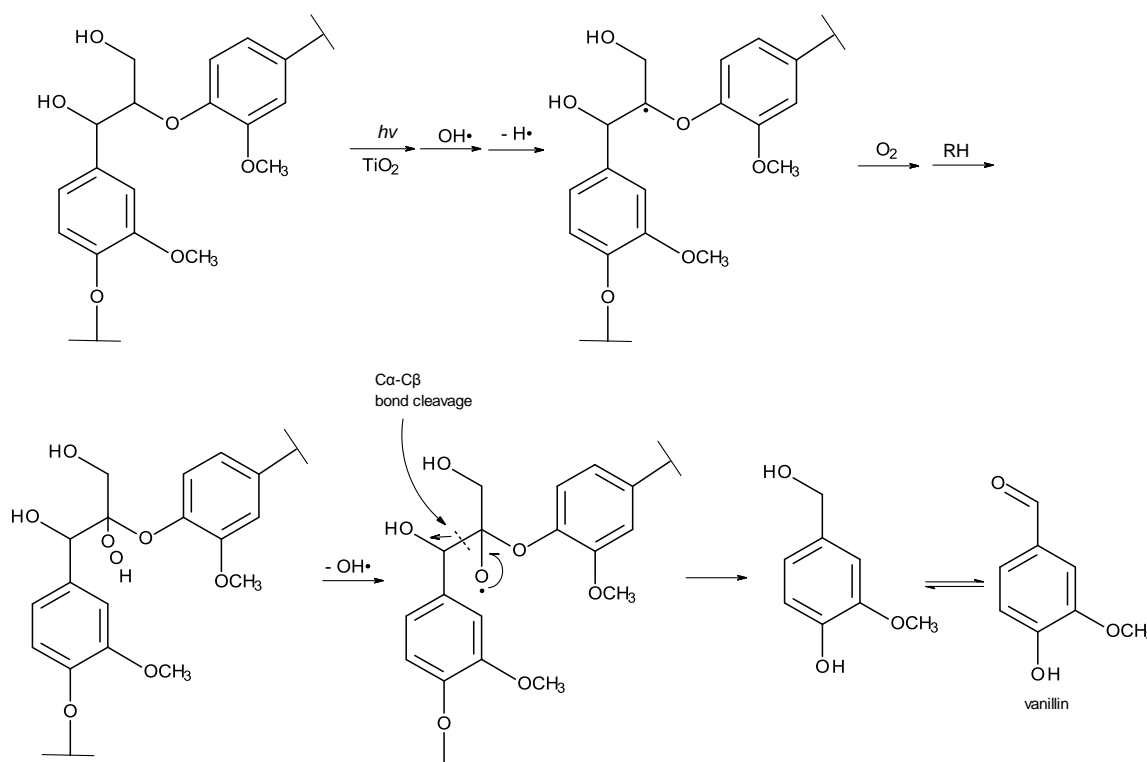


Figure 8: Supposed lignin degradation scheme by autooxidation induced by TiO_2 / poly (ethylene oxide) [55].

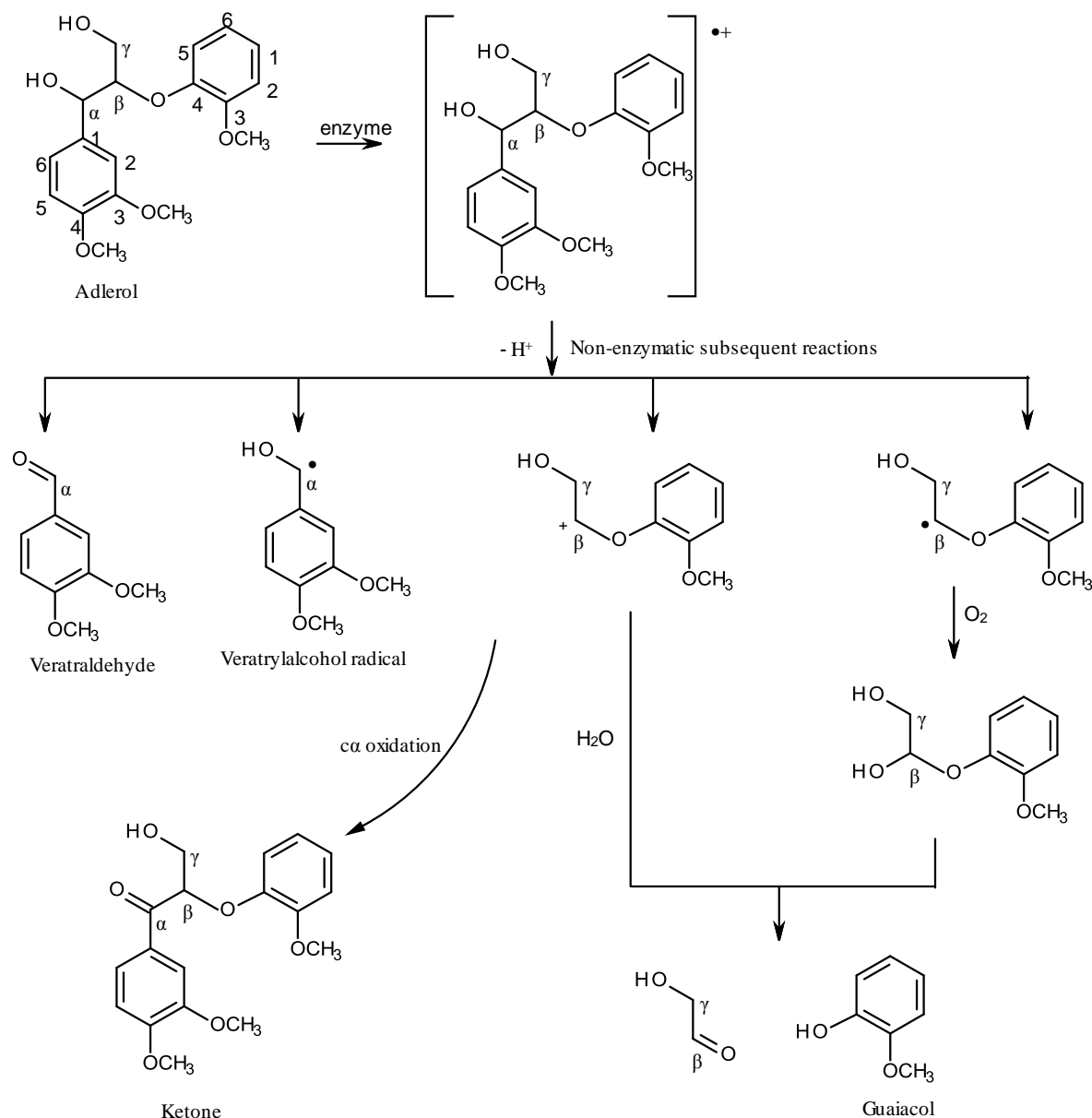


Figure 9: Proposed radical reaction scheme initiated by enzyme (lignolytic heme peroxidase) for the conversion of adlerol possessing C β -O-4 bonds into smaller units, summarized by Busse et al. [31], abstracted from Tien and Kirk [56], Kirk et al.[57], Lundell et al.[58], Schoemaker et al.[59] and Palmer et al.[60].

Figure 9 [31] illustrates the formation of a radical cation formed as a result of enzyme (lipase) mediated reaction of adlerol. Adlerol is characterized by a C β -O-4 bond and considered to be a lignin model compound. With the formation of the radical species, subsequent non-enzymatic reactions such as radical reactions can take place generating a wide variety of products and complex compounds. In summary this involves:

- Cleavage of side-chain e.g. C α -C β bond cleavage.
- Cleavage of C-H bond.
- Demethoxylation.

- Cleavage of ether-bond (e.g. addition of solvent (H₂O)) [60].
- Hydroxylation (e.g. through oxygen incorporation via O₂ or H₂O from the solvent) of benzylic methylene groups.
- Formation of phenol (by nucleophilic attack, e.g., addition of solvent (H₂O)) [60].
- Cleavage of aromatic caused by reactions with perhydroxy radicals (HOO•) [60].
- The free-radical species (R•) are highly reactive [60] which in turn can bind molecular oxygen (O₂) forming the products and a superoxide anion radical (O₂•⁻) [59] via degradation of an organic peroxy radical intermediate (ROO•) [60].
- Formation of a ketone [61] through C α -oxidation (e.g. due to proton loss [59]; or direct hydrogen abstraction in the presence of active oxygen species [62]).

4.3. Conclusion

It is widely assumed that the photocatalytic degradation of lignin follows a radical reaction pathway which is similar to that considered in thermal, electrochemical and biochemical processes. However, reporting on the degradation pathway of lignin derivatives and even that of lignin model compounds is still a major challenge. This is probably due to the complex nature and variety of possible degradation products. Indeed the mechanism is far more complex considering other factors such as type of lignin, type of catalyst, pH, illumination source and additives.

5. Photocatalysis of lignin derivatives: state of the art

5.1. Influence of process parameters

Varying process parameter is aimed at improving the photocatalytic efficiency of a system. The basic process parameters, such as catalyst concentration [63; 64; 36], substrate concentration [64; 65], addition of metal ion to TiO₂ catalyst [66; 63; 67; 68; 15], pH [69; 64], illumination [70; 64; 36; 38], and their influence shall be discussed in this chapter.

Table 2 gives an overview of reaction conditions including type of catalyst applied while Table 3 portrays parameters, analytical methods and results achieved by some researchers. It is worthwhile noting that, comparing the different photochemical processes poses a big challenge because of the wide variables involved. These discrepancies start from the source and type of lignin followed by the differences in reactor design, illumination source, intensity of radiation and different types of TiO₂ catalyst such as Fischer scientific rutile TiO₂ [36], TiO₂ (TiO₂-TP-2 of Fujititan) [65], just to name a few.

Table 2: Summary of starting conditions for the photocatalytic degradation of lignin derivatives.

Reference	Lignin source	Catalyst	Reaction conditions
Machado et al. [46]	Peroxyformic acid lignins from eucalyptus grandis wood (EL1) EL1 + sodium borohydride	TiO ₂ and H ₂ O ₂	Lignin conc.: 0.25mg/mL, T=25°C, pH 11, UV Vis radiation $\lambda > 300\text{nm}$, 400W mercury lamp, cylindrical pyrex glass reactor, constant oxygen bubbling.
Ksibi et al. [69]	Water soluble lignin obtained from black liquor.	TiO ₂ -P25 (Degussa)	Lignin conc.: 90mg/L, T=20°C, pH 8.2, UV-radiation $\lambda > 290\text{nm}$, pyrex reactor open to air, philips HPK 125W lamp.
Kansal et al. [64]	Lignin from wheat straw kraft digestion	TiO ₂ P25 (Degussa) and ZnO	Lignin conc.: (10–100 mg/L) in 100mL, ZnO catalyst dose (0.5–2.0 g/l), pH of the solution (pH 3–11), solar illumination, oxidant concentration ($3.06 \times 10^{-6}\text{M}$ to $15.3 \times 10^{-6}\text{M}$), thin bed film slurry pond reactor, oxidant: sodium hypochlorite solution (4% available Cl ₂).

Reference	Lignin source	Catalyst	Reaction conditions
Dahm and Lucia [36]	Whitewater from industrial process water that exits paper machines	Fischer Scientific rutile TiO ₂	Lignin conc.: 40mg/L in 500mL batch reactor, T=21°C-42°C, Rayonet photochemical chamber, 16 VWR 8-W black light, phosphor (350-nm) lamps, constant oxygen bubbling. power of illumination: 128 to 64W, light intensity: 223-445mW/cm ³ .
Portjanskaja and Preis [66]	Lignin, purchased from Aldrich	TiO ₂ P25-N (Degussa)	Lignin conc.: 100mg/L, pH 8, batch reactor system, reactor open to air, Phillips TLD 15W/05 low-pressure luminescent mercury UV-lamp, UV-radiation $\lambda > 360\text{nm}$, power density of irradiation = 0.7mW/cm ² , visible light source.
Tanaka et al. [65]	Lignin from coniferous wood	TiO ₂ (TiO ₂ -TP-2 of Fujititan)	Lignin conc.: (0.003 to 0.03%), UV-radiation $\lambda > 310\text{nm}$, cylindrical reaction vessel.
Tonucci et al. [38]	Ca ²⁺ and NH ₄ ⁺ lignin derivatives	TiO ₂ as Degussa P25+ Polyoxometalates (POM), H ₂ O ₂	Open quartz tubes (20mL) reactor, T=20°C, 1atm, multi rays of ten UV lamps of 15W power each, UV-radiation $\lambda > 254\text{nm}$.
Miyata et al. [55]	Picea glehnii wood flour	TiO ₂ /polyethylene oxide (PEO)	Reactor: open petri dish, T= 30 °C, t= 48h, 400W mercury lamp.
Shendeet al. [15]	Kraft lignin	TiO ₂ -ZnO-ZrO ₂	Lignin conc.: 1mg/mL in 10mL, 250W Xenon lamp and AM 1.5G lamp filter, power density of irradiation: 100mW/cm ² , Solar lamp simulator.
Tian et al. [71] and Pan et al. [34]	Kraft lignin from black liquor	Ta ₂ O ₅ -IrO ₂ and PbO ₂ thin film TiO ₂ Nanotube/ PbO ₂	Lignin conc.: 30% (w/w), UV-radiation $\lambda > 365\text{nm}$, t= 10min, power density of irradiation: 20mW/cm ² , blue wave TM50 AS UV spot lamp, EG&G 2273 potentiostat/galvanostat to apply current, Ti/TiO ₂ NT/PbO ₂ electrode as working electrode and Pt coil as outer electrode and Ag/AgCl as reference electrode.
Awungacha Lekelefac et al. [72; 73]	Lignin sulfonate from paper waste water	TiO ₂ as Degussa P25, TiO ₂ from sol-gel process of TiOSO ₄ , TTIP	Lignin conc.: 500mg/L in 200mL, Osram Planon light source, irradiance: 30-40W/m ² . UV-radiation λ : 280-420nm, t=20h, reactor open to air, recirculation system, flow rate 22.5mL/min.

Table 3: Parameters, analytical methods and results from different work groups.

Reference	Parameter studied	Analytics	Result
Machado et al. [46]	Role of hydroxyl radicals, irradiation of lignin in the absence and presence of photocatalyst TiO ₂ and H ₂ O ₂	Ultra Violet-Visible (UV-Vis) spectroscopy Ionization Absorption Spectroscopy (IAS), Size Exclusion Chromatography (SEC)	A sharp decrease in the phenolic content observed for reactions involving direct photolysis. SEC: a reduction of almost 50% in the average molecular weight of lignin equal to 1.4kD after 90min of irradiation.
Ksibi et al. [69]	Irradiation of lignin in the absence and presence of photocatalyst TiO ₂ – P25	UV-Vis spectroscopy, ¹³ C-Nuclear Magnetic Resonance (NMR) Solid state, Total Ion gas Chromatography (TIC), Induction Coupling Plasma (ICP), Chemical oxygen demand (COD)	56% degradation rate with TiO ₂ catalyst after 420min, reaction time. Ethylacetate-extractable products showed vanillin, vanillic acid, palmitic acid, biphenyl structures and 3,4,5-trimethoxy benzaldehyde. Presence of magnesium and calcium ions. COD removal is higher for the initially low concentrations of lignin solution.
Kansal et al. [64]	Catalyst dose, pH, oxidant concentration, initial substrate concentration ,ZnO catalyst in slurry and immobilized mode	UV-Vis spectroscopy, COD	Optimum catalyst dose is 1g/L. Optimum oxidant concentration: 2×10 ⁻⁶ M. Gradual decrease of absorption peak indicating decomposition of organics. COD removal is higher for the initially low concentrations of lignin solution.
Dahm and Lucia. [36]	Catalyst dose, illumination intensity	UV-Vis spectroscopy, Total Organic Carbon (TOC), Capillary Ion electrophoresis Analysis (CIA)	Gradual decrease in absorption peak indicating decomposition of organics. Optimal catalyst dose of 10mg/m. Higher illumination intensities correlated well with higher initial degradation rate. 74% disappearance of TOC.

Reference	Parameter studied	Analytcs	Result
Portjanskaja and Preis [66]	Influence of ferrous ions N-doped catalyst effect Sprayed catalyst on support and submersed catalyst	COD, UV-Vis spectroscopy, biochemical oxygen demand (BOD), colorimetric measurement at 570nm	Addition of Fe ²⁺ , up to 2.8mg/L leads to 25% increase in photocatalytic efficiency. Sprayed catalyst exhibited 1.5 times higher efficiency than the one attached by submersion. Negligible effect of N doped catalyst. Increase of aldehyde concentration over reaction time. Neutral media was most beneficial for biodegradability. 80% of free phenols removed under neutral conditions.
Tanaka et al. [65]	Catalyst loading, lignin concentration, illumination time	UV-Vis spectroscopy, TOC, Gel Permeation Chromatography (GPC), ¹ HNMR, Fourier Transformation Infra-Red (FTIR) spectroscopy	FTIR measurement revealed a fast transformation of aromatic moiety present in lignin. Characteristic bands of aromatic rings, methoxy and aliphatic side chains. Decrease in TOC values over time. Decrease in degradation rate with increase catalyst dosage. But after catalyst threshold value is attained, catalyst increase causes a decrease in degradation rates. FTIR peaks are shifted towards lower molecular weight region after photocatalysis.
Tonucci et al. [38]	Test of catalytic systems to obtain fractions with reduced degrees of polymerization. Comparison of thermal and photochemical reactions	¹ HNMR, Gas Chromatography – Mass Spectroscopy (GC-MS)	POMs are less selective when used as photocatalysts. No appreciable bleaching of the solution was seen when POM was used as thermal catalyst. Derived chemicals from experiment: vanillin, hydroxylmethoxy-acetophenone, coniferyl alcohol, coniferyl aldehyde, methanol, formic acid, acetic acid, and sometimes small amounts of C-2 and C-3 alcohols.
Miyata et al. [55]	Examination of cell wall structure of lignin (wood flour)before and after photocatalysis	GC-MS, Scanning Electron Microscopy (SEM), ¹ H-NMR	High delignification activity, delignification confined to the surface of lignin. Derived chemicals experiment: vanillin.

Reference	Parameter studied	Analytics	Result
Shende et al. [15]	Test of combined action of bio,- and photocatalytic systems	UV-Vis spectroscopy, GC-MS, X-ray Dispersive Energy Spectroscopy and X-ray Diffraction Analysis (EDX, XRD), SEM	Detection of following chemicals: acetyl guaiacol, 4-ethoxymethyl-2-methoxy phenol, methoxyphenyloxime, guaiacol, succinic acid, acetyl guaiacol, vanillic acid and vanillin.
Tian et al. [71] and Pan et al. [34]	Test of combined action of electro,- and photocatalytic systems	UV-Vis spectroscopy, FTIR, SEM, X-ray (EDX), High Performance liquid Chromatography (HPLC), COD	Detection of following chemicals: carbonyl functionality, vanillin and vanillic acid.
Awungacha Lekelefac [72; 73]	Comparison of degradation rates by different catalyst	HPLC, Fluorescence and UV-Vis spectroscopy, SEM, TOC	<p>UV-Vis results reveal faster degradation of the aliphatic moiety compared to the aromatic moiety of lignin sulfonate obtained from paper waste water.</p> <p>Peaks observed during HPLC analysis. Some of the peaks produced after photocatalysis had fluorescence signals. This suggests the production of new substances and fluorophores.</p> <p>Coatings produced through sol- gel procedures are stable and can be used many times.</p>

5.1.1. Influence of catalyst

One aspect to successfully implement photocatalysis is the choice of an appropriate photocatalyst. The majority of catalysts used are based on TiO₂ as summarized in Table 2. ZnO has also been applied either as single catalyst [64] or in a combination with other catalyst such as TiO₂ [72]. De Lasa et al. [74] described ZnO as being less active than TiO₂. They add that the use of ZnO is particularly relevant when the oxidative degradation rate becomes limited. This is opposite to what Kansal et al [64] reported by saying, ZnO is more reactive than TiO₂. However, TiO₂ (mainly anatase) remains the most used catalyst as can be depicted from Table 2. TiO₂ is reported to be favored because of its non-toxic property, cost efficiency, chemical and biological inertness. Moreover TiO₂ possesses the most efficient photo-activity and the highest stability, thus making it suitable for industrial use [75].

ZnO has been described to degrade lignin under visible light sources [64; 76] whereas TiO₂ is mostly applied in connection to UV-light sources as highlighted in Table 2. However, both ZnO and TiO₂ possess energy band gap energy of 3.2 e.V. [41].

Additives such as SiO₂ [77], polyethylene oxide (PEO) [55], polyethylene glycol (PEG) [78] have been added to TiO₂ catalyst, particularly when applying immobilized catalyst. Addamo et al. [77] noted a high adhesion of TiO₂ to glass support material when pre-coating was done with SiO₂. Moreover the pre-coating might have other advantages such as hindering diffusion of Na⁺ ions from the glass material into the nascent TiO₂ film during heat treatment processes. Analogous to the addition of SiO₂, polyethylene glycol (PEG) has also been introduced to mitigate catalyst surface activity, modify surface hydrophobicity and also reduce agglomeration tendency of the TiO₂ gel or TiO₂ particles in the suspensions [78]. By a proper surface modification, interaction between catalyst and substrate can be enhanced [72; 77].

Kansal et al. [64] varied catalyst (ZnO) dose from 0.5g/L to 2.0g/L for 0.1g/L kraft lignin solutions and found out that there was an optimum catalyst threshold value at 1 g/L which gives a catalyst to substrate ratio of 1:10.

Dahm et al. [36] examined catalyst dose from 2×10^{-3} g/L to 1.2×10^{-2} g/L for lignin solutions (from white water liner mill) of 4×10^{-2} g/L (catalyst to lignin ratio: 5×10^{-3} - 3×10^{-2}) at pH 8 and obtained best energy efficiency values and lignin degradation rates with a catalyst loading of 1.0×10^{-2} g/L.

In contrast, Ma et al. [63] applied far higher catalyst concentration compared to Dahm and Lucia [36]. Catalyst concentration was varied between 1g/L - 10g/L Pt/TiO₂. Best catalysis dose with respect to reaction turnover was obtained at 5g/L Pt/TiO₂. With the increase of

catalyst dose at pH 7, the reaction rate increased from 6.1×10^{-3} l/min (1 g/L TiO₂) to 7.1×10^{-3} l/min (5 g/L TiO₂) and 9.9×10^{-3} l/min (10 g/L TiO₂).

Catalyst effect has been explained on the basis that optimum catalyst loading is dependent on the initial solute concentration. An increase in catalyst dosage leads to a corresponding increase of total active surface area for reactions [79]. To that, at higher TiO₂ concentrations, the photon flux is more easily intercepted by the catalyst before penetrating into the bulk of the system. At the same time, due to an increase in turbidity of the suspension with high dose of photocatalyst, there is a decrease in penetration of UV light and hence photo-activated volume of suspension or solution decreases [80].

In summary, researchers have obtained best catalyst to lignin relations for different reaction designs and thus a general recommendation on catalyst dose is not possible. However, when lignin solution is treated with increasing catalyst loads, a corresponding increase in degradation rate is observed until a threshold value is reached [64; 63; 66; 36].

5.1.2. Influence of metal ion (doping) and additives

The purpose of adding metal ions to photocatalysts is to mitigate band gap energy through the introduction of intra band gap states and as a consequence produce a bathochromic shift in the absorption spectrum [11]. Altering the absorption spectral range gives the possibility to exploit both the visible light spectrum and UV light sources. Metal ion doping is also introduced to serve as electron or hole traps in order to minimize recombination between generated electron – hole pairs [11].

Portjanskaja and Preis [66] studied the addition of Fe²⁺ ions to an acidic lignin solution and found an increase in photocatalytic oxidation (PCO) efficiency. The optimum Fe²⁺ ions quantity was 2.8 mg/L while using 100 mg/L lignin solution. Upon further elevation of Fe²⁺ ions concentration, a corresponding reduction of the photocatalytic oxidation efficiency of lignin was noted. Likewise, Ohnishi et al. [67] made a comparative study by doping platinum (Pt), silver (Ag) and gold (Au) ions to TiO₂. In these reactions, 50 mg of catalyst (TiO₂) was used with the addition of an equivalent 1.5 wt % (based on TiO₂) metal ion. The addition of noble metals brought about a faster decolorization of lignin. Au showed better results than Ag, followed by Pt. In the same context, adding sodium hypochlorite as oxidant to Pt/TiO₂ catalyst, an additional five fold degradation rate was observed compared to that without doping [63]. Contradictory to the results described above, negligible effect of photocatalytic efficiency due to doping has been reported as well. Awungacha Lekelefac et al. [72] obtained little or no change in degradation rate by doping TiO₂-P25-SiO₂ catalyst with Pt ions (1 wt% relative to

TiO₂ catalyst). Likewise Portjanskaja and Preis [66] noted a negligible change of photocatalytic efficiency of TiO₂ when doped with nitrogen. Sarkanen et al. [42], Gellerstedt and Lindfors [81] reported the bias of peroxides to oxidation with reagents such as permanganate to favor aromatic moieties. Oxidation agents like permanganate oxidizes predominantly aliphatic chains in alkaline and neutral media. However, by the application of H₂O₂ (Fenton system), lignin disappeared completely [38]. Tonucci et al. [38] concludes that in order to satisfactorily conserve the organic material, the best compromise appears to be the TiO₂ photosystem, which shows low carbon consumption, good preservation of the aromatic rings and greatly reduced mineralization.

In summary, different results have been obtained concerning the influence of noble metal ion addition. While some authors report an improvement in the photocatalytic efficiency upon their addition, others report their addition as having no considerable influence. However, for reactions in which an improvement in the photocatalytic efficiency was noticed, there was a threshold value to be considered. When the concentration of dopant surpasses this threshold value, electron hole recombination is favored and this has a negative impact to photocatalysis. In such a case, the space-charge layer gets narrower and p-type dopants attract electrons and by virtue become negative. They would now then act as hole acceptor attracting holes. On the other hand n-type dopants which act as electron donor centers and possess excess electrons attract holes as well [11].

5.1.3. Influence of lignin concentration

Once the initial lignin concentration becomes higher exceeding a threshold value an inhibitory effect on the photodegradation was noted [64; 69; 36]. This threshold value varies and depends on the reaction system and reaction parameters such as optical density, catalyst concentration and reaction volume. From literature, different authors have implemented varying lignin concentrations probably to suit their reaction design. For example Ksibi et al. [69] uses 90mg/L; Awungacha Lekelefac et al. [72] applied lignin starting concentration of 500mg/L while Kansal et al. [64] applied concentrations between 10mg-100mg/L.

Explanations arising from the findings are as follows: at low lignin concentrations the incidental photonic flux irradiated interact with the catalyst generating hydroxyl radicals (OH●) which allow a faster degradation [29]. On the other hand, high initial lignin concentrations may lead to tight adsorption which can suppress CO₂ evolution [65] and hence maintain chemical oxygen demand (COD) values. Moreover, low delignification yields may be due to an inhibitory effect because of autooxidation by low molecular weight lignin degradation products

formed [55]. Also, due to the polymer structure of lignin which is cross linked, this makes it difficult for radical species, acid and the aldehyde compounds produced to spread into the inner region of the substrate hence limiting auto oxidation. As a worst case, this might be the rate-determining step of delignification which is hindered [82; 83; 84].

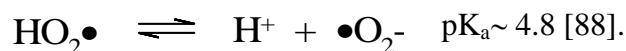
In summary, the time taken for complete degradation depends on the initial concentration of lignin and faster degradation occurs at low lignin concentrations.

5.1.4. Influence of pH

Varying pH entails an alteration in the properties of semiconductor–liquid interface [85], mainly related to the acid–base equilibrium of the adsorbed hydroxyl group [43]. Furthermore, pH also impacts lignin degradation rates [69; 64; 67]. In this context several studies were carried out with partly contradictory outcomes.

Kansal et al. [64] made pH investigations from 3-11 under solar light illumination using ZnO as catalyst. Maximum degradation was reached in alkaline conditions (pH 11). This is supported by Villasenor and Mansilla[86], reporting an almost complete decolorization of kraft black liquor from pine wood at pH value of 11.6 in combination with ZnO catalyst. Similar results were achieved by Ohnishi et al. [67] for bleaching alkaline lignin in aqueous solution with TiO₂ and ZnO as catalyst. High activities at neutral pH were also reported by Ohnishi et al. [67]. In contrast, Ma et al. (2008) [63] observed higher reaction rates and rapid degradation of a synthetic lignin wastewater (prepared by dissolving commercial lignin powder in aqueous solution; pH 11) in acidic solution (pH 3) than in alkaline solutions at pH 11; for either TiO₂ or Pt/TiO₂ catalysts.

Reconsidering the photocatalytic principle, the formed superoxide anion radicals ($\bullet\text{O}_2^-$) are in a pH-dependent equilibrium with perhydroxyl radicals ($\text{HO}_2\bullet$) as follows [87]:



$\bullet\text{O}_2^-$ undergoes dismutation reaction resulting in H₂O₂ and O₂ competing to any other $\bullet\text{O}_2^-$ -triggered reaction. In case of low pH operation conditions in aqueous solutions, HO₂• becomes dominant whose reactivity is considerably higher compared to $\bullet\text{O}_2^-$ [89]. Subsequently, HO₂• initiates substrate (S) oxidation to the radical cation (S⁺•) and is itself reduced to H₂O₂ [90]. Thus, increased degradation rates can be reasonably expected supporting the results made by Ma et al. [63] in an acidic environment. $\bullet\text{O}_2^-$ are extremely reactive in organic solvents [89].

Another aspect is the solubility of kraft lignin (soluble at $\text{pH} > 10.5$) which reduces with decreasing pH , whereas lignosulfonate should remain unaffected by pH in aqueous solution. Moreover, β -O-4 bonds have been described to be stable at acidic pH [20]. In fact, this could additionally explain the elevated degradation of kraft lignin made by Kansal et al. [64], and Villaseñor and Mansilla [86]. Nevertheless, the contradictory results gained by Ma et al. [63] still exist under the assumption that kraft lignin was used (which would be supported by the high pH of 11, obviously necessary for dissolving the lignin powder). Although most photocatalytic reactions described in literature are in an aqueous milieu, lignin raw material and its fission products may however vary considerably. Therefore the optimal pH is most likely to be reaction specific and has to be evaluated experimentally in principle.

5.1.5. Influence of Illumination

Many of the studies found in literature so far have not dealt on this subject per se. What is found is the use of different illumination sources, each having a specified power and lamp type. However, all tend to emit UV-light between the range 280-420nm. Other illumination sources include the visible light spectrum.

In general terms, illumination influences in that, it initiates photocatalysis by generating electron-hole pair in the semiconductor particles [42; 43]. Dahm and Lucia [36] altered illumination intensity while observing lignin degradation. In this study 0,04g/L lignin was used and light intensity was varied between 223-445mW/cm³. It was found out that higher illumination intensities correlated well with higher initial degradation rates and hence total lignin degradation [36]. Neppolian et al. [29] report degradation to be proportional to radiation intensity and best results are achieved for low lignin concentrations because of enhanced interaction between catalyst and incidental photonic flux.

In summary, high illumination power causes a corresponding high initial degradation rate at low lignin concentrations because maximum light penetration into the reaction medium is favored.

5.2. Process analytical methods

Various analytical techniques have been used to monitor lignin degradation. At the beginning of this sub-chapter, analytics revealing compounds formed from lignin degradation is treated. This includes for example, gas chromatography (GC) and ¹H NMR (nuclear magnetic resonance). This is then followed by results of qualitative analytic measurements such as

ultraviolet-visible (UV-Vis) spectroscopy and dissolved carbon (DC). A list of authors, analytical techniques applied and results achieved are outlined in Table 3.

Portjanskaja and Preis [66] studied lignin degradation by measuring the removal of phenols through colorimetric measurements. As a result of 24h photocatalytic oxidation under neutral media conditions, 80% of free phenols were removed. Gas chromatography (GC) result from Ksibi et al. [69] attested vanillin, vanillic acid, palmitic acid, biphenyl and 3,4,5-trimethoxy benzaldehyde structures after the photocatalysis of lignin from black liquor. This is in accordance with the findings of Tonucci et al. [38] reporting the formation of vanillin, hydroxylmethoxy-acetophenone, coniferyl alcohol, coniferyl aldehyde, methanol, formic acid, acetic acid and small amounts of C-2 and C-3 alcohols as degradation products.

^1H NMR spectral analysis of lignin before illumination and after 24h of illumination showing characteristic bands of aromatic rings, methoxy and aliphatic side chains were compared with each other. Results revealed that the aromatic ring degraded faster than the aliphatic chain [65]. Fourier transformation infrared spectroscopy (FTIR) showed bands corresponding to CH_3 , CH_2 and CH which remained unchanged after illumination while bands corresponding to aromatic rings disappeared as a result of illumination [65; 34].

Results obtained from the combination of photochemical and electrochemical oxidation from Tian et al. [71] and Pan et al. [34] were similar to that of Tanaka [65]. Here, ^{13}C -NMR confirmed the presence of the carbonyl functionality and the presence of vanillin and vanillic acid after 12h photochemical-electrochemical oxidation. Their results showed that the combination of a photocatalytic and an electrochemical oxidation significantly enhanced the efficiency of lignin degradation due to anodic potential bias which suppresses the recombination of photogenerated electrons and holes [34].

Ultraviolet spectrophotometry offers a convenient method to qualitatively and quantitatively analyze lignin in solution [91]. This is reflected by the large number of publications using this technique [69; 64; 66; 65; 63; 68; 92; 38; 36; 15]. This is most likely due to its simplicity to interpret lignin degradation. Lignins absorb UV light with high molar extinction coefficients because of the several methoxylated phenylpropane units of which they are composed [38]. Figure 10 depicts a series of photometric scans of lignin sulfonate from paper waste water showing a gradual reduction of absorbance during photocatalytic treatment [72]. Here, the absorption peaks are around 210nm and 280nm. Absorbance decreases with time implying the decomposition of lignin and the deterioration of chromophor groups [72].

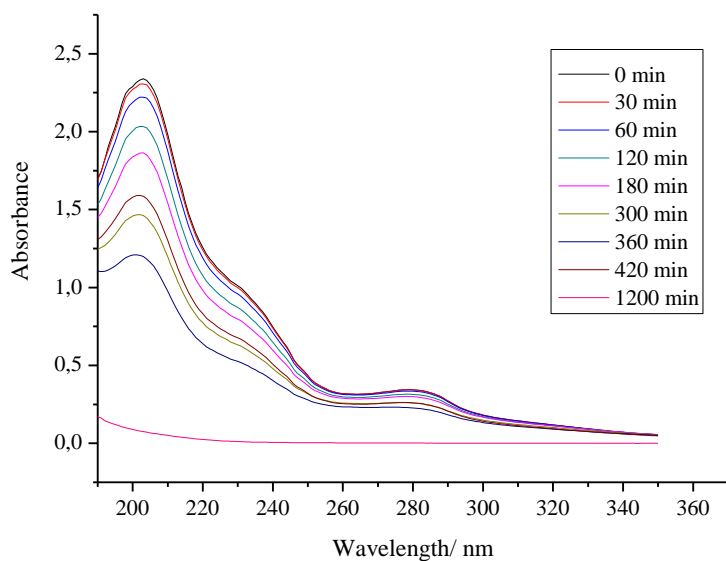


Figure 10: Time dependent UV-Vis absorption spectra of aqueous lignin solution from waste paper water irradiated with UV light (280-420nm) for different time intervals. The spectra are obtained for sol-gel derived TiO_2 nanocrystalline coating (TiO_2 -P25- SiO_2) [72].

Peaks at 210nm correspond to portions of the unsaturated chains while those at 280nm correspond to unconjugated phenolic hydroxyl groups [15] and the aromatic moiety [67] of the lignin molecule. Ohnishi et al. [67] report the absorption tailing arising from the color of lignin. Lignin degradation has been reported either at wavelength around 280nm corresponding to unconjugated phenolic hydroxyl groups [68; 64; 65; 15] or for both wavelengths (210nm and 280nm) [67; 38; 72]. Kobayakawa et al. [93] noted some other absorbance at wavelengths lower than 250nm and pointed out that this could be due to the modification of lignin fragmentations leading to the formation of transient species like methanol, ethanol, formaldehyde, formic acid and oxalic acid among others.

Analytical methods to effectively quantify lignin degradation by calculating the oxygen demand by organic substances and remaining organic carbon before and after photocatalysis have been studied. Amongst the methods are dissolved carbon (DC) [65; 68; 36], chemical oxygen demand (COD) [69; 64; 66; 67; 92], biochemical oxygen demand (BOC) [66], dissolved organic carbon (DOC) [63] and American dye manufacture institute value (ADMI) [63]. COD and BOD describe the oxygen demand by organic substances to be converted to CO , CO_2 , H_2O and NH_3 . Total organic carbon (TOC) describes the amount of carbon bound in an organic compound while DOC describes the dissolved fraction of organic carbon. ADMI measures the amount of dyestuff in water [64].

Decolorization of lignin solution has been reported to be another parameter observed during photocatalytic degradation. Color is an indirect indicator of the lignin amount. The higher the color intensity of the solution, the greater is the lignin content (high concentrated

lignin solutions, e.g. black liquor, appear dark brown) [94]. Thus, color changes can be interpreted as conversion of lignin to transient species or conversion to CO_2 and H_2O . In the latter case, decolorization must not necessarily be observed. Awungacha et al [72] observed a gradual change from the characteristic yellow lignin (when highly diluted) to a colorless liquid after a period of 20h with sol-gel derived TiO_2 nanocrystalline coatings on sintered borosilicate glass as depicted in Figure 11. A corresponding decrease in dissolved Carbon (DC) values close to 82% was observed for TiO_2 -P25- SiO_2 catalyst confirming degradation. This is shown in Figure 12.

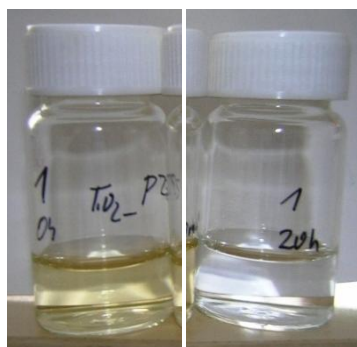


Figure 11: Gradual change from the characteristic yellow lignin sulfonate to a colorless liquid after a period of 20h. Catalyst: TiO_2 -P25 (Degussa)+TEOS, UV-light, room temperature (25°C), lignin concentration: 0.5g/L [72].

These findings are analogous to that of Ohnishi et al.[67] reporting the bleaching of lignin sulfonate which becomes colorless over time when illuminated continuously. Additionally, the chemical oxygen demand (COD) value decreases, generating carbon dioxide and a small amount of carbon monoxide as the main gaseous products. COD removal was reported to be effective at low lignin concentrations as compared to high lignin concentrations [64].

Another applied analytical technique is fluorescence detection directly coupled to a high performance liquid chromatography (HPLC) as a means to identify non aliphatic component in the complex mixture of lignin degradation products [72]. Fluorescence emission in lignin is attributed to aromatic structures such as conjugated carbonyl, biphenyl, phenylcoumarone and stilbene groups [95; 96]. Awungacha et al. [72] observed peaks on the HPLC and fluorescence chromatograms suggesting the production of new substances and fluorophores.

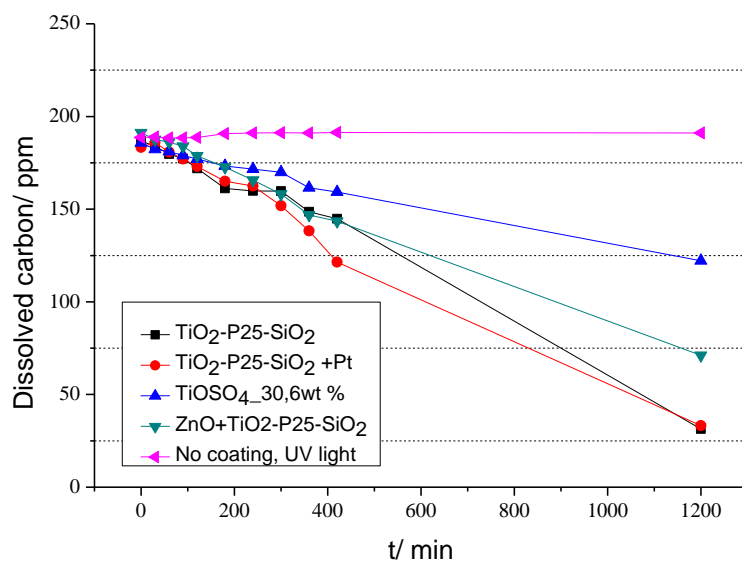


Figure 12: Variation of DC with time of aqueous lignin sulfonate solution from paper waste paper water irradiated with UV light (280-420nm) for different time intervals. The spectra are obtained for sol-gel derived TiO₂ nanocrystalline coatings (TiO₂-P25-SiO₂+Pt, TiO₂-P25-SiO₂, TiOSO₄_30.6wt%, ZnO+TiO₂-P25-SiO₂) [72].

6. Material

The laboratory instruments, materials and chemicals used in this work are outlined in Table 4 - Table 6.

6.1. Laboratory apparatus

Table 4: Laboratory equipment

Apparatus	Manufacturer/ source	Description/ Model
Analytical balance	Sartorius Micro	
Autosampler vial	NeoLab	
Alu-vial cover	NeoLab	
Drawing software	Accelrys draw	Accelrys draw 4.1
Filter support for syringe	Schleicher&Schüll	
Fluorescence spectrometer	Varian Cary Eclipse	Varian Cary Eclipse
Furnace	Heraeus Instruments	MR 170
HPLC	Hewlett Packard	HP1090
Laboratory drying chamber	Heraeus Instruments	
MSQ Plus Tune	ThermoFisher Scientific	Version: 2.0; SP2
MSQ	ThermoFisher Scientific	20905
Magnetic stirrer	H+P Labortechnik, oberschleissheim	Monotherm
Micropipette	Eppendorf, Hamburg	
Programmable fluorescence detector	HP	HP1040A
pH meter	Mettler Toledo	Fire Go
Pre-filter	Sartorius Stedim	Minisart RC 15
Roller pumps	Ismatec, Switzerland	Ecoline
Rasterelectronmicroscope	Zeiss Evo Göttingen	Evo LS 10
RO Water filter	Millipore Millipak	
Spectrophotometer	Thermo-Scientific	Genesys 10S
Total organic carbon (TOC)	Shimadzu	TOC-5000A
UV-A meter	Dr. Hoenle UV-technology	UV-A meter
UV-light plates	Osram	wavelength between 280- 420nm
Ultrasonic cleaner	Eumax	
UHPLC	Knauer	Platin blue
Water jet vacuum pump	16mmbar vacuum	

Xcalibur
Zentrifuge

Thermofisher scientific
Eppendorf

Version: 2.1.0.

6.2. Work material

Table 5: Table of materials used

Apparatus	Manufacturer/ source	Description/ Model
Polystyrene divinylbenzene adsorbent resin, Chromabond ®(HR-P)	Macherey Nagel, Düren.	Chromabond ®(HR-P)
Borosilicate glass tubes	ROBU-Germany	Borosilicate glass tubes
Sintered glass particles	ROBU-Germany	Por.00 (~ 30% void), Por. 0 (~ 30% void), grain size diameter between 200-400µm
Membrane module, Ultraflux AV Paed	Fresenius, Bad Homburg	Filtration and dialysis system, surface area: 0.2m ² , high cut off, average pore size <0.02µm
Cuvette	Carl Roth, Karlsruhe	Rotilabo
Pipette tips	Eppendorf, Hamburg	
Syringe filter	Carl Roth	0,45µm pore size
Cross flow mono-tubular ceramic membrane	Atech Innovation GmbH	Poresize: 100nm, inner diameter: 16mm, outer diameter: 25.4mm, 20kD molecular weight cut-off

6.3. Chemicals

Table 6: Table of chemicals used

Chemical name	Chemical Formula/ description	Manufacturer/ source
Lignin sulfonate	Bleaching effluent from paper waste water	Sappi-Ehingen AG
Zinc Oxide	ZnO(5 m ² /g)	Sigma Aldrich-Germany
chloroplatinic acid hydrate	H ₂ PtCl ₆ .6H ₂ O	Sigma Aldich(99.999%)
Titanium (IV) oxide sulfate dehydrate	TiOSO ₄ .2H ₂ O	Alfa Aesar
Tetraethylortosilicate (TEOS)	SiO ₄ (C ₂ H ₅) ₄	Merck
polyethylene glycol	Aldrich	(average Mn 300)
Titanium tetraisoproxide	C ₁₂ H ₂₈ O ₄ Ti	Sigma Aldich (97%)
Titanium dioxide - P25	TiO ₂ P25. Aeroxide [®] , surface area 50m ² /g and average particle size 30nm. 70% anatas and 30% rutil	Evonik-Hanau
Methylene blue	C ₁₆ H ₁₈ N ₃ SCl	Merck
Ammonium monovanadate	NH ₄ VO ₃	Merck
Ammonia solution	NH ₃	Merck
Ammonium carbonate	NH ₄ CO ₃	Merck
Iron nitrate	Fe(NO ₃) ₃	Merck
Cerium oxide	CeO ₂	Sigma Aldich
Cerium sulphate	CeSO ₄	Sigma Aldich
Samarium(III)nitrate hexahydrate	Sm(NO ₃) ₃ .6H ₂ O	Sigma Aldich
Selenium oxide	SeO ₂	Sigma Aldich
Gadolinium (III)nitrate hexahydrate	Gd(NO ₃) ₃ .6H ₂ O	Sigma Aldich
Ytrium nitrate hexahydrate	Y(NO ₃) ₃ .6H ₂ O	Sigma Aldich
Vanadium (V) oxide	V ₂ O ₅	Sigma Aldich

Chemical name	Chemical Formula/ description	Manufacturer/ source
Iron (III) oxide	Fe ₂ O ₃	Sigma Aldich
Cobalt oxide	Co(II)O	Sigma Aldich
Chromium (VI) oxide	CrO ₃	Sigma Aldich
Chloroform	CHCL ₃	Merck
Methanol	CH ₃ OH	Merck, Darmstadt, 99,8% HPLC grade
Ethanol	CH ₃ CH ₂ OH	Merck
Ethylacetate	C ₄ H ₈ O ₂	Merck
Hexane	C ₆ H ₁₄	Merck
Hydrochloric acid	HCL	Merck, 37%
Biphenyl-4-ol	C ₁₂ H ₁₀ O	Merck, Hohenbrunn, 98%
Iron (III) chloride	FeCl ₃	Sigma Aldich
Diphenylmethan	C ₁₃ H ₁₂	Alfa Aesar, Karlsruhe, 99%
Diphenylether	C ₁₂ H ₁₀ O	Alfa Aesar, Karlsruhe, 98%
Eugenol	C ₁₀ H ₁₂ O ₂	Alfa Aesar, Karlsruhe, 98%
4-Methoxy-biphenyl	C ₁₀ H ₁₂ O	Alfa Aesar, Karlsruhe, 98%
Phthalan	C ₈ H ₁₀ O	Alfa Aesar, Karlsruhe, 98%
Benzylphenylether	C ₁₃ H ₁₁ O	Alfa Aesar, Karlsruhe, 97%
Benzol	C ₆ H ₆	Sigma Aldich
Tyrosin	C ₉ H ₁₁ NO ₃	Merck
Siringaldehyde	C ₉ H ₁₀ O ₄	Alfa Aesar, Karlsruhe, 98%
Maleic acid	C ₄ H ₄ O ₄	Merck, Hohenbrunn, 99%
4-Hydroxybenzoic acid	C ₇ H ₆ O ₃	Merck, Hohenbrunn, 99%
Vanillic acid	C ₈ H ₈ O ₄	Merck
4-Hydroxy-3-methoxy cinnamaldehyde	C ₁₀ H ₁₀ O ₃	Sigma Aldrich, Steinheim, 98%
4-Hydroxy-3,5- dimethoxybenzoic acid	C ₉ H ₁₀ O ₅	Merck, Hohenbrunn, 99%
Coumaric acid	C ₉ H ₈ O ₃	Sigma Aldrich, Steinheim, 98%
Phenol	C ₆ H ₆ O	Merck, Hohenbrunn, 96%
Vanillin	C ₈ H ₈ O ₃	Sigma Aldrich

Chemical name	Chemical Formula/ description	Manufacturer/ source
Sinapyl alcohol	$C_{11}H_{14}O_4$	Sigma Aldrich
O/M/P Cresol	$C_7H_8O_2$	Merck
Toluene	C_7H_8	Merck
Tert-butylphenol	$C_{10}H_{14}O$	Sigma Aldrich, 99%
Potassiumdihydrogen phosphate dihydrate	$KH_2PO_4 \cdot 2H_2O$	Merck
Potassium hydrogen phosphate	$KHPO_4$	Merck
Ammonium carbonate	NH_4CO_3	Merck
Ammonium bicarbonate	NH_4HCO_3	Merck
Formic acid	CH_2O_2	Fluka, Steinheim, 98%, MS- grade
Acetonitrile	C_2H_3N	Merck, Darmstadt, 99,9%, LC grade

7. Analytical methods

Analytical techniques reported in this work are: UV-Vis spectroscopy, high performance liquid chromatography (HPLC), gas chromatography (GC), dissolved carbon (DC) and scanning electron microscopy (SEM).

7.1. UV-Visible spectroscopy

The concentration of lignin in the reaction mixture was determined by correlating absorbance of an aliquot solution to the calibration curve of lignin at different concentrations. This was done using an UV-visible (Thermo-Scientific Genesys 10S) spectrophotometer (at 203nm and 280nm) with deionized water as reference. The percentage degradation was calculated as follows:

$$\text{Degradation (\%)} = \left(\frac{C_0 - C}{C_0} \right) \times 100 \dots\dots\dots(1)$$

C_0 is the initial concentration of lignin and C is the concentration of lignin after photo-irradiation. The photocatalytic decomposition of the organic molecules follows the Langmuir-Hinshelwood kinetics, which may be represented as [37; 97]:

$$\frac{-dC}{dt} = -kCC_{OH} \cdot \dots\dots\dots(2)$$

C is the concentration of lignin and C_{OH} the hydroxyl radical concentration. It is assumed that the hydroxyl ion produced during the reaction is consumed and its concentration in reaction is far less than that of lignin in reaction. By this assumption, the rate would depend only on the lignin concentration (pseudo-stationary hypothesis) [98]. The rate expression can thus be written as follows:

$$-\ln\left(\frac{C}{C_0}\right) = kt \dots\dots\dots(3)$$

The linear plot of $\ln(C/C_0)$ versus t gives the rate constant, k (slope).

7.2. High performance liquid chromatography (HPLC, HP1090)

Column type: Hypersil BDS C18 Column, length 250mm, Inside diameter: 4.0mm. Particle size: 5µm Flow: 0.8mL/min, mobile phase gradient, 0.01M KH₂PO₄ 95% and 5% methanol - 70% methanol: 0-50min, 70% methanol: 50min-70min, mobile phase (eluent) degassed in helium, column temperature: 50°C, injection volume: 25µL, draw speed 83µL /min. Diode array detection (DAD) wavelength: 240nm, 260nm, 280nm.

7.3. Programmable fluorescence detector attached to HPLC (HP1040A)

FLD Signal: Pmt gain 13

Emission wavelength: 240nm. Excitation wavelength: 330nm

7.4. Gas chromatography (GC)

Column type: WCOT fused silica, stationary phase: CP-Sil 5CB, column length: 10m, inside diameter: 0.53mm, outside diameter: 0.70mm, film thickness: 5.0µm.

Temperature program: initial temp: 50°C, initial time: 3min, final temperature: 270°C, rate: 6°C/min, final time: 5min, pressure: 9.0Kpa; flow: 5.2mL/min, velocity: (40.7cm/sec), split flow: 5.2mL/min, split ratio: 1.00:1.

8. Experimental

8.1. Description of reaction systems

Three experimental procedures were implemented for the reactions. In the first one, lignin sulfonate solution was pumped through the reactor using roller pumps in a continuous manner with a flow rate of 22.5mL/min. Samples were collected at intervals or at the end of the reaction. Figure 13 depicts this reaction procedure.

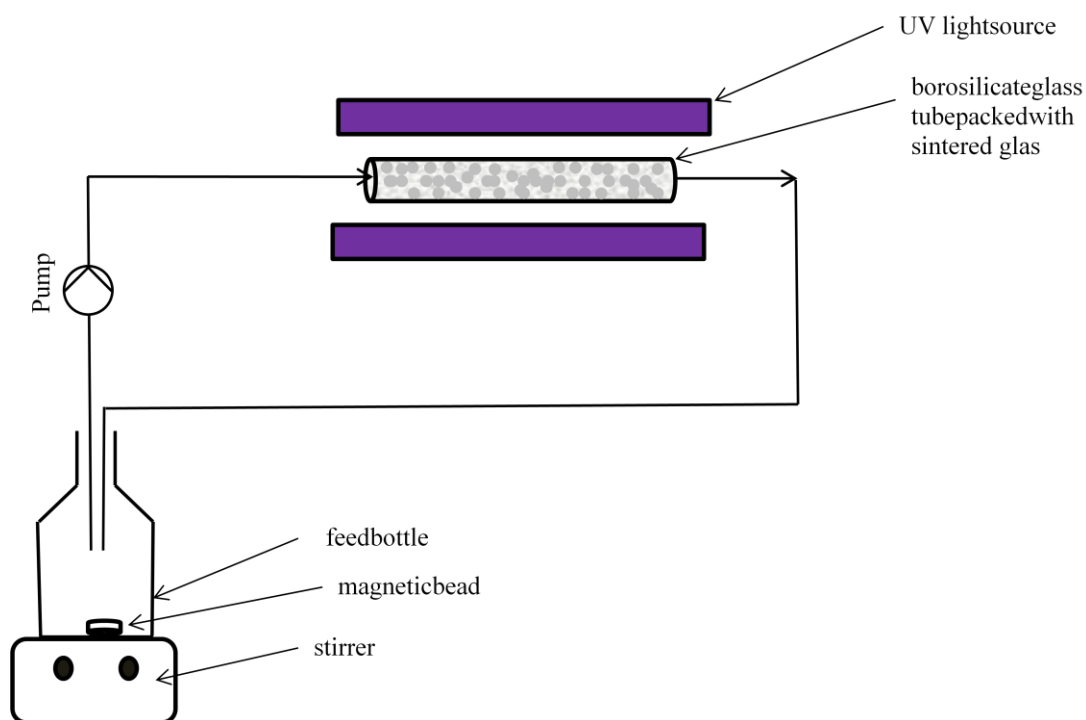


Figure 13: Experimental setup for the photocatalytic degradation of lignin sulfonate.

The second procedure involved a reaction-extraction pathway in which solid phase extraction (SPE) followed after reaction. SPE was carried out with highly porous polystyrene divinylbenzene adsorbent resin (HRP). In the third procedure, the reactor was connected to a dialysis filter fitted with a HRP extraction column which ran in a cycle process. This is depicted in Figure 14. This was aimed to directly extract smaller molecules produced and preferably aromatic and phenol like compounds from the aqueous medium.

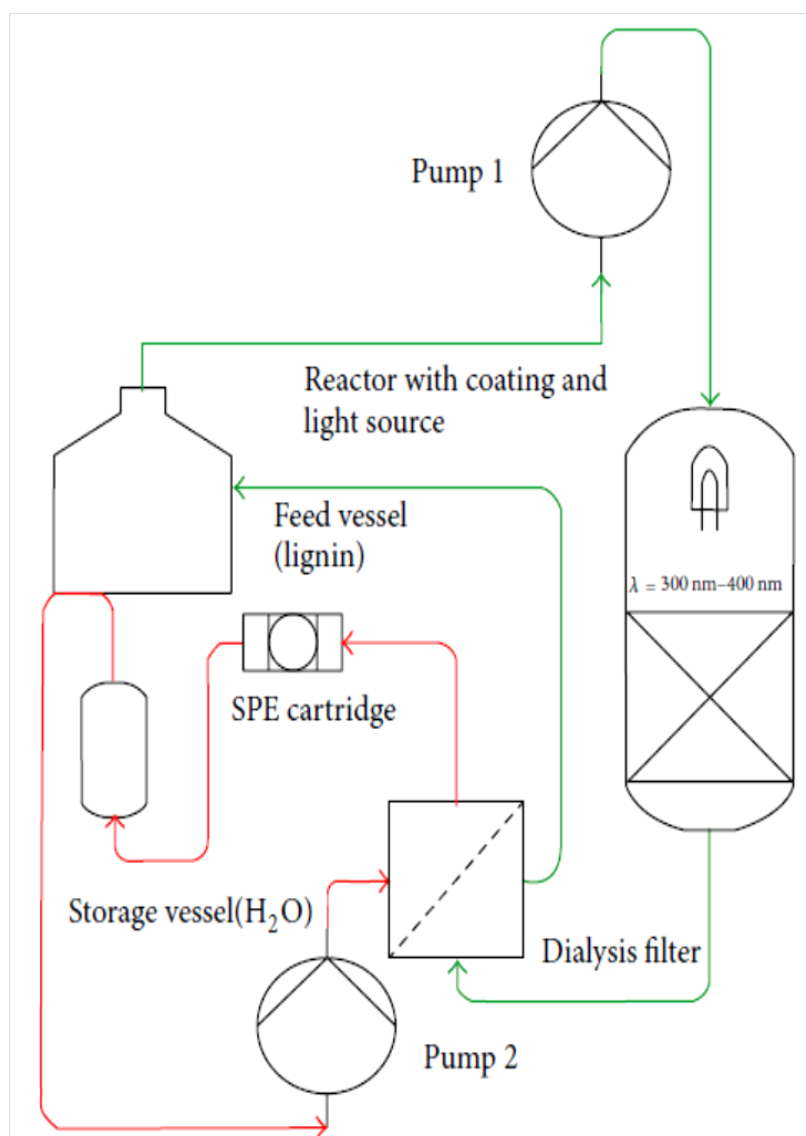


Figure 14: Photocatalytic cycle process with integrated solid phase extraction and dialysis membrane

8.2. Reactor characterization

The reaction design consisted of TiO₂ coatings on sintered glass (150-250 μm nominal pore size), packed in a borosilicate tube 26 cm long, 1 cm outer diameter and 6 mm internal diameter. Glass particle grain size was between 200-400 μm. The tube was placed between two planar dielectric barrier discharge lamps (Osram planon) emitting UV-light at wavelength between 280-420 nm. This construction enabled the incident light from the broad surface-light source to be evenly distributed all over the surface of the glass tubes. Figure 15 illustrates the photocatalytic reactor.

8.2.1. Brunauer-Emmett-Teller (BET) surface area

The BET specific surface area of a borosilicate tube containing the sintered glass particle before coating was $0.015\text{m}^2/\text{g}$ (from manufacturer product data sheet attached at appendix: Figure 50). This gives an estimation of 0.17m^2 for 11.5g of sintered glass particles contained in the borosilicate glass tube.

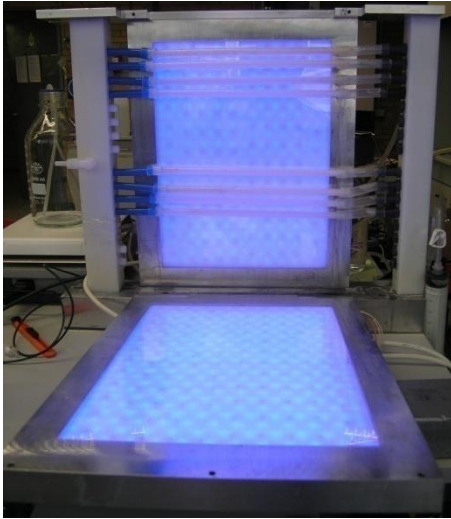


Figure 15: Photocatalytic reactor

8.2.2. Flow measurements

For fluid flow through a bed of approximately spherical particles, the Reynolds number (Re) used to characterize laminar or turbulent flow regimes is defined as follow [99]:

$$\text{Re} = \frac{\rho V D}{\mu(1-\varepsilon)} \dots\dots\dots(6)$$

Where ρ is the density of lignin sulfonate solution (kg/m^3), μ is the dynamic viscosity of $0.5\text{g}/\text{L}$ lignin sulfonate solution ($\text{Pa}\cdot\text{s}$), ε is the voidage and V is the superficial velocity (m/s).The voidage was calculated from the correlation equation of packed beds [100].

$$\varepsilon = 0.293 + (0.684) dr^{-0.85} \cdot \frac{1}{(1,837 dr - 1)^{0.5}} \dots\dots\dots(7)$$

Where $dr = \frac{dt}{dp}$, dt is internal diameter of tube (6mm) and dp is diameter of particle (0.3mm).

The particle must be spherical and $dr > 1.86$ [100].

The superficial velocity V was calculated from:

$$V = \frac{\text{Volume flow rate}}{\text{cross sectional area of tube}} \dots\dots\dots(8)$$

8.2.2.1. Results of flow measurements

It is assumed that the packed bed reactor design had a good distribution of the flow over the diameter of the tube. For packed bed reactors, laminar conditions apply when $Re < 2000$ and fully turbulent when $Re > 2000$ [99]. Using equation 6, a value of 56 was obtained which characterizes a laminar flow. Table 7 outlines the values used to characterize the flow type of reactor.

$R_{i,tube}$	$A_{tube}[m^2]$	ρ_{lignin} [kg/m ³]	V_{lignin} [m/s]	$D_{particles}[\mu m]$	μ_{lignin} [kg/(m•s)]	$\varepsilon(\text{voidage})$	Re
0.30cm	2.83×10^{-5}	1000	0.013	300	1×10^{-4}	0.30	56

Table 7: Parameters for flow characterization in the photocatalytic reactor.

8.3. Photonic efficiency of reactor

For quantification and classification of a photocatalytic process, parameters such as quantum yield and photonic efficiency are necessary in order to improve the engineering applications of photocatalytic technologies. In this work, because of the undefined molar mass of lignin sulfonate which is needed to calculate the reaction rate in mol/L.s, methylene blue (MB) was chosen as test substance and its rate expression was used. MB has a known molar mass and has been described in some publications [101; 102; 97].

The photonic efficiency (ξ) was calculated as follows:

$$\xi = \frac{d[c]/dt}{I^0} \dots\dots\dots(9)$$

Where $d[c]/dt$ is the reaction rate extrapolated from MB degradation profile with units mol/(L•s)

I^0 is the incident photon flow determined by UV-A radiometric measurements with units Einstein•mol/(L•s)

A photon has a distinct energy quanta E_p which is defined by:

$$E_p = h \cdot f = h \cdot \left(\frac{c}{\lambda}\right) \dots\dots\dots(10)$$

With Planck's constant: $h=6.63 \times 10^{-34}$ [Js]; speed of light, $c=2.998 \times 10^8$ [m/s]; frequency, f [1/s]; wavelength (λ) in [m].

The number of photons N_p can be calculated by:

$$N_p = \frac{E}{E_p} = \frac{E(\lambda \times 10^{-9})}{(h \cdot c)} \dots\dots\dots(11)$$

E is the irradiance with units $[W/m^2]$, λ is the wavelength in $[m]$ and $h \cdot c = 1.988 \times 10^{-25} J \cdot m$

N_p can be expressed as follows:

$$N_p = E \cdot \lambda \cdot (5.03 \times 10^{15}) [1/(m^2 \cdot s)] \dots\dots\dots(12)$$

The photon flux I^0 can be determined by:

$$I^0 = \frac{N_p}{N_A}$$

with Avogadro number, $N_A = 6.022 \times 10^{23} \text{mol}^{-1}$

$$I^0 = \frac{E \cdot \lambda \cdot (5.03 \times 10^{15}) [1/(m^2 \cdot s)]}{6.022 \times 10^{23} [1/mol]} \dots\dots\dots(13)$$

$$I^0 = E \cdot \lambda \cdot (0.83 \times 10^{-8}) [mol / (m^2 \cdot s)] \dots\dots\dots(14)$$

$$I^0 = E \cdot \lambda \cdot (0.83 \times 10^{-2}) [\mu mol / (m^2 \cdot s)] \dots\dots\dots(15)$$

The calculated values of the photonic efficiencies (ξ) (Table 8) was averaged on the wavelength spectrum (360nm) of the lamp emission centered in the range 280-420nm. The irradiance (E) of the reactor, determined from radiometric measurements was between 30-40W/m². The irradiance was averaged at 34W/m² from 20 data points.

Table 8: Data obtained for the calculation of photonic efficiency (rate of degradation to incident photonic flux) of the different catalyst with MB as substrate.

Photocatalyst	Photon flux (I^0) [mol/(m ² •s)] or [Einstein•mol/(L•s)]	Reaction rate [mg/(L•min)]	Reaction rate [mol/L•s]	photonic efficiency (ξ) [mol /Einstein]	photonic efficiency [%]
TiOSO ₄ _30.6 wt. %	1.03x10 ⁻⁴	0,05	2.61x10 ⁻⁹	2.54x10 ⁻⁵	0.003
TiO ₂ -P25-SiO ₂	1.03x10 ⁻⁴	0,0215	1.12x10 ⁻⁹	1.09x10 ⁻⁵	0.001
TiO ₂ -P25-SiO ₂ +Pt	1.03x10 ⁻⁴	0,0236	1.23x10 ⁻⁹	1.2x10 ⁻⁵	0.001
TiOSO ₄ _30.6wt.%+ZnO	1.03x10 ⁻⁴	0,0178	9.27x10 ⁻¹⁰	9.1x10 ⁻⁵	0.001

8.4. Discussion

Determining photonic efficiency mathematically (radiometry) from lignin degradation experiments poses a major challenge because of the undefined molar mass of lignin. The values of photonic efficiency resulting from this study (concentration of MB is 14mg/L with a reaction volume of 200mL) are relatively low compared to that found in literature. For example, Hidalgo et al. [103; 104] reported photonic efficiency of 4% while using 3mg/L glucose dissolved in water and TiO₂ catalyst derived from tinanyloxysulphate (TiOSO₄). The reason for such low values may be attributed to the following:

- The surface area of the catalyst: the catalytic coating used in this study was same to that described by Hidalgo et al.[103; 104] in which photonic efficiency as much as 4% was attained. However just one tube containing coated sintered glass particles was used in this study in comparison to eight tubes applied by Hidalgo et al. [103; 104]. One tube was used because of the high adsorption of MB on the coatings.
- In this study a concentration of 14mg/L with a reaction volume of 200mL is applied compared to just 3mg/L (200mL) described by Hidalgo et al. [103; 104].
- The nature of the substrate: unlike glucose which is linked by single C-C bonds (bond strength of 347 kJ/mol), methylene blue or lignin contains aromatic rings made up of conjugated (carbon carbon) bonds with bond strength 518kJ/mol. Double bonds (C=C) have bond strength of 636 kJ/mol [105]. So it is expected that compounds such as glucose degrade faster compared to MB for example.
- Catalyst-substrate interaction: MB showed strong adsorption unto the catalytic coatings probably because of its cationic nature [73]. So, a proper choice has to be made which data points are to be considered for graphical extrapolation. In this work, an adsorption equilibrium time for MB experiments was determined experimentally to be 1h. Reaction rates are usually considered at the beginning of photocatalytic reaction processes because of the slow nature of reactions which is rate determining [52]. In this step, processes such as absorption of photons of light by catalyst, production of electrons and other oxidizing species amongst other take place before a faster reaction takes place [106]. Moreover at the beginning of a photocatalytic reaction there is less influence of side products and subsequent degradation of formed species.
- Light intensity: the irradiance (E) of the reactor was determined by radiometric measurements ranging between 30-40W/m². This means irradiance and consequently

photonic efficiency depended on which spot of the reactor the UVA/B-meter (pointer) was placed. In this study, an average at 34W/m^2 was determined from 20 data points.

- Range of UV-light emission: the photocatalytic reactor emitted UV-light in the range 280-420nm. This means irradiance and consequently photonic efficiency calculations depended on which wavelength was chosen. In this study, the calculated value of the photonic efficiencies (ξ) was done with a wavelength averaged at 360nm.

8.5. Conclusion

For the circulating packed bed reactor laminar flow conditions apply with Reynolds number 56. Determining photonic efficiency from lignin degradation experiments through radiometric calculations poses a major challenge because of the undefined molar mass of lignin.

The photonic efficiency of a catalyst depends strongly on the type and concentration of substrate. Other factors include the rate of electron transfer, the rate of charge recombination, crystal structure, surface area of catalyst, porosity and surface hydroxyl group density [11].

9. Catalyst preparation and characterization

9.1. Introduction

Catalyst synthesis in this study was via the sol-gel route. Sol-gel route is a wet-chemical process which offers advantages such simplicity in the synthesis of sols, homogeneity of coatings and ability to deposit coatings on larger and odd shaped substrates. Furthermore, a simple modification of the film composition can be performed directly in the sol-gel process.

Table 9 shows the catalytic coatings prepared listed in different categories. This shall be discussed below.

9.2. Categories of catalytic coatings, mode of catalyst selection

The coatings consisted of either of titania, silica or zinc on sintered borosilicate glass. The categories are divided based on precursor type and additive used for catalyst synthesis as follows: category 1: Tinanyloxysulphate (TiOSO_4) as precursor, category 2: Titanium isopropoxide (TTIP) as precursor, category 3: zinc oxide (ZnO) catalyst, category 4: TiO_2 -P25 (aeroxide, TiO_2 , Evonik Industries) based catalyst, category 5: TiO_2 doped with transition metals, category 6: TiO_2 modified with lanthanides and actinides, category 7: TiO_2 surface modification with PEG and SiO_2 , and category 8: TiO_2 modified with nitrogen.

Category 1 describes tinanyloxysulphate (TiOSO_4) as precursor. TiOSO_4 precursor used in this study had been reported by Hidalgo [104; 103] to yield high photonic efficiency between 4-7%. Such a value is uncommon for heterogeneous photocatalysis and this was worth testing. Photonic efficiency values commonly found in literature are below 1% and it is one of the main setbacks for heterogeneous photocatalysis. Titanium isopropoxide (TTIP) has so far not been described in literature in connection to lignin degradation experiments. From the alkoxide process, photochemical active TiO_2 catalyst can be derived [11; 77].

ZnO has been described to absorb over a large fraction of the electromagnetic spectrum [64; 76] which renders its applicability to visible light sources whereas TiO_2 is mostly applied in connection to UV-light sources as highlighted in Table 2 and as explained in chapter 4.2.1. Moreover, the advantage of sol-gel in catalyst preparation was exploited to combine catalysts to act as co-catalyst. For example, TiO_2 -P25+ SiO_2 / ZnO; TiOSO_4 _30.6wt% / ZnO and TiO_2 -P25+ SiO_2 / TiOSO_4 _30.6wt%.

Category 4 and category 9 present TiO_2 -P25 based catalyst mostly applied in suspension systems. From the results of Addamo et al. [77], high adhesion of TiO_2 -P25 on glass support material was noted when pre-coating was done with SiO_2 . Furthermore SiO_2 is beneficial

because it hinders possible diffusion of Na^+ ions from the glass material into the nascent TiO_2 film during the heat treatment process [77].

Analogous to the addition of SiO_2 , polyethyleneglycol (PEG) was introduced to influence catalyst surface activity (category 7). PEG being unpolar in nature was introduced to modify surface hydrophobicity and also limit the agglomeration tendency of the TiO_2 gel or TiO_2 particles in the suspensions. Also, surface modifications can enhance interaction between catalyst and substrate [78]. It was therefore worth testing such a system with TiOSO_4 as precursor for TiO_2 catalyst. Nitrogen addition as dopant was aimed to mitigate intra band gap states [11] and this was tested by the addition of NH_3 and NH_4VO_3 to TiO_2 catalyst (category 8). In addition, metal ions as dopants (e.g. Fe, Co) were mixed to the gels of TiO_2 catalyst (category 5).

Category 1	Category 3	Category 5	Category 6	Category 7	Category 8
12.6wt.%_TiOSO ₄	ZnO + P25-TiO ₂	TiOSO ₄ + 1%_Cr(VI)O	TiOSO ₄ + 1%_CeSO ₄	TiOSO ₄ +PEG	TiOSO ₄ + (NH ₄) ₂ CO ₃
30.6 wt.%_TiOSO ₄	ZnO + TiOSO ₄	TiOSO ₄ + 1%_Fe ₂ O ₃	TiOSO ₄ + 1%_Sm(NO ₃) ₃	TiO ₂ -P25+SiO ₂	TiOSO ₄ + NH ₃
	ZnO-SiO ₂	TiOSO ₄ +V ₂ O ₅	TiOSO ₄ + CeO ₂	TiO ₂ P25+SiO ₂ +Pt	TiOSO ₄ + NH ₄ VO ₃
Category 2	Category 4	TiOSO ₄ + 1%_Co(II)O	TiOSO ₄ + 1%_SeO ₂	ZnO + TiO ₂ -P25	Category 9
TTIP	TiO ₂ -P25+SiO ₂	TTIP+Fe	TiOSO ₄ + 1%_Gd(NO ₃) ₃	ZnO + TiOSO ₄	ZnO + TiOSO ₄
TTIP+Pt	TiO ₂ -P25+SiO ₂ +Pt	TiOSO ₄ +Pt	TiOSO ₄ + 1%_Y(NO ₃) ₃	ZnO-SiO ₂	ZnO + TiO ₂ -P25
TTIP+Fe					TiOSO ₄ + TiO ₂ -P25

Table 9: Catalytic coatings divided into categories.

9.3. Catalyst synthesis

9.3.1. Preparation of TEOS solution

Tetraethylortosilicate (TEOS) sol was prepared by adding dropwise 77mL of 2-propanol mixed with 5mL of H_2O and 4mL of HNO_3 to 22mL TEOS at room temperature. The resultant solution was stirred for 2h.

9.3.2. Preparation of TiOSO_4 _30.6wt% gel

In a 200mL beaker 45.9g of TiOSO_4 (Alfa Aesar) was weighed and 104mL of water was added. The suspension was stirred till a clear solution was obtained. The solution was heated up

to 85°C while adding 5N NaOH dropwise until a pH of 5.5 was reached. The temperature was maintained for 8h under stirring. After that, the gel was washed 3 times with 75mL water each time. The gel was re-suspended in distilled water using 150mL of water and then sonicated for 6h. After sonication the gel was ready for coating.

9.3.3. Preparation of TiO₂-P25 suspension

TiO₂-P25 (aeroxide, TiO₂, Evonik Industries) suspensions were prepared by adding 8.75g TiO₂-P25 to 50mL water and sonicated for 60min. Tetraethylortosilicate (TEOS) layers were applied on the glass substrate before coating with TiO₂-P25.

9.3.4. Preparation of ZnO suspension

12g of ZnO was added to 150mL of water and stirred for 1h. In a separate beaker, nitric acid (65%) was added dropwise to 60mL TEOS solution till a pH 1.55 was reached. ZnO suspension was then mixed with TEOS by adding dropwise TEOS to ZnO suspension and stirred for 2h at room temperature.

9.3.5. Preparation of ZnO +TiO₂-P25-SiO₂suspension

TiO₂-P25 suspension was prepared by adding 5.25g TiO₂-P25 in 30mL water and sonicated for 60min. From the previously prepared ZnO/TEOS-suspension, 20mL was added to TiO₂-P25 suspension and left to mix for 2h at room temperature.

9.3.6. Preparation of TiOSO₄_30.6wt%+PEG gel

In a beaker, 7.4g of PEG-300, 45.9g of TiOSO₄ and 104mL of water were mixed together. The suspension was stirred till a clear solution was obtained. The solution was heated up to 85°C while adding 5N NaOH dropwise until a pH of 5.5 was reached. The temperature was maintained for 8h under continual stirring. Following that, the gel was washed 3 times with 75mL water each time. The gel was re-suspended in distilled water using 150mL of water and then sonicated for 6h. After sonication the gel was ready for coatings.

9.3.7. Preparation of doped TiO₂ catalyst

The amount of dopant used was 1wt% relative to TiO₂ concentration in the gel or suspension in question. The metal precursor was directly added to the gel and then stirred for 30min prior to coating. For example 86 mg of NH₄VO₃ was added in a 75mL TiO₂ gel derived from TiOSO₄_30.6wt%. Table 9 portrays catalytic coatings synthesized. Amongst the catalyst, following were prepared with the addition of a metal ion (dopant) to TiO₂: TiO₂-P25-SiO₂+Pt, TiOSO₄_30.6wt%+Pt, TTIP+Pt, TTIP+Fe, TiOSO₄_30.6wt%+NH₃, TiOSO₄_30.6wt%+NH₄VO₃, TiOSO₄_30.6wt%+(NH₄)₂CO₃, TiOSO₄_30.6wt%+Cr(IV)O, TiOSO₄_30.6wt%+Fe₂O₃, TiOSO₄_30.6wt%+V₂O₅, TiOSO₄_30.6wt%+Co(II)O, TiOSO₄_30.6wt%+CeSO₄, TiOSO₄_30.6wt%+Sm(NO₃)₃, TiOSO₄_30.6wt%+CeO₂, TiOSO₄_30.6wt%+SeO₂, TiOSO₄_30.6wt%+Gd(NO₃)₃, TiOSO₄_30.6wt%+Y(NO₃)₃.

9.3.8. Preparation of TiOSO₄_30.6wt% + TiO₂-P25 suspension

TiO₂-P25 suspensions was prepared by dissolving 3,5g TiO₂-P25 in 20mL water and sonicated for 60min. To this suspension 30mL of TiOSO₄_30.6wt% gel was added and sonicated for 1h at 25°C.

9.3.9. Preparation of TTIP gel

TiO₂ gel was prepared by mixing 36mL of titanium tetraisopropoxide (TTIP), 400mL of H₂O and 3.8mL of HNO₃ (65% w/w). The mixture was stirred for 24h at room temperature (25°C) and then left to stand for 6h (ageing time).

9.3.10. Coating procedure of TEOS on glass

TEOS was pumped through both sides of the glass tube and then left to dry at 150°C. The oven temperature was then raised to 300°C and maintained for 3h. Coating with TiO₂-P25 then followed.

9.3.11. Coating procedure of gels and suspensions on glass

The gel was pumped with use of a roller pump through each side of the glass tubes to ensure a homogeneous coating (Figure 16). This was done each time for 3min with the

pumping rate set at 10mL/min. After coating, the tubes were placed in an oven and heating rate was set at 5°C/min. When the oven attained 110°C, the tubes were left to dry for 2h. In order to carry out the calcinations step, the oven temperature was raised to 500°C with heating rate still maintained at 5°C/min. The oven temperature was maintained at 500°C for 1h. After the oven had cooled down, the tubes were removed from the oven and were now ready for photocatalytic experiments.

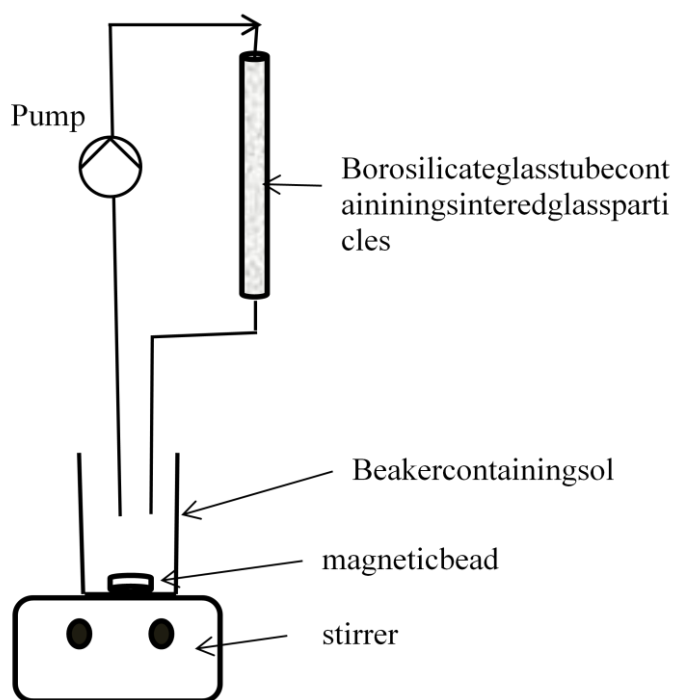
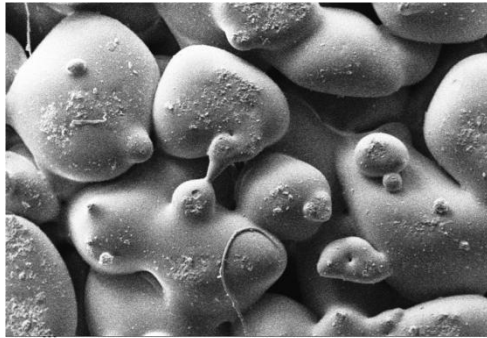


Figure 16: Catalyst coating on sintered glass via pumping of gel in a circulatory manner through borosilicate glass tube

9.4. Results and discussion

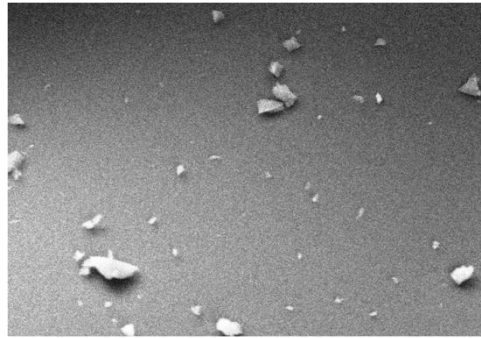
35 different coatings were synthesized. Scanning electron microscopy (SEM) and Energy dispersive spectroscopy (EDS) were done to characterize the coatings. In this chapter, SEM images shall be presented for the 3 best coatings which effectively degraded lignin. The weight of coating on the glass tubes was in the range 0.12g-0.19g.

9.4.1. Morphology of coatings



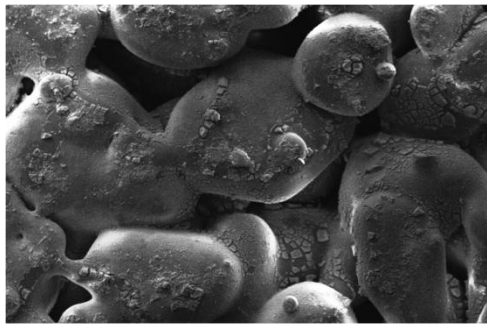
200μm

(a) 50x



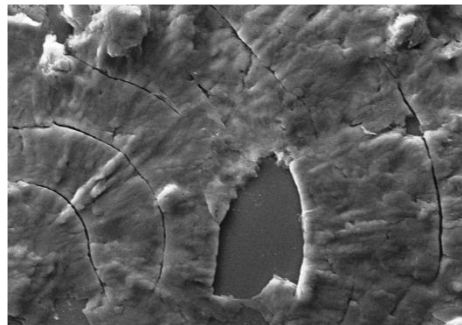
10μm

(b) 1000x



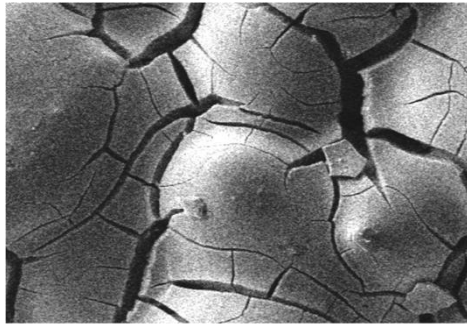
200μm

(c) 50x



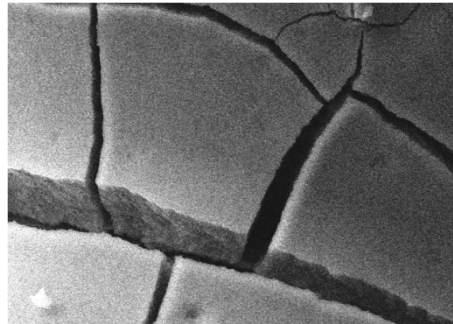
10μm

(d) 1000x



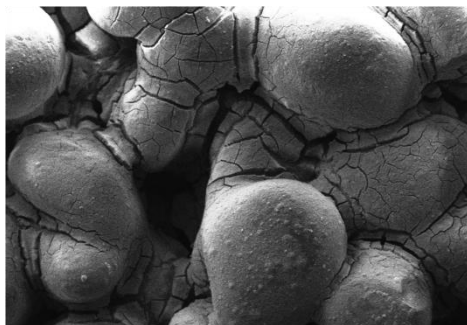
100μm

(e) 100x



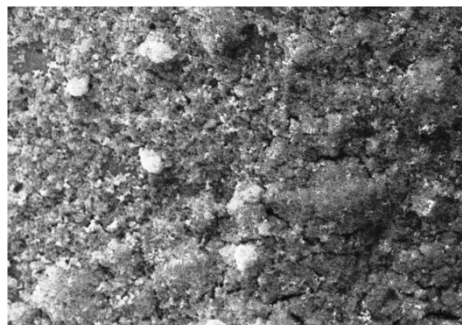
10μm

(f) 2000x



200μm

(g) 50x



10μm

(h) 1000x

Figure 17: SEM images for uncoated borosilicate sintered glass ((a) and (b)), TiO_2 (TiOSO_4 +30.6wt%) coating on borosilicate glass ((c)and (d)), TiO_2 -P25- SiO_2 ((e) and (f)), ZnO + TiO_2 -P25- SiO_2 ((g) and (h))

Scanning electron microscopy (SEM) was the primary tool for characterizing the surface morphology and fundamental physical properties of the material surface such as porosity and distribution of the coating. In Figure 17; SEM images are shown for uncoated and coated glass with different catalyst. Samples consisted of sintered glass plates cut to a size of 1cm^2 dipped into the gel or suspension. Drying and calcination were done same as was the case with borosilicate glass tubes [73]. The micrographs for the uncoated sintered glass in Figure 17(a) and Figure 17(b) show structures formed by glass particles of approx. $200\text{-}400\mu\text{m}$ in size sintered together. Figure 17c -Figure 17h shows micrographs of the coated glass material. Figure 6e and 6h consist of a double coating whereby TEOS was first coated and $\text{TiO}_2\text{-P25}$ follows. Significant agglomeration of the particles is also observed. Some fissures are also seen at joints between sintered particles and on the glass particles as a result of drying. It is worthwhile noting these micrographs originate from sintered glass plates whereby the drying mechanism could be harsher as heat radiations directly strike on them as compared to a borosilicate glass tube encasing sintered glass particles. However, the coatings were considerably well distributed all over the surface of the sintered glass.

It can be adopted that the coatings had a crystalline structure due to the thermal treatment (also known as calcination) at 500°C . It is also supposed that, the crystal phases involved both rutil and anatase since as the transformation of anatase to rutil is in the temperature range between $600\text{-}700^\circ\text{C}$ [107]. Rutil is known to be the stable phase of TiO_2 whereas anatase and brookite are metastable at all temperatures and transform to rutil when they are heated. Moreover anatase is typically the majority product of inorganic syntheses and is the main constituent of nanocrystalline materials [108]. Aeroxide[®] $\text{TiO}_2\text{-P25}$ obtained from Evonik consisted of 70% anatase and 30% rutil.

9.5. Conclusion

The advantage of sol-gel in catalyst preparation was exploited to combine catalyst to act as co-catalyst. Commercial obtainable $\text{TiO}_2\text{-P25}$ widely applied in suspension systems was effectively immobilized on sintered glass support with the aid of tetraethylortosilicate (TEOS) solution which acted as support material. The catalytic films had very good adherence on the sintered glass and the films retained a constant efficiency when re used after washing with water. The coatings were considerably well distributed all over the surface of the sintered glass. This is very promising for their potential use as immobilized catalyst in batch or flow reactors.

10. Evaluation of photocatalytic active coating by methylene blue

10.1. Introduction

Prior to lignin degradation experiments, a comparative quality test was done with methylene blue (MB) as substrate with 35 different coatings obtained via sol-gel route described in the preceding chapter. The aim of comparing the catalysts was to select the most active catalysts and test their activity with the more robust and recalcitrant lignin sulfonate from paper waste water. Ten coatings out of 35 coatings synthesized could effectively degrade MB. A comparative study of the effectiveness and photocatalytic activity of these coatings shall be the subject of this chapter.

MB was used as model dye because of its heteroatomic chemical nature consisting of C, H, N and S. Secondly, MB is widely used as colorants and there is a change in colour when it degrades over time. Thirdly, MB has a defined molar mass and has been well characterized in literature to test the efficiency of coatings by degradation experiments [101; 102; 97]. Fourthly, methylene blue is a dye substance that the chemical and textile industry face the challenge to adequately dispose it from waste water. This means, this work presents a reaction design which can remediate the pollution problem (e.g. chemicals and colored waste water in the ecosystem that poison and damage aquatic life) in waste water discharged from pulp and paper mills on the one hand and on the other hand, proposes a catalyst system which can be used for lignin sulfonate degradation.

The most frequently used approaches to treat waste water are physicochemical methods such as adsorption [109], chemical methods such as chlorination, ozonation [110] and biological methods [111]. However with the use of heterogeneous catalytical systems as that developed in this study, advantages such as catalyst re-use, minimization of catalyst leaching or resistance to extreme physical and chemical conditions are exploited.

This chapter starts with an overview of the degradation pathway of MB followed by results achieved from the comparative degradation study with different catalyst.

10.2. Degradation pathway of MB

Figure 18 depicts the heteroatomic chemical structure of MB consisting of C, H, N and S atoms. Houas [97] reports the degradation pathway of MB as follows:

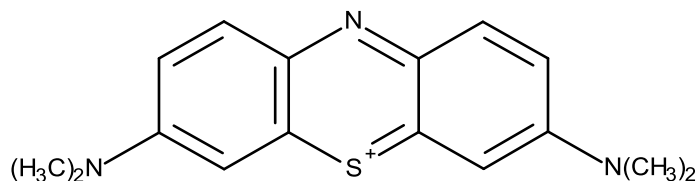


Figure 18: The chemical structure of methylene blue (drawn with symyx draw).

- MB degradation begins with cleavage of C-S⁺=C functional group via a columbic interaction between C-S⁺=C functional group and basic TiO₂ [101].
- Opening of the central aromatic ring containing both heteroatoms, S and N. The origin of H atoms necessary to C-H and N-H bond formation can be gained from the proton reduction by photogenerated electrons [102], [112].
- Formation of a sulfoxide, a sulfone and a sulfonic group as observed in Fenamiphos degradation [101].
- The sulfoxide group can undergo a second attack by an OH• radical producing the sulfone (non-detected) and causing the definitive dissociation of the two benzene rings. The sulfone can be attacked by OH• giving sulfonic acid.
- Radical R-C₆H₄• can subsequently react with OH• giving phenolic compounds [102].
- Progressive degradation by OH• attacking dimethyl-phenyl-amino groups, aldehydes which decarboxylate into CO₂.

Conclusively, the degradation leads to the conversion of organic carbon into harmless gaseous CO₂ and that of nitrogen and sulfur heteroatoms into inorganic ions, such as nitrate and ammonium, and sulfate ions, respectively [97].

10.3. Photocatalytic experiments

The photocatalytic activity of the coatings was tested by the photooxidation of methylene blue dissolved in water at a concentration of 14 mg/L in 200mL as feed volume. The reaction procedure involved MB pumped through the reactor using roller pumps in a continuous manner with a volume flow rate of 22.5mL/min and Reynolds number (Re) of 56. The BET specific surface area before coating of a borosilicate tube containing the sintered glass particle was 0.015m²/g (from manufacturer product data sheet attached at appendix (Figure 50)). This gives

an estimation of 0.17 m^2 for 11.5g of sintered glass particles contained in the borosilicate glass tube.

Samples were collected at intervals up till a period of 4h reaction time. Figure 13 depicts this reaction procedure in which the borosilicate glass tubes containing coated sintered glass particles tube was placed between two planar dielectric barrier discharge lamps (Osram planon) emitting UV-light of wavelength around 280-420nm.

Reactions were carried out at room temperature. Blank experiments were performed in the absence of UV light illumination as well as with uncoated sintered glass plates. The concentration of methylene blue in the reaction mixture was measured at regular intervals by measuring the absorbance of an aliquot solution. This was done using a UV-visible (Thermo-Scientific Genesys 10S) spectrophotometer (at 665nm) with deionized water as reference. A Beer-Lambert diagram was established to correlate the absorbance at 665nm to MB concentration. The percentage degradation was calculated using equations (1). Equations (2) and Equations (3) are the rate expression used. The linear plot of $\ln(C/C_0)$ versus t gives the rate constant, k (slope).

10.4. Results

Absorption maxima appear at wavelength 291nm and 665nm in the UV-Vis spectrum. An example of such a spectrum is represented in Figure 19. The coating consisted of TiOSO_4 _30.6wt% under photocatalysis of MB for a period of 4h. The samples were collected at intervals; (-60, -15, 0, 30, 60, 90, 120, 150, 180) min. Minus (-) 60 and 15min means that, a sample was collected 60min and 15min before the UV-light was put on. This was to ensure that the adsorbance equilibrium between catalyst and substrate has been reached and that the photo reaction starts when UV lights switched on. Absorption in the visible range at 665nm was chosen to study MB degradation.

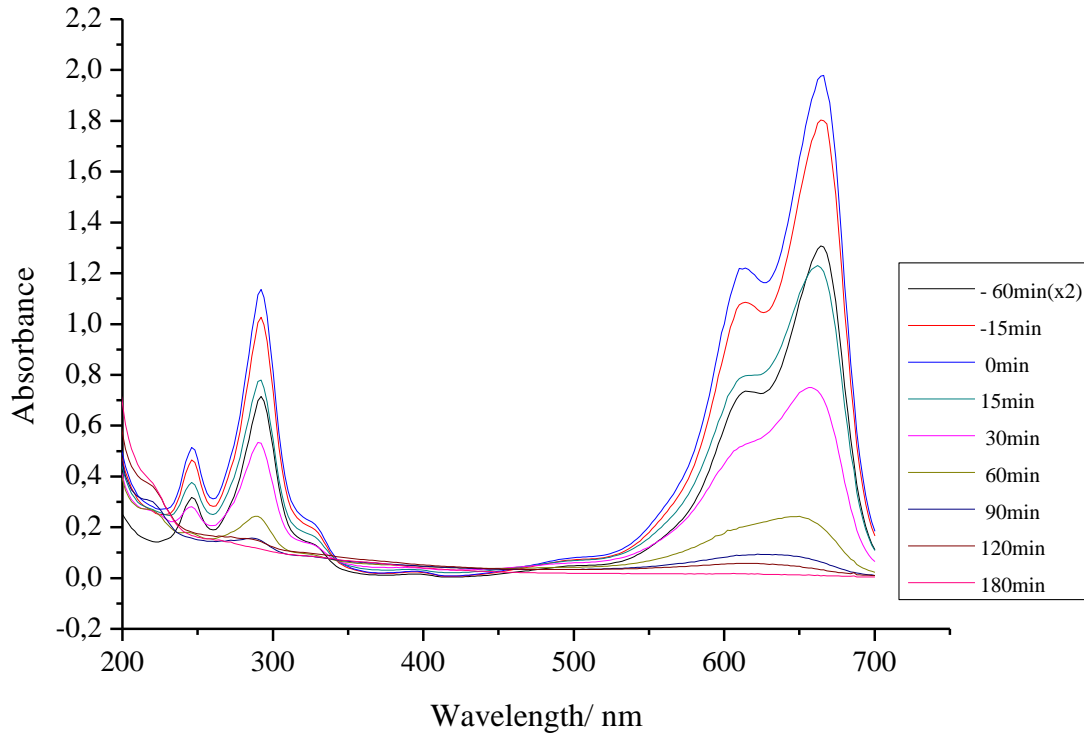


Figure 19: Typical time dependent UV-Vis absorption spectra of aqueous MB solution irradiated with UV light (280-420nm) for different time intervals. The spectrum is obtained for sol-gel derived TiO_2 from titanyloxysulphate

Figure 20 shows an absorbance –time diagram of MB. The reaction was performed in the dark with uncoated sintered glass. No significant adsorption is noted. With the presence of TiO_2 coating, one notes a very strong adsorption till approx. 60min suggesting adsorption equilibrium is attained after 60min recirculation in the dark (Figure 21). For all experiments, MB was hence recirculated through the reactor for 60min before UV light was put on. The adsorption mechanism is a result of columbic interaction between MB which has a cationic configuration and OH^- ions present on the surface of TiO_2 nanocrystallites [97]. The time dependent UV-Vis absorption spectra of aqueous MB shows a decrease in absorbance for peaks at 665nm and 291nm as MB blue degrades (Figure 19). A shoulder at around 665nm was observed. Other peak formation was noted at wavelengths 220nm and 240nm. This suggested the formation of intermediate products. Absorbance for both the intermediate peak and parent MB peak reduced with time and after 3h no peaks were observed indicating destruction of MB dye and intermediate products.

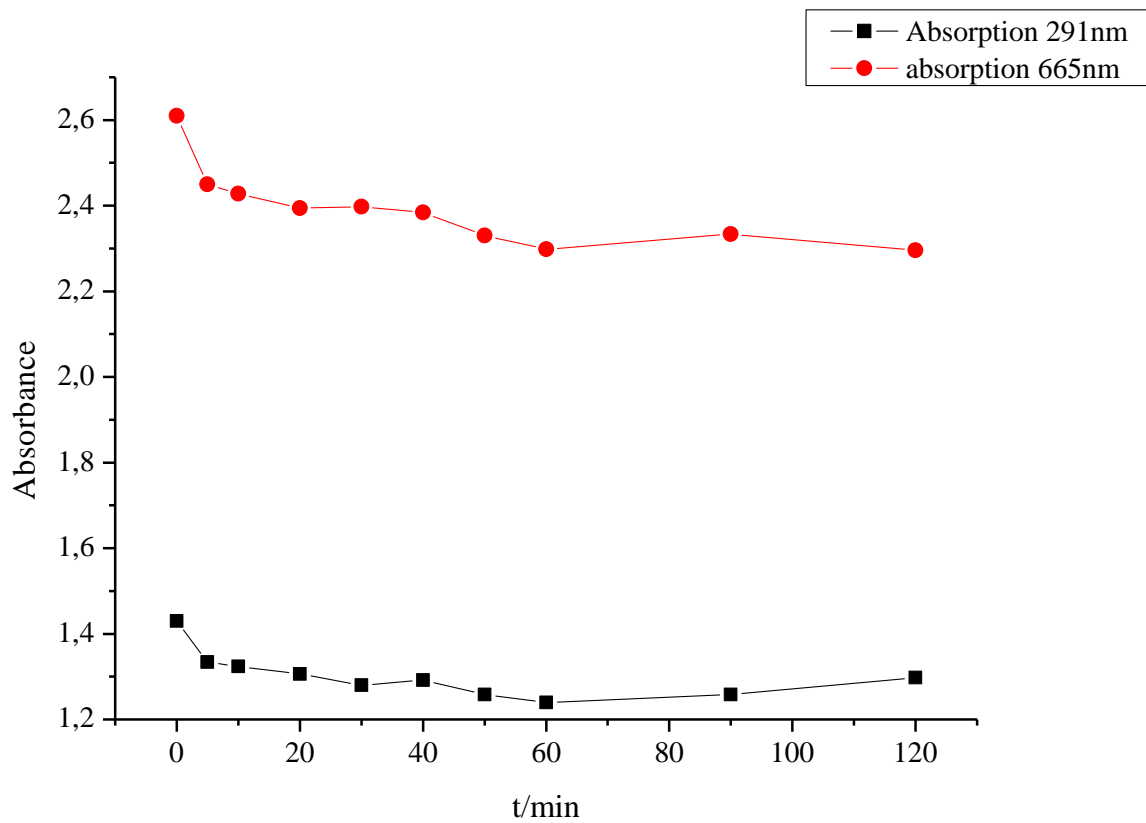


Figure 20: Absorption-time diagram, uncoated glass and no lights

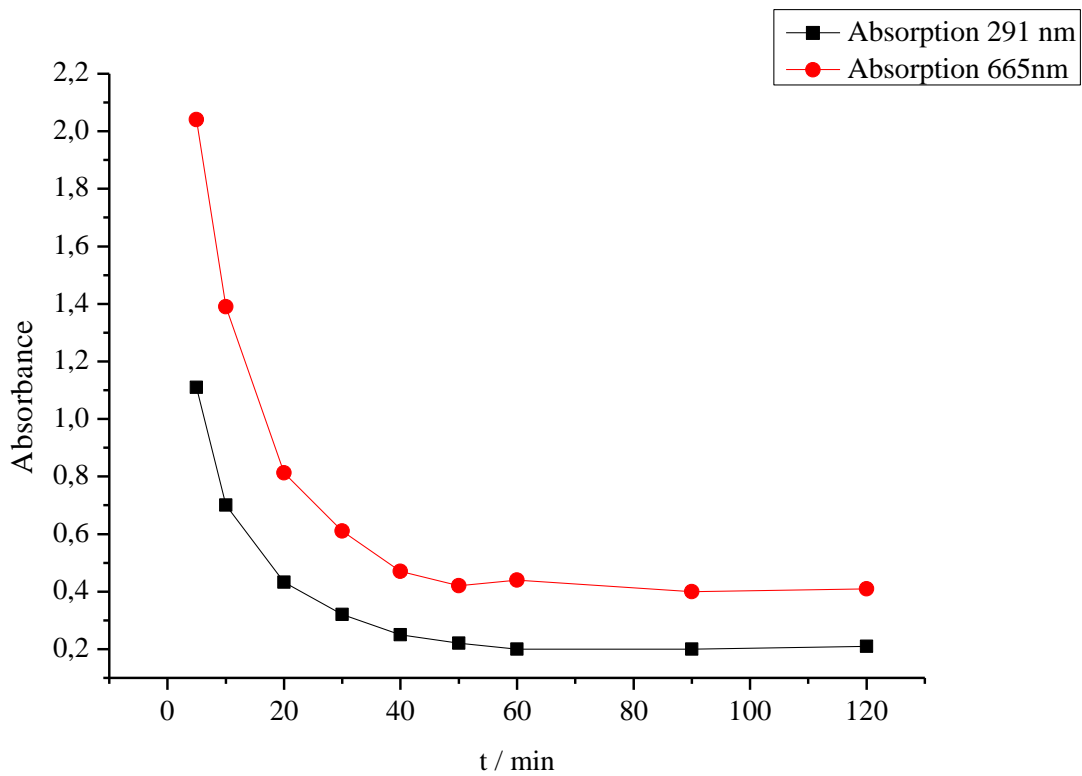


Figure 21: Absorption-time diagram, coated glass and no lights

Decolorization of MB solution was observed during the photocatalytic degradation experiments. Figure 22 depicts the decolorization pattern obtained with $\text{TiOSO}_4\text{-}30.6\text{wt}\%$ + $\text{TiO}_2\text{-P}25$ catalyst over time. From left to right, samples were collected after (-60, -15, 0, 30, 60, 90, 120, 180)min.

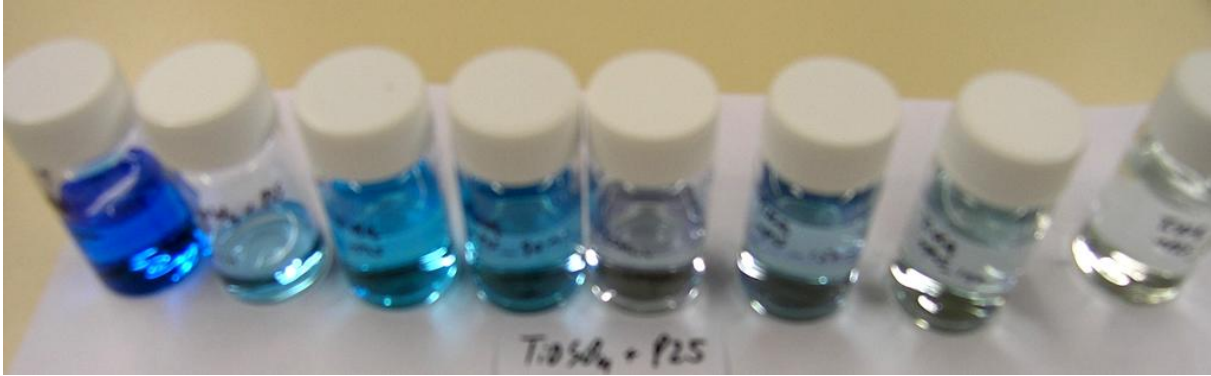


Figure 22: MB decolorization with $\text{TiOSO}_4\text{-}30.6\text{wt}\%$ + $\text{TiO}_2\text{-P}25$ catalyst

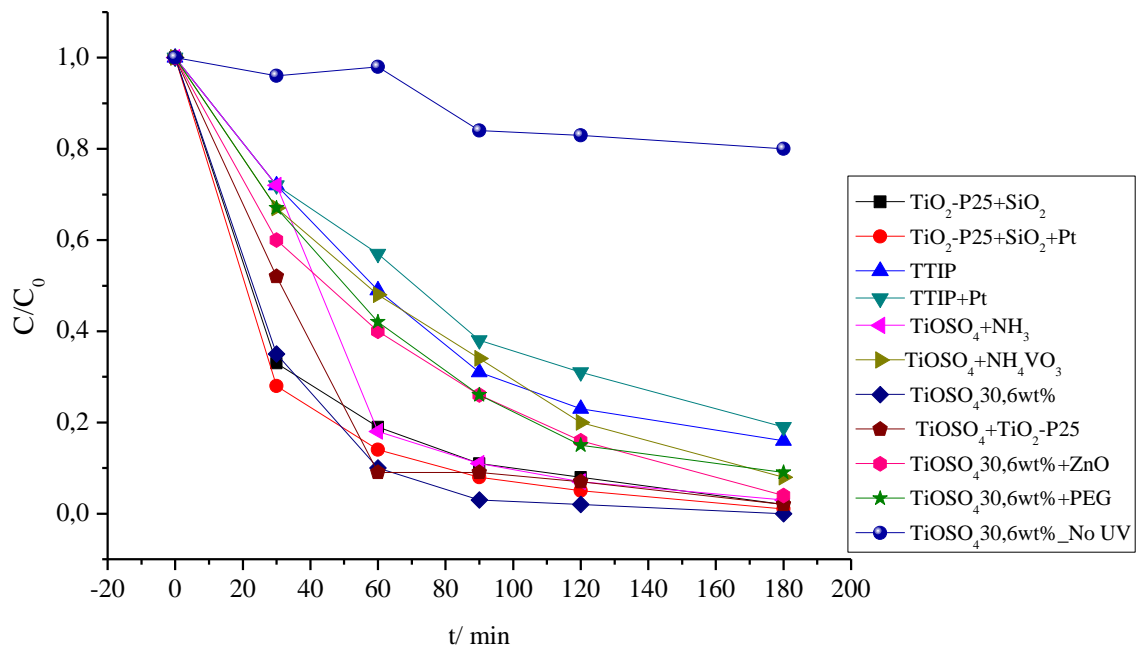


Figure 23 shows the change in MB concentration in the recirculating reactor. A decrease in MB concentration in the presence of UV light is observed for all catalytic systems. However in the absence of UV light with coated glass material, a slight change in concentration close to 20% attributed to adsorption effects was observed. UV light brought along the source of photons needed by the catalyst for electron excitation and hence reaction. Once the photons intercepts with the catalyst, they absorb light generating surface trapped electron hole pairs, which undergo the interfacial processes of oxygen reduction and methylene blue oxidation.

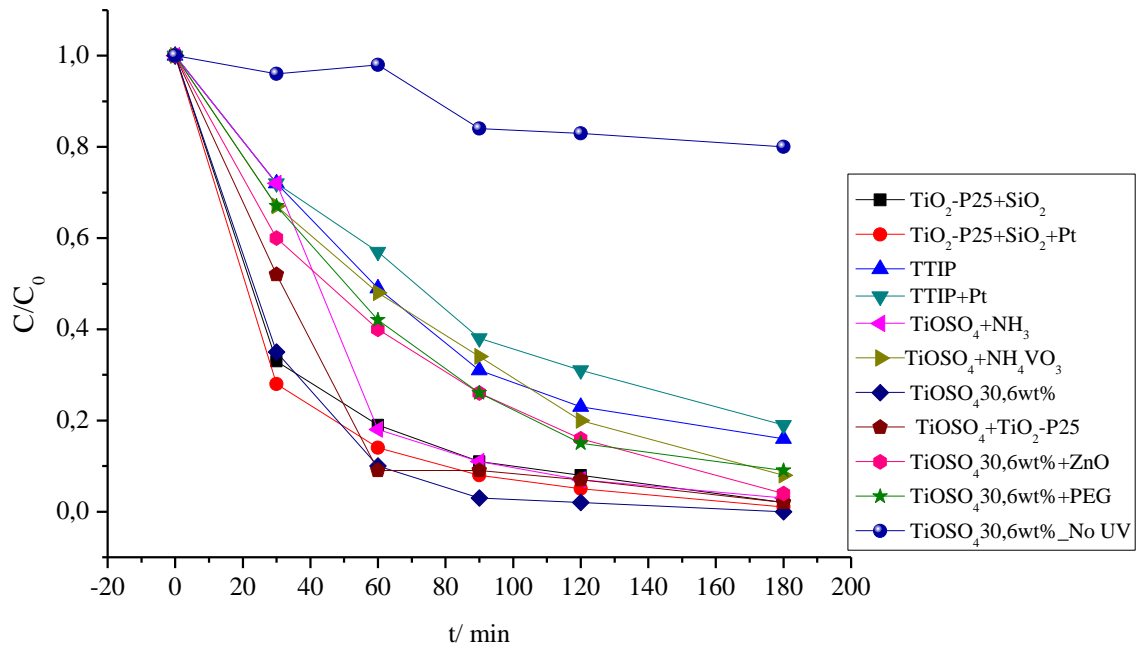


Figure 23: Change in concentration of MB with time. MB initial concentration: 14mg/L, UV radiation $\lambda > 280\text{nm}-420\text{nm}$, recirculating reactor open to air, absorption at 665nm and immobilized catalysts.

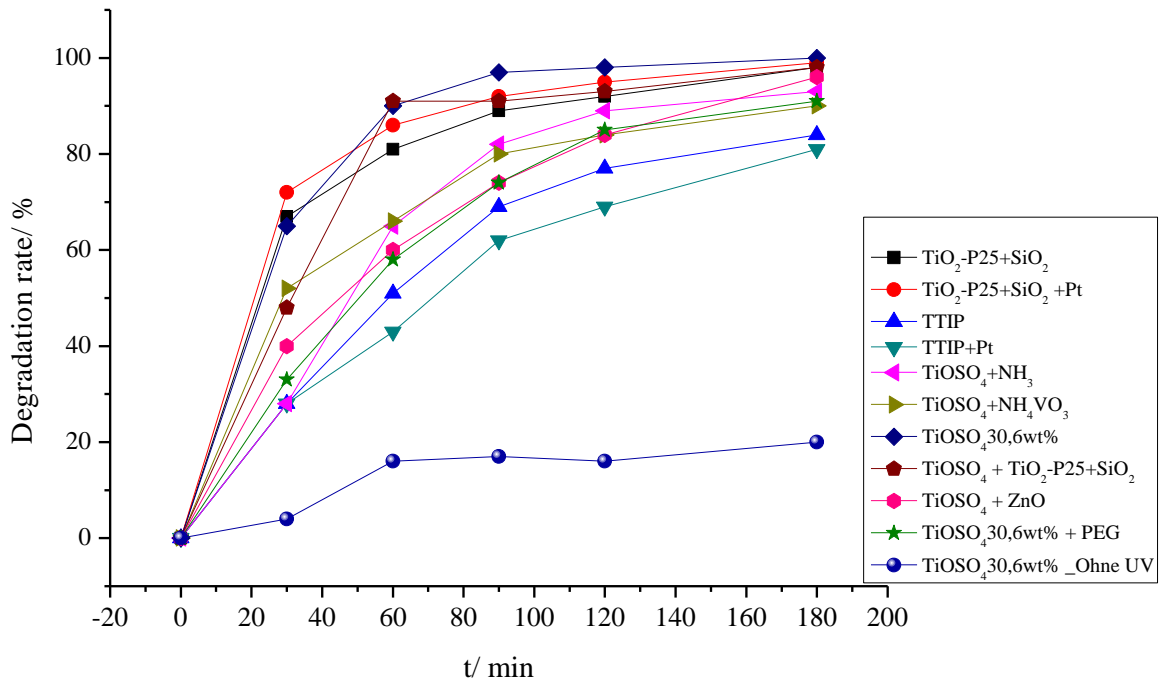


Figure 24: Degradation kinetic of MB using diverse immobilized catalyst under UV light. MB initial concentration: 14mg/L, UV radiation $\lambda > 280\text{nm}-420\text{nm}$, recirculating reactor open to air, absorption at 665nm and immobilized catalysts.

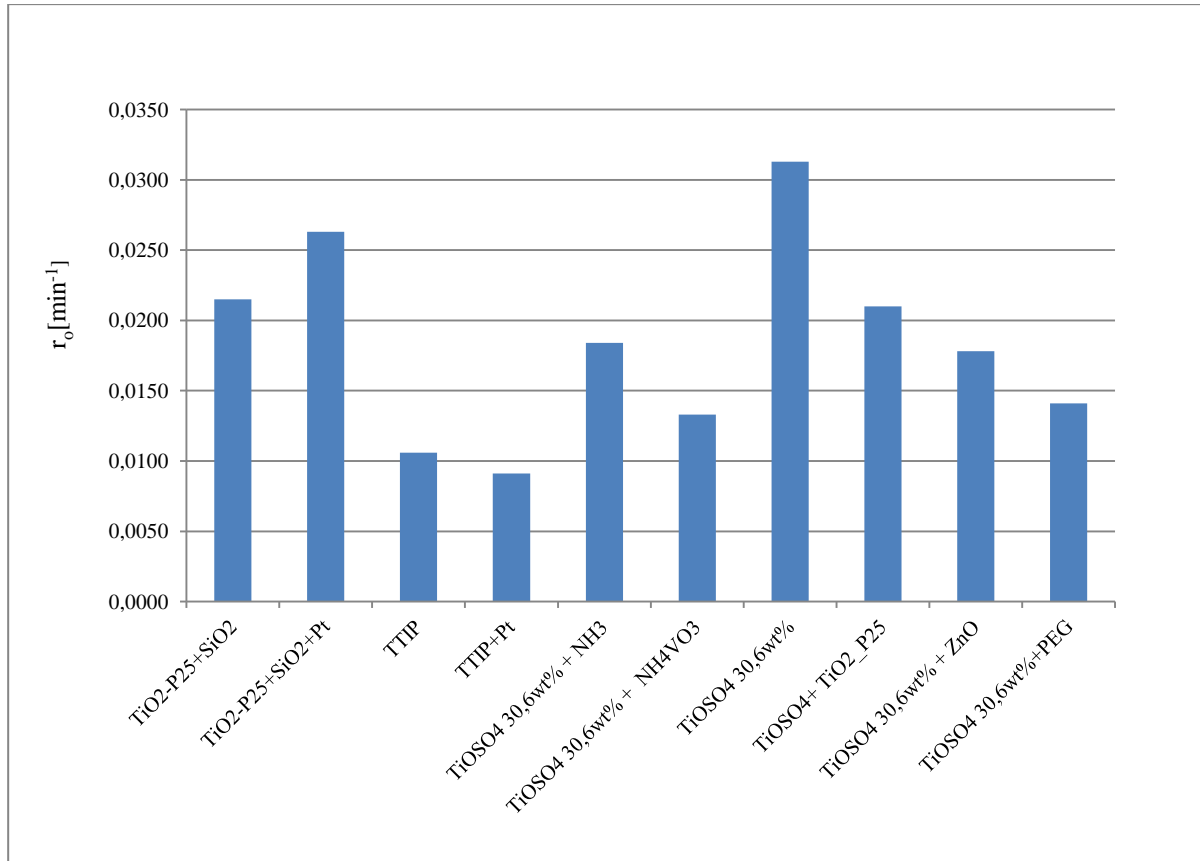


Figure 25: Reaction rates of the photocatalytic degradation of MB(14mg/L) under UV light on immobilized catalysts

TiO₂-P25+SiO₂, TiO₂-P25+SiO₂+Pt, TiOSO₄_30.6wt% showed highest degradation rates close to 100% after 90min illumination with degradation rates exceeding 50% after 30min. TTIP+Pt and TTIP showed lowest degradation rates (Figure 24). TiOSO₄_30.6wt% showed highest reaction rate of 0,0313 1/min followed by TiO₂-P25+SiO₂+Pt, TiO₂-P25+SiO₂ and TiOSO₄+TiO₂_P25 showing reaction rates of 0,0263min⁻¹; 0,0215min⁻¹ and 0,0210min⁻¹ respectively (Figure 25).

The aim of combining catalysts was to achieve optimum catalytic activity by increasing total active surface area and hence the availability of more active sites on catalyst surface. TiO₂-P25 was made to bind on the glass substrate by the aid of TEOS. SiO₂ which comprises TEOS has been widely applied as catalytic support materials due to its stabilizing role as binding system [113]. Moreover because TEOS in solution is colorless and while coated it remains colorless, it therefore had no adverse effect on the turbidity of the reaction or transparency of the coatings. This transparent nature assures the photon flux to be easily intercepted by the catalyst. On the contrary case there would be a decrease in penetration of UV light and hence the photo activated volume of the reactant solution decreases [80]. TEOS could

also have an adverse effect in compromising the viscosity of the gel, morphology and crystalline nature of catalyst on glass, and composition of catalyst to be impregnated.

Nitrogen addition as dopant so as to mitigate intra band gap states [11] was tested by the addition of NH_3 and NH_4VO_3 to TiOSO_4 as catalyst precursor. Reaction rates achieved for NH_3 and NH_4VO_3 were $0,0184\text{min}^{-1}$ and $0,0133\text{min}^{-1}$ making a difference of 39% which was far still lower than that obtained by using unmodified TiOSO_4 . The reaction rate of $\text{TiOSO}_4_{30.6\text{wt\%}}_{\text{NH}_3}$ was 70% lower than that of $\text{TiOSO}_4_{30.6\text{wt\%}}$. Addition of PEG (polyethylene glycol), ZnO, NH_3 and NH_4VO_3 to the catalytic system all gave degradation rates greater than 50% after 60min of reaction. After 90min reaction time degradation rates reached were in the order $\text{TiOSO}_4_{30.6\text{wt\%}} > \text{TiO}_2\text{-P25+SiO}_2\text{+Pt} \approx \text{TiOSO}_4_{30.6\text{wt\%}}+\text{TiO}_2\text{-P25} > \text{TiO}_2\text{P25+SiO}_2 > \text{TiOSO}_4_{30.6\text{wt\%}}+\text{NH}_3 \approx \text{TiOSO}_4_{30.6\text{wt\%}}+\text{NH}_4\text{VO}_3 > \text{ZnO}+\text{TiOSO}_4_{30.6\text{wt\%}} \approx \text{TiOSO}_4+\text{PEG} > \text{TTIP} > \text{TTIP+Pt}$. Degradation values were 97%, 92%, 91%, 89%, 82%, 80%, 74%, 74%, 69%, and 62% respectively. Use of PEG was to prevent the aggregation of Titania particles in the gel [114]. Adding Pt to $\text{TiO}_2\text{-P25+SiO}_2$ system brought about a corresponding increase in reaction rate close to 10% probably because of the formation of intra-band gaps and thus reducing electron-hole pair recombination.

10.5. Conclusion

This work presents a comparative study of coatings produced via sol-gel basis on sintered glass particles in a borosilicate glass tube. Following catalytic systems were presented: $\text{TiO}_2\text{-P25+SiO}_2$, $\text{TiO}_2\text{-P25+SiO}_2\text{+Pt}$, TTIP, TTIP+Pt, $\text{TiOSO}_4\text{+PEG}$, $\text{TiOSO}_4\text{_{30.6wt\%}}$, $\text{TiOSO}_4\text{_{3.6wt\%+NH}_3}$, $\text{TiOSO}_4\text{_{30.6wt\%+NH}_4\text{VO}_3}$, $\text{TiOSO}_4\text{_{30.6wt\%+TiO}_2\text{-P25+SiO}_2}$ and $\text{ZnO+TiOSO}_4\text{_{30.6wt\%}}$.

A comparative study to access the degradation rate of the different coatings was done with MB. Illumination of uncoated glass material gave negligible changes in MB degradation after long irradiation time of 3h. A decrease in MB concentration in the presence of UV light was observed. However in the absence of UV light with coated glass material, a slight change in concentration close to 20% attributed to adsorption effects was observed. The effect of adding Pt as metal ion was monitored with $\text{TiO}_2\text{-P25}$ and TTIP gels. $\text{TiO}_2\text{-P25+SiO}_2$, $\text{TiO}_2\text{-P25+SiO}_2\text{+Pt}$ and $\text{TiOSO}_4\text{_{30.6wt\%}}$ coatings showed highest degradation rates close to 100% after 90min illumination with degradation rates exceeding 50% after 30minutes. TTIP+Pt showed lowest degradation rates. New absorption peaks in the UV-spectrum suggested the formation of intermediate products which disappeared in course of reaction indicating destruction of MB dye and intermediate products [115; 116; 97].

11. Photocatalysis of lignin in circulating packed bed reactor

11.1. Introduction

This chapter reports on stable catalytic coatings and their photocatalytic activity studied by degradation experiments of lignin sulfonate from paper waste water under UV light illumination. The synthesis of immobilized catalyst on porous glass support material via the sol-gel route is reported in chapter 9.3. $\text{TiO}_2\text{-P25-SiO}_2\text{+Pt}$, $\text{TiO}_2\text{-P25-SiO}_2$, $\text{TiOSO}_4\text{-30.6wt\%}$, $\text{ZnO+TiO}_2\text{-P25-SiO}_2$ catalyst were used in this study because they had shown highest catalytic activity out of the 35 different synthesized catalyst both with use of MB as test substance and with use of lignin sulfonate. The morphology of the coatings are described in chapter 9.4.1.

In this section, degradation rates, reaction rates, dissolved carbon (DC), formation of peaks and fluorescence of products formed from the photocatalytic degradation of lignin sulfonate is discussed. Through simultaneous reaction-extraction pathways applying dialysis filtration and highly porous polystyrene divinylbenzene adsorbent resin (HR-P) for solid phase extraction (SPE), an attempt was made to isolate smaller molecules produced from photocatalytic degradation (Figure 14). Moreover relatively high lignin sulfonate (0.5g/L) concentrations were used in the reactions. Following analytical techniques were used to monitor lignin degradation: UV-Vis spectroscopy, DC, SEM, HPLC, and fluorescence spectroscopy. UV-Vis spectroscopy revealed a faster reduction in the concentration values for the aliphatic moiety compared to the aromatic moiety. Peaks were observed by both fluorescence spectroscopy and HPLC suggesting the production of new substances and fluorophores. Figure 13 and Figure 26 depict the circulating packed bed photoreactor while Figure 14 depict the circulating packed bed photoreactor with integrated dialysis filtration column and solid phase extraction column.

11.2. Experimental

The degradation experiments of lignin sulfonate were carried out with a starting concentration of 0.5g/L in 200mL deionized water. The tube was placed between two planar dielectric barrier discharge lamps (Osram Planon) emitting UV-light of wavelength around 280-420nm. The broad surface of the light source insured incident light to be well distributed all over the surface of the glass tubes.

The reactions were carried out in 3 procedures. In the first one, lignin sulfonate solution was pumped through the reactor using roller pumps in a continuous manner with a flow rate of 22.5mL/min. Samples were collected at intervals up to a period of 20h reaction time. Reactions

were carried out at room temperature. Blank experiments were performed in the absence of UV light illumination as well as with uncoated sintered glass tubes. For all experiments, lignin was recirculated through the reactor for 60 min before UV-light was put on. This was to ensure uniform wettability within the packed bed and same starting reaction conditions for all experiments. The second procedure involved a reaction-extraction pathway in which extraction followed after reaction with the use of highly porous polystyrene divinylbenzene adsorbent resin (HRP). In the third procedure, the reactor was connected to a dialysis filter fitted with a HRP extraction column operating in a cycle process. This is depicted in Figure 14. The aim was to directly extract smaller molecules produced and preferably aromatic and phenol like compounds from the aqueous medium.

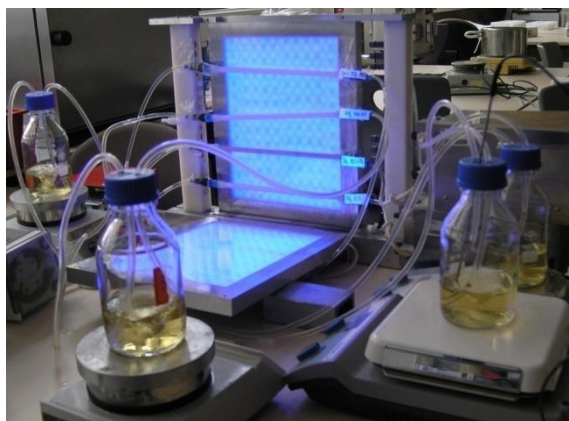


Figure 26: Photocatalytic reaction setup. Lignin sulfonate is pumped through the reactor using roller pumps in a continuous manner.

11.3. Analytics

The concentration of lignin sulfonate in the reaction mixture was determined by correlating absorbance of an aliquot solution to the calibration curve of lignin at different concentrations. This was done using an UV-visible (Thermo-Scientific Genesys 10S) spectrophotometer (at 203nm and 280nm) with deionized water as reference. Equation (1) was used to calculate percentage degradation while Equations (2) and Equations (3) were used to calculate the reaction rate constant resulting from the linear plot of $\ln(C/C_0)$ versus t (see section 7.1, page 35). Dissolved carbon (DC) content of lignin sulfonate over time was done using a TOC analyzer (Shimadzu TOC-5000A). HPLC and fluorescence detection were done on an HP1090 liquid chromatograph and HP1040A programmable fluorescence detector respectively.

11.4. Results

11.4.1. Degradation experiments

Figure 27 shows a time dependent UV-Vis spectra of lignin sulfonate. Absorption peaks were observed at 203nm and 280nm. A shoulder was observed around 230nm. Lignin absorbs UV light with high molar extinction coefficients because of the several methoxylated phenylpropane units of which they are composed of [38]. The absorption peaks decrease gradually indicating the decomposition of lignin sulfonate and hence deterioration of the chromophore groups present. Peaks around 203nm correspond to portions of unsaturated chains [38; 67] while those around 280nm correspond to unconjugated phenolic hydroxyl groups [15] and aromatic rings [67] of lignin sulfonate. Ohnishi et al. [67] report the absorption tailing arising from the color of lignin.

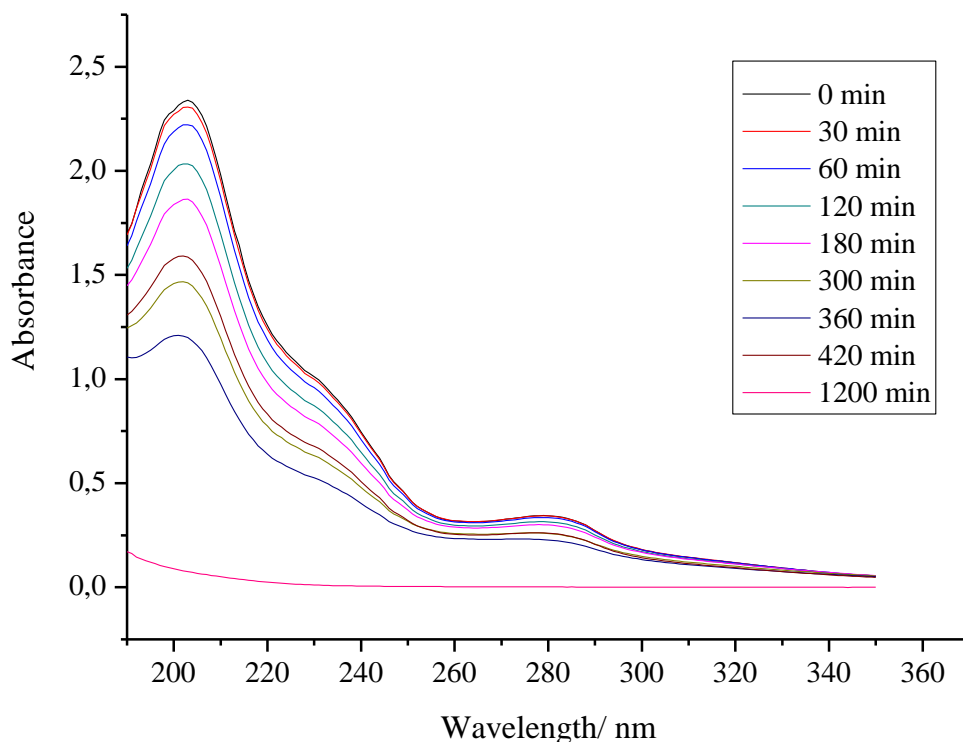


Figure 27: Time dependent UV-Vis absorption spectra of aqueous lignin sulfonate solution. Concentration: 0.5g/L in 200mL, reaction time: 20h, catalyst: sol-gel derived $\text{TiO}_2\text{-P25-SiO}_2$, reaction at room temperature, UV radiation (280-420nm).

Preliminary reactions carried out involved lignin sulfonate degradation experiments performed on uncoated glass in the presence of UV- light as well as on coated glass particles in the absence of UV-light. Results obtained revealed no significant change in absorbance over a 20h period indicating no major degradation and adsorption. Houas et al. [97] note that at

catalytic surfaces experiencing unfavourable conditions such as repellent interactions, there may be no adsorption. It can further be argued that because of the nature of lignin used in this work (lignin sulfonate) the sulfonate groups attached to lignin render it anionic. Likewise because of the basic nature of the reaction medium (pH 9) and the negatively charged surface hydroxyl (OH^-) ions generated from the photochemical reactions, adsorption conditions do not prevail.

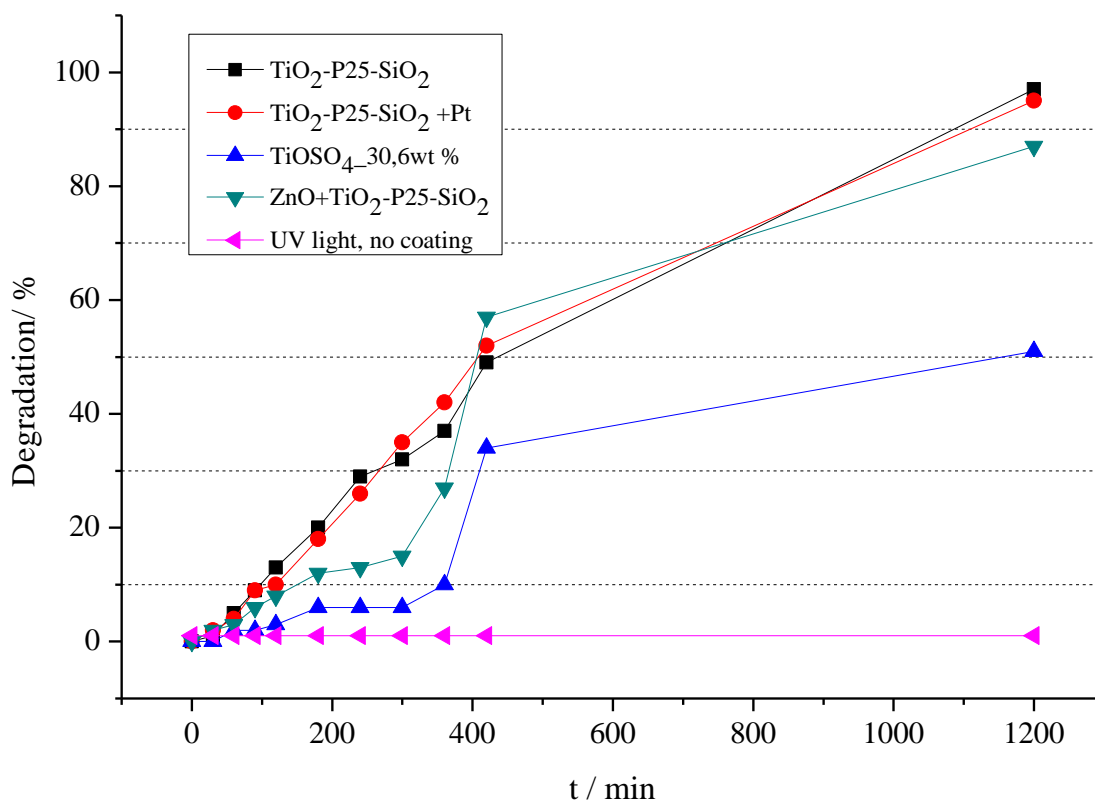


Figure 28: Effect of different catalyst on percentage degradation of lignin sulfonate under UV light at wavelength 203nm (lignin sulfonate concentration: 0.5g/L in 200mL, reaction time: 20h, reaction at room temperature, UV radiation (280-420nm)).

Figure 28 and Figure 29 depict the degradation of lignin sulfonate by different catalyst at wavelength 203nm and 280nm respectively. Degradation of lignin sulfonate prevailed in the presence of a catalyst. An abrupt degradation increase was observed for $\text{TiOSO}_4_{30.6\text{wt}\%}$ and $\text{ZnO}+\text{TiO}_2\text{-P25-SiO}_2$ catalysts between 240min and 300min. Here, the slow reaction at the beginning is the rate determining step [52]. In this step, processes such as absorption of photons of light by catalyst, production of electrons and other oxidizing species amongst other take place before a faster reaction takes place [106]. An almost linear degradation pattern was noted for $\text{TiO}_2\text{-P25-SiO}_2+\text{Pt}$ and $\text{TiO}_2\text{-P25-SiO}_2$ throughout the complete reaction time. Degradation rates of 97%, 95%, 87% and 51% were attained by coatings $\text{TiO}_2\text{-P25-SiO}_2+\text{Pt}$, $\text{TiO}_2\text{-P25-SiO}_2$,

ZnO+TiO₂-P25-SiO₂ and TiOSO₄_30.6wt% respectively after 20h reaction time for the straight chain lignin sulfonate moiety (Figure 28). Similar degradation values are also observed for the aromatic moiety after 20h (Figure 29). TiOSO₄_30.6wt% catalyst was less reactive compared to the others because of the relatively low degradation values it produced. Less than 40% degradation was achieved after 420min for both the aromatic and aliphatic moiety. Comparing the degradation rates of the aromatic moiety against that of the straight chain moiety after 420min approximately, it was observed that higher degradation values were attained by the aliphatic moiety. In detail, for the aliphatic moiety degradation rates of 49%, 52%, 57% and 34% were noted while for the aromatic moiety degradation rates of 34%, 32%, 41%, 36% were observed for TiO₂-P25-SiO₂+Pt, TiO₂-P25-SiO₂, ZnO+TiO₂-P25-SiO₂ and TiOSO₄_30.6wt% respectively. This suggests a faster transformation of the aliphatic side chains as compared to the aromatic species. A similar conclusion was reached by Tanaka et al [65] whereby Fourier transform infrared spectroscopy (FTIR) measurements were studied.

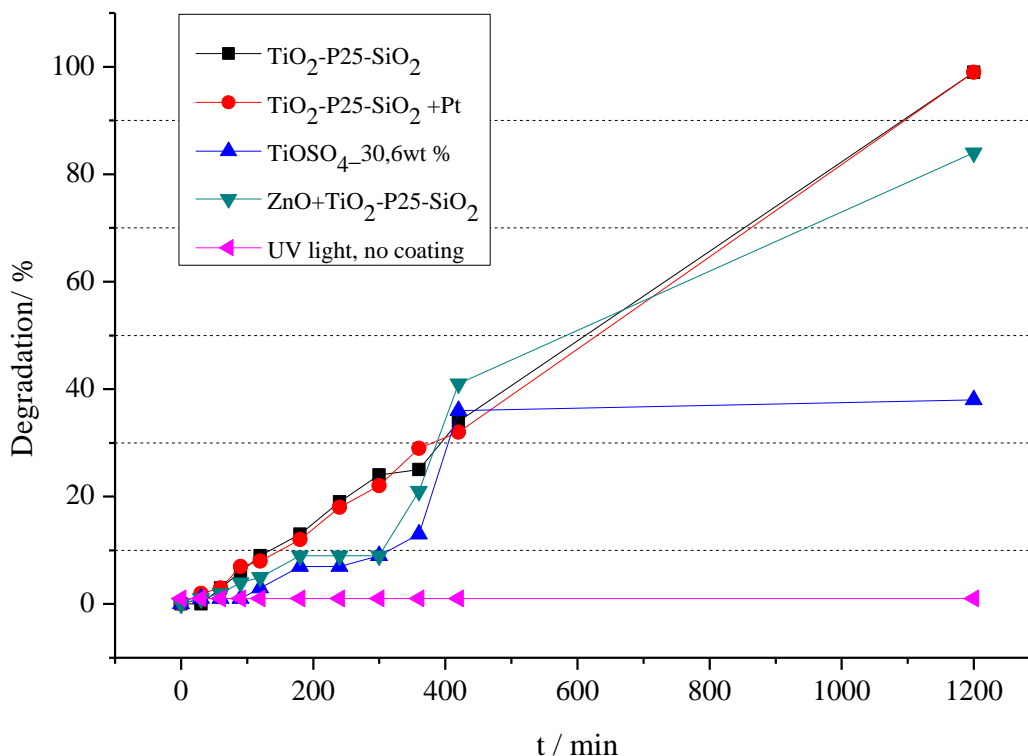


Figure 29: Effect of different catalyst on percentage degradation of lignin sulfonate under UV light at wavelength 280nm (lignin sulfonate concentration: 0.5g/L in 200mL, reaction time: 20h, reaction at room temperature, UV radiation (280-420nm)).

Comparing the degradation values of lignin sulfonate by using plain TiO₂-P25-SiO₂ and that with the combination of ZnO and TiO₂-P25-SiO₂, a higher degradation rate was observed

for ZnO and TiO₂-P25-SiO₂ after 420min; both for the straight chain moiety and aromatic moiety. However after 20h reaction time, TiO₂-P25-SiO₂ had a higher degradation value; both for the straight chain moiety and aromatic moiety. Degradation rates of 49% and 57% were observed after 420min for TiO₂-P25-SiO₂ and ZnO+TiO₂-P25-SiO₂ catalysts respectively. Meanwhile after 20h reaction time, values of 97% and 87% were attained by TiO₂-P25-SiO₂ and ZnO+TiO₂-P25-SiO₂ catalyst respectively. This means ZnO+TiO₂-P25-SiO₂ catalyst was more active during the first 420min and its activity decreased in the proceeding time.

Adding (doping) Pt as metal ion to TiO₂-P25-SiO₂ slightly improved the degradation values compared to that of plain TiO₂-P25-SiO₂ catalyst. Values of 49% and 52% were attained after 420 min reaction time for TiO₂-P25-SiO₂ and TiO₂-P25-SiO₂+Pt catalyst respectively whereas after 20h reaction time, values of 97% and 95% were attained by TiO₂-P25-SiO₂ and TiO₂-P25-SiO₂+Pt catalyst respectively. These results indicate Pt contributed to a slight increase in degradation rate which is in accordance to some published results [66; 67]. However this effect cannot be interpreted here because of high degradation rates already attained by the unmodified catalyst (TiO₂-P25-SiO₂).

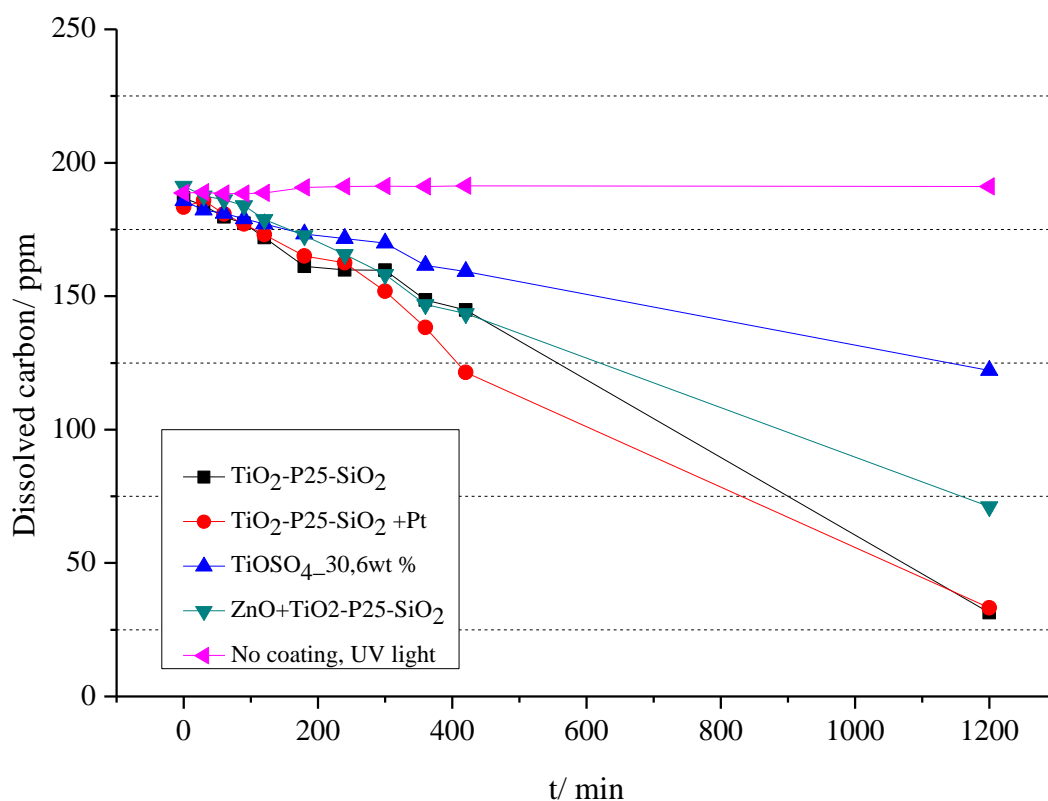


Figure 30: Removal of dissolved carbon in lignin sulfonate. Concentration: 0.5g/L in 200mL, reaction time: 20h, reaction at room temperature, UV radiation (280-420nm).

In order to effectively quantify lignin degradation, dissolved carbon (DC) measurements were done (Figure 30). DC describes the amount of carbon bound in a compound. DC in lignin sulfonate of initial concentration 500mg/L decreased from 185ppm to 144ppm, 121ppm, 159ppm and 143ppm after 420min for the catalysts: $\text{TiO}_2\text{-P25-SiO}_2$, $\text{TiO}_2\text{-P25-SiO}_2 + \text{Pt}$, $\text{ZnO} + \text{TiO}_2\text{-P25-SiO}_2$ and $\text{TiOSO}_4\text{-30.6wt\%}$ respectively. This value further decreased to 31ppm, 33ppm, 122ppm and 71ppm making a DC removal of 84%, 82%, 61% and 34% for $\text{TiO}_2\text{-P25-SiO}_2$, $\text{TiO}_2\text{-P25-SiO}_2 + \text{Pt}$, $\text{ZnO} + \text{TiO}_2\text{-P25-SiO}_2$ and $\text{TiOSO}_4\text{-30.6wt\%}$ respectively. Hence, DC removal was in the order $\text{TiO}_2\text{-P25-SiO}_2 + \text{Pt} \sim \text{TiO}_2\text{-P25-SiO}_2 > \text{ZnO} + \text{TiO}_2\text{-P25-SiO}_2 > \text{TiOSO}_4\text{-30.6wt\%}$. Decrease in DC has been reported to generate carbon dioxide and small amounts of carbon monoxide as the main gaseous products [67].

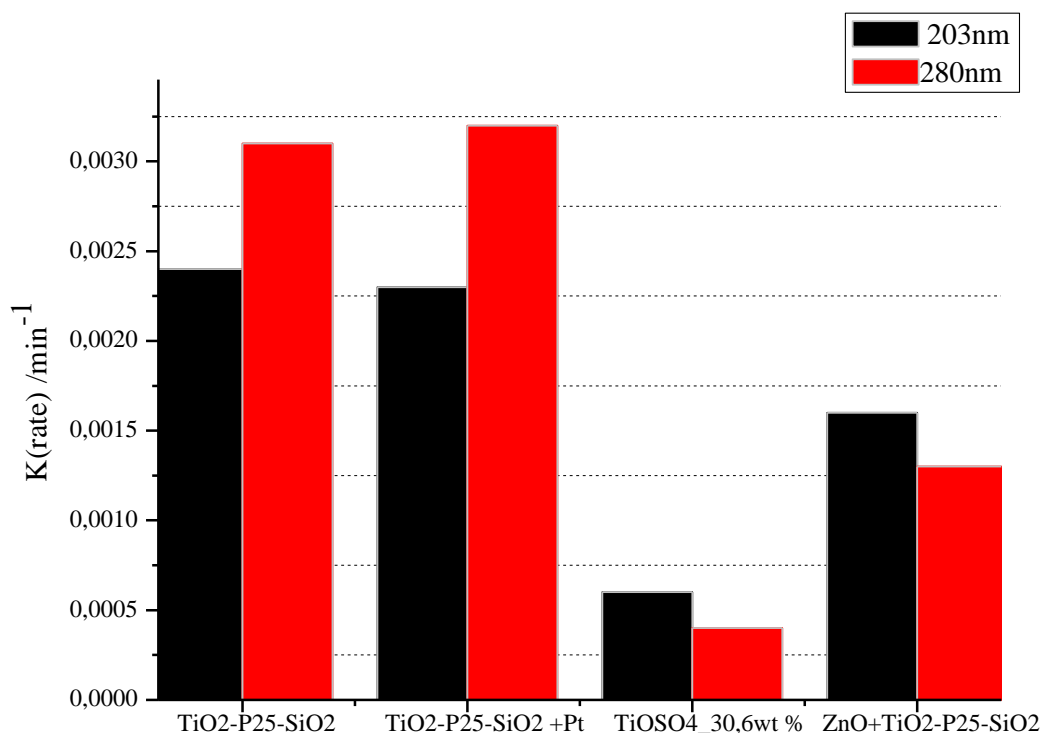


Figure 31: Reaction rates of the photocatalytic degradation of lignin sulfonate (500mg/L) under UV light on immobilized catalysts. Concentration: 0.5g/L in 200mL, reaction time: 20h, reaction at room temperature, UV radiation (280-420nm).

The rate constant values for the different catalyst are shown in Figure 31. Reaction rate was in the order $\text{TiO}_2\text{-P25-SiO}_2 + \text{Pt} \sim \text{TiO}_2\text{-P25-SiO}_2 > \text{ZnO} + \text{TiO}_2\text{-P25-SiO}_2 > \text{TiOSO}_4\text{-30.6wt\%}$ for both the aromatic and aliphatic side chain wavelength regions.

Comparing $\text{ZnO} + \text{TiO}_2\text{-P25-SiO}_2$ and $\text{TiO}_2\text{-P25-SiO}_2$, adding ZnO to $\text{TiO}_2\text{-P25-SiO}_2$ had an adverse effect to reaction rate probably because ZnO occupies some of the active sites on the catalyst support and it does not optimally absorb UV light in the domain of the wavelengths

transmitted by the photo reactor ($280 < \lambda < 420\text{nm}$) and as a consequence, there are limitations of electron transfer between the band gaps [64].

12. Comparative catalyst study in an optimized work up procedure involving simultaneous reaction-extraction of waste water lignin sulfonate

12.1. Introduction

A comparative study was done regarding the formation of peaks and fluorescence of products from the photocatalytic degradation of lignin sulfonate. In this study different catalytic coatings were tested on their photocatalytic activity to produce new products (peaks) and also to evaluate if the new peaks were fluorescent. Fluorescent signals indicate the presence of polyaromatic hydrocarbons or heterocycles. Fluorescence emission in lignin is attributed to aromatic structures such as conjugated carbonyl, biphenyl, phenylcoumarone and stilbene groups [95; 96]. Moreover, through a simultaneous reaction-extraction pathway applying dialysis filtration and highly porous polystyrene divinylbenzene adsorbent resin (HR-P), an attempt was made to isolate smaller molecules produced from the photocatalytic degradation of lignin. Following analytical techniques were used in this study: HPLC and fluorescence detection.

The assessment of the catalysts was done by comparison of peaks on the chromatogram before and after photocatalysis. This means, a good catalyst should degrade lignin sulfonate, generate new product peaks and possibly produce compounds which fluoresce. Moreover these compounds should preferably be low molar mass aromatic compounds such as phenol.

12.2. Experimental

The experiments were carried out with a starting concentration of 0.5g/L lignin sulfonate dissolved in 400mL deionized water. During each experimental run, eight tubes containing same coated catalyst obtained from sol-gel processes were placed between the planar dielectric barrier discharge lamps emitting UV-light of wavelength in the range 280-420nm (see chapter 9.3 for procedure of catalyst synthesis). The reactor was connected in series to a dialysis filter membrane such that lignin sulfonate solution leaving the reactor directly went into the dialysis filter system. This was done using roller pumps in a continuous manner with a flow rate of 22.5mL/min. The filtrate from the dialysis membrane was further connected to an SPE unit with use of a cartridge containing the solid phase. This line also ran in a continuous manner such that incoming molecules were directly extracted. Before fitting the SPE cartridge into the

reaction setup, it was first conditioned with 10mL methanol and rinsed with 20mL water. The SPE unit consisted of highly porous polystyrene divinylbenzene adsorbent resin (HR-P). At a given time period the cartridge was replaced with a freshly conditioned one. Once the cartridge was removed, it was flushed with air before elution with 10mL methanol. The methanol solution, now containing the extract was then analyzed via HPLC in line with a fluorescence detector. Samples were collected at the beginning and at the end of the reactions (4h). Figure 14 depicts the reaction and extraction procedure.

Batch reactions were also done and this involved 500g crushed glass coated with catalyst. The reaction procedure was such that 0.5g/L lignin sulfonate (reaction volume of 1000mL) was stirred from above while the beaker containing both catalyst and lignin sulfonate was placed on the UV discharge lamp plates.

12.3. Results

Results and discussion in this section shall cover aspects observed only with catalysts that produced new peaks. The peak intensity is denoted by milli absorbance units (mAU).

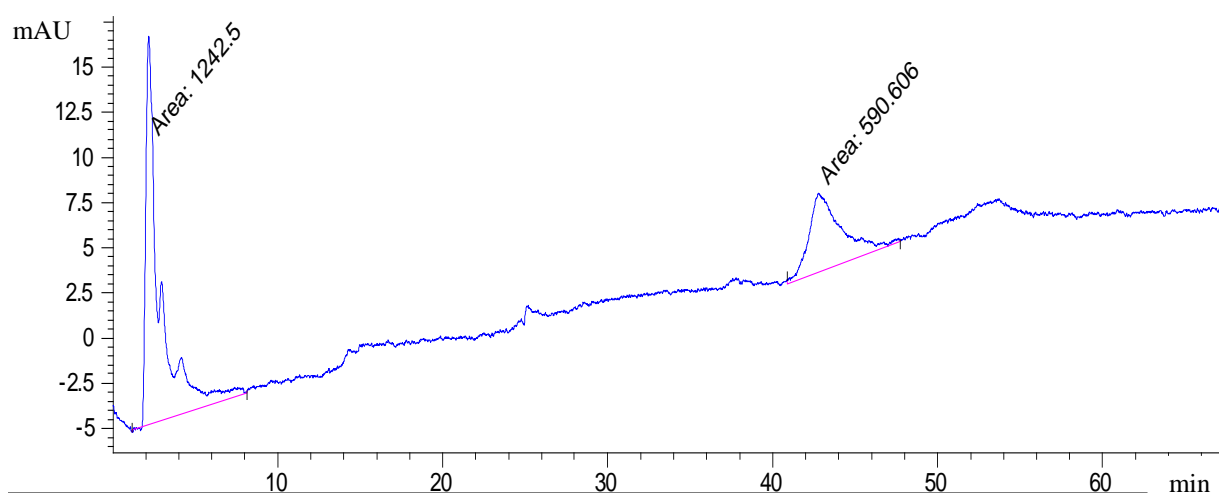


Figure 32: 2 g/L lignin through reactor before illumination. Catalyst: $\text{TiO}_2\text{-P25-SiO}_2$, reaction at room temperature, absence of UV radiation, absence of dialysis filter and SPE with HP-R.

Figure 32 illustrates an HPLC chromatogram of 2g/L lignin sulfonate during calibration. Lignin sulfonate peak is at r.t. ~2min. Methanol (used as eluting agent during SPE) peak also lie at r.t. close to 2min. (Figure 33).

Figure 33 depicts an HPLC chromatogram and a fluorescence chromatogram in which both measuring apparatus were coupled. The Y-axis describes the the fluorescence detection intensity. This chromatogram was obtained after photocatalysis of waste water lignin sulfonate with use of $\text{TiO}_2\text{-P25-SiO}_2$ catalyst. The red and blue color run on the chromatogram depicts the HPLC results at the beginning and after 4h of reaction respectively. The green color depicts the fluorescence signals. Peaks were observed on both HPLC and fluorescence detection suggesting the production of new substances (Figure 33). Some of the peaks had fluorescent signals e.g. the peaks at r.t. 42 and 46min.

Color of line	red	blue	green
Time /h	0h	4h	4h, fluorescence

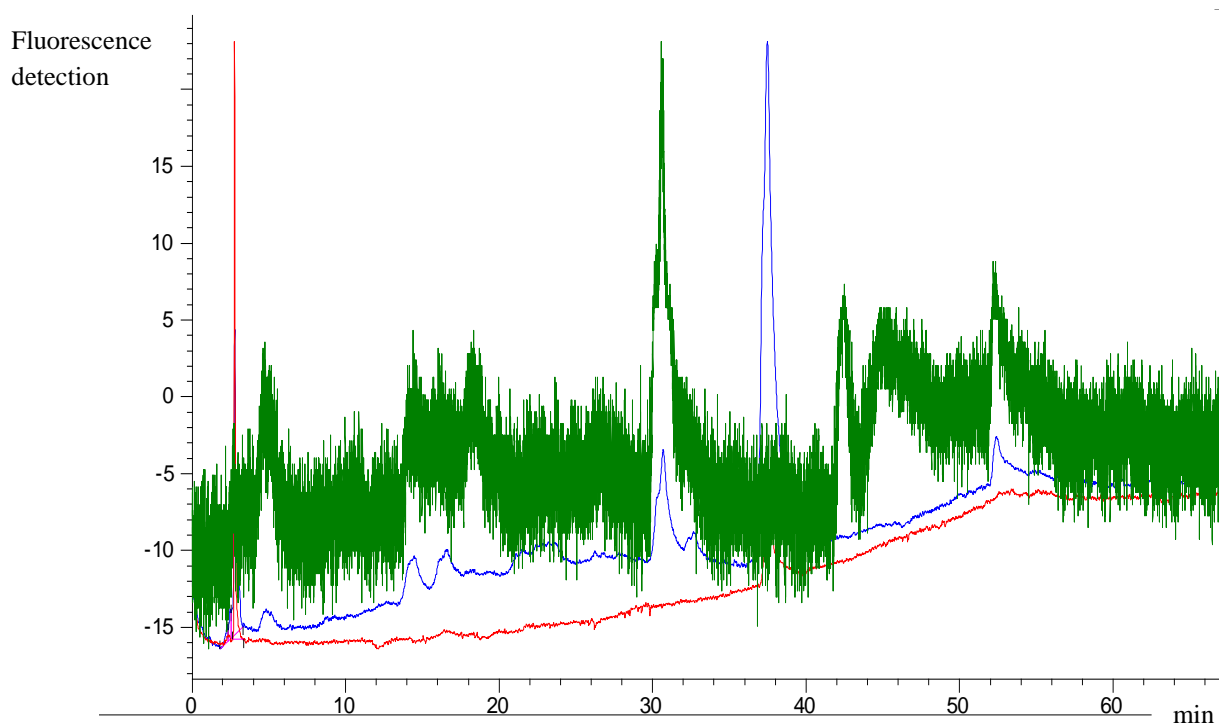


Figure 33: HPLC chromatogram and fluorescence peaks of lignin sulfonate solution. Reaction volume: 200mL, concentration of lignin sulfonate: 0.5g/L, reaction time: 4h, catalyst: $\text{TiO}_2\text{-P25-SiO}_2$, reaction at room temperature, presence of UV radiation, simultaneous reaction, dialysis filter and SPE with HP-R cartridge during reaction.

With the use of $\text{TiO}_2\text{-P25-SiO}_2$ catalyst, new fluorophores were detected as soon as 5min and can be observed spread along the spectrum till around 55mins. Also, broad peaks were found, both on the HPLC chromatogram and on the fluorescence chromatogram. The peaks at r.t. 37min and at 42min in some HPLC chromatograms originated from the photocatalytic reaction system. From this experiment, the peak at r.t. 37min was present during blank experiments when water was circulated in the photocatalytic reaction system in the presence of

UV-light. The peak at r.t. 37min was also present when methanol was circulated in the reactor in the absence or presence of UV light. This peak had a relatively big area and it was a setback because it could mask peaks resulting from lignin degradation. For example, if a substance like xylols having a r.t. of ~ 37min were produced, they could be masked in the HPLC chromatogram.

During measurements, diode array detector (DAD) wavelength was set at 240nm and not all degradation products could be detected at this particular wavelength. In fact, one of the challenges to analyze lignin through HPLC is to set the DAD wavelength for maximum detection. These difficulties arise because of the vast range of possible products arising from lignin degradation. Furthermore, broad peaks were found both on the HPLC and fluorescence chromatograms indicating that distinct emission decay peaks cannot be produced due to superimposition of the different fluorophores.

A summary of results obtained from the application of the different catalyst is shown in Table 10. The (+) and (-) signs denotes the presence and absence of a peak at a given retention time respectively. The last column gives an overall observation of the catalyst.

Results revealed that catalysts produced different product chromatograms. That is, depending on which catalyst was used, a particular chromatogram was generated and the retention time of the products was not necessarily that observed from other catalyst. However some peaks at r.t. 30, 42, 53, 60 appeared in most chromatograms and a summary this is found in Table 10. The following catalysts produced many peaks in descending order: $\text{TiO}_2\text{-P25-SiO}_2 > \text{TiOSO}_4\text{-30.6wt\%+ TiO}_2\text{-P25} > \text{TiOSO}_4\text{-30.6wt\%}, \text{ZnO+TiO}_2\text{-P25-SiO}_2$

Table 10: Peaks at particular retention in relation to catalyst tested

Catalyst	Retention time of peaks /minutes				others peaks	Fluorescence Peaks	Observation
	30	42	53	60			
TTIP	-	+	-	-		42, 60	many small peaks
TTIP+Pt	+	+	+	-		30, 52, 42,	many small peaks
TiOSO ₄ -30.6wt%+ Pt	+	+	+	-		30, 52, 42,	many small peaks
TiO ₂ -P25-SiO ₂ +Pt	+	+	+	-		30, 52, 42,	many small peaks
TiO ₂ -P25-SiO ₂	+	-	+	-	5,14,16	5,14, 16, 30, 42, 45, 52	many small peaks
				-			
TiOSO ₄ -30.6wt%+NH ₄ CO ₃	+	+	+	-		30, 52, 42,	many small peaks
TiOSO ₄ -30.6wt%+CeO	+	+	+	-		30, 52, 42,	many small peaks
TiOSO ₄ -30.6wt%+NH ₃	+	+	+	-		30, 52, 42,	many small peaks
TiOSO ₄ -30.6wt%+NH ₄ VO ₃	+	+	-	-		30, 52, 42,	many small peaks
TiOSO ₄ -18,3wt%	+	-	-	-	5, 14, 16,	5, 12, 14, 18, 30, 42,	many small peaks
TiOSO ₄ -30.6wt%	+	-	-	-	5, 14, 16,	5, 12, 14, 18, 30, 42,	many small peaks
TiOSO ₄ -30.6wt%+ TiO ₂ -P25	+	-	-	-	5, 12, 14, 16,	5, 12, 14, 18, 30, 42,	many small peaks

ZnO+TiO ₂ -P25-SiO ₂	+	+	-	-	5, 14,16, 30, 40	5,14, 16, 18, 26, 30, 42	many small peaks
ZnO+ TiOSO ₄ _30.6wt%	+	-	-	-	14,22, 23. 24, 30	18, 26, 30, 43	many small peaks
ZnO+TEOS	+	-	-	-	8, 14,22, 38, 45, 58	30, 58, 45	many small peaks
TiOSO ₄ _30.6wt%+CeSO ₄	-	+	-	-		30, 53	no peaks
TiOSO ₄ _30.6wt%+sm(NO ₃) ₃	-	+	-	-		30, 54	no peaks
TiOSO ₄ _30.6wt%+CeO	-	+	-	-		30, 55	no peaks
TiOSO ₄ _30.6wt%+SeO	-	+	-	-		30, 56	no peaks
TiOSO ₄ _30.6wt%+Gd(NO ₃) ₃	-	+	-	-		30, 57	no peaks
TiOSO ₄ _30.6wt%+Y(NO ₃) ₃	-	+	-	-	12, 16, 34,	30, 44, 55	few peaks
TiOSO ₄ _30.6wt%+Cr(IV)O	-	+	-	-	12, 16, 34,	30, 44,	
TiOSO ₄ _30.6wt%+Fe ₂ O ₃	+	+	+	-	12, 16, 34,	5, 30, 33, 42, 54	many small peaks
TiO ₂ - P25-SiO ₂ -Batch	-	+	+	-	12,16, 18, 52, 58	big margins of signals	many small peaks
TiO ₂ -P25+ TiOSO ₄ _30.6wt% Batch	-	+	+	-	8, 12,16, 18, 52, 59	big margins of signals	many small peaks
ZnO_TEOS_ Batch	-	+	-	-	8, 12,16, 52, 60	big margins of signals	many small peaks
TiOSO ₄ _30.6wt%_Batch	-	+	-	-	12,16, 28, 32, 46	big margins of signals	many small peaks

The results below compare reactions without UV light (pattern 1) and reactions with the presence of UV light (pattern 2, 3 and 4). Also, comparison is made between solid phase extraction (SPE) during the reaction (pattern 1, 3 and 4) and after reaction (pattern 2). Additionally, comparative fluorescence results between SPE samples (pattern 1, 2 and 3) and the aqueous raffinate (pattern 4) from continuous extraction are made.

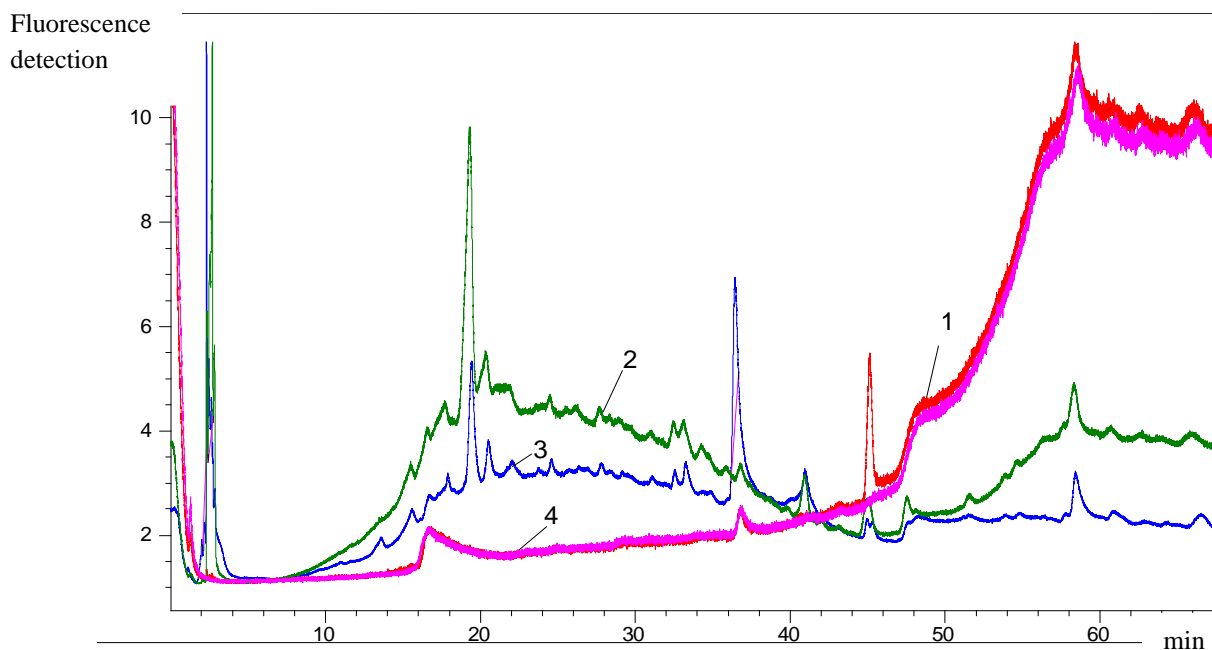


Figure 34: Fluorescence chromatogram of lignin sulfonate degradation product. Emission spectrum, λ_{em} : 240nm, λ_{ex} : 330nm, concentration: 100mL 0.5g/L, reaction time: 20h, catalyst: TiOSO₄_30.6wt%, reaction at room temperature.

- (1): absence of UV radiation, SPE with HP-R cartridge after reaction suspended in methanol.
- (2): presence of UV radiation, SPE with HP-R cartridge after reaction suspended in methanol.
- (3): presence of UV radiation, simultaneous SPE with HP-R cartridge during reaction.
- (4): presence of UV radiation, aqueous raffinate from continuous extraction.

Comparing procedure (2) and procedure (3) (Figure 34) it was observed that the fluorophores produced had similar retention times and similar peak areas. This indicated that it did not matter if extraction was done after the reaction or during the reaction. No peaks were observed for (1) reinforcing the necessity of UV light for lignin sulfonate degradation. The absence of peaks for (4) suggests that degradation was complete and all produced substances were adsorbed on the SPE cartridge. Moreover, tailing was observed for samples (1) and (4) that did not contain degradation products dissolved in it.

12.4. Conclusion

Commercial obtainable TiO₂-P25, well known for its high chemical purity and well defined physico-chemical properties widely applied in suspension systems was effectively immobilized on sintered glass support with the aid of tetraethyl ortosilicate (TEOS) solution which acted as support material. TiO₂ -P25 contains anatase and rutile phases in a ratio of about 3:1. Under the photocatalytic reaction condition, the anatase and rutile agglomerates are considered to decompose and are in contact with each other, leading to a synergy effect such as decrease recombination rates of electrons [117]. The catalytic films synthesized had very good adherence on the sintered glass and the films retained a constant efficiency when re-used after washing with water. The coatings were considerably well distributed all over the surface of the sintered glass. Moreover, the reactor design in this work effectively degraded relatively high concentration of lignin sulfonate solutions (500mg/L) from paper waste water.

UV-Vis spectroscopy revealed a faster transformation of the aliphatic side chains as compared to the aromatic species. Adding Pt as metal ion to TiO₂-P25-SiO₂ catalyst showed a negligible effect on degradation rates. The reaction rate of the catalytic systems was in the order TiO₂-P25-SiO₂ +Pt ~ TiO₂-P25-SiO₂>ZnO+TiO₂-P25-SiO₂>TiOSO₄_30.6wt%.

Peaks were observed on HPLC and fluorescence chromatograms suggesting the production of new substances and fluorophores. Through simultaneous reaction-extraction pathways applying dialysis filtration and highly porous polystyrene divinylbenzene adsorbent resin (HR-P), an attempt was made to isolate smaller molecules produced from photocatalytic degradation.

13. A photocatalytic study of lignin standard (model) compounds

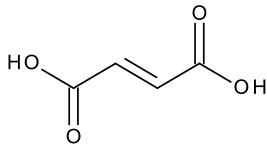
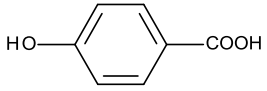
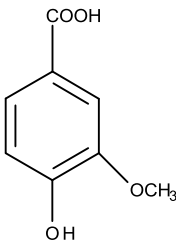
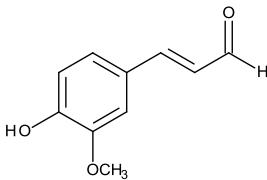
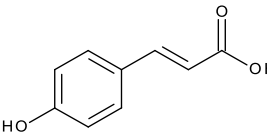
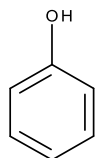
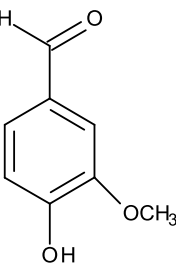
13.1. Introduction

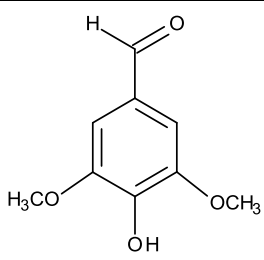
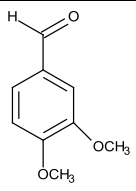
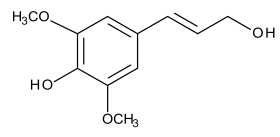
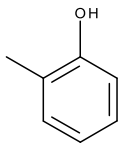
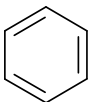
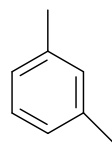
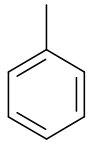
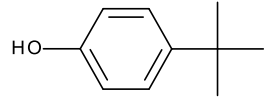
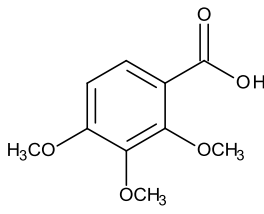
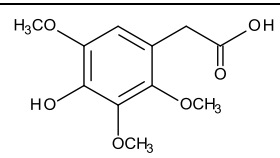
This study was done to get information about the retention times (r.t.) of possible lignin degradation substances (standard compounds) as a means to identify products arising from the photocatalytic degradation of lignin sulfonate through peak superimposition. Also, some of these standard compounds were subjected to photocatalysis to ascertain their degradability. In this case, HPLC analysis would confirm peaks disappearance or formation as a result photocatalysis. The retention time of the standard compounds as well as calibrations were determined by dissolving 1g/L of the substance in methanol (Table 11). However information such molar mass or chemical structure of substance produced was not covered in this study.

This chapter starts by giving an overview of some lignin standard compounds, their chemical formula and retention time from HPLC measurement by the method described below. Column type: Hypersil BDS C18 Column, length 250mm, Inside diameter: 4.0mm. Particle size: 5um Flow: 0.8mL/min, mobile phase gradient, 0.01M KH_2PO_4 95% and 5% methanol - 70% methanol: 0-50min, 70% methanol: 50min-70min, mobile phase (eluent) degassed in helium, column temperature: 50°C, injection volume: 25 μL , draw speed 83 μL /min. Diode array detection (DAD) wavelength: 240nm, 260nm, 280nm.

The procedure used in selecting the standard compounds for photocatalysis are further described. The selection was based on the characteristic linkage type found in the standard compound which should reflect that found in the polymeric structure of lignin. After that a description of possible degradation pathways and possible products formation with focus on the radical mechanism was treated. Finally the experimental setup and results obtained from the time dependent photo-catalytic experiments of the standard substances were treated.

Table 11: Retention time, molar mass and chemical structure of standard compounds

Compound	Chemical formula	Molar mass [g/mol]	Chemical structure	Retention time, HPLC / min
Maleic acid	$C_4H_4O_4$	116.07		3
4-Hydroxybenzoic acid	$C_8H_8O_4$	138.12		9
Vanilic acid	$C_8H_8O_4$	168.14		11
4-Hydroxy-3-methoxy cinnamaldehyde (coniferyl aldehyde)	$C_{10}H_{10}O_3$	178.18		12
Coumaric acid	$C_9H_8O_3$	164.16		15
Phenol	C_6H_6O	94.1		15.5
Vanillin	$C_8H_8O_3$	152.14		16

Siringaldehyde	$C_9H_{10}O_4$	182.17		18
Veratraldehyde	$C_9H_{10}O_3$	166.17		19
Sinapyl alcohol	$C_{11}H_{14}O_4$	210.2		19.5
o/m/p-Cresol	C_7H_8O	108.14		25
Benzol	C_6H_6	78.11		32.5
3,5 Dimethyl benzol (xylol)	C_8H_{10}	106.17		38
Toluene	C_7H_8	92.14		46
Tert-butylphenol	$C_{10}H_{12}O_2$	150.22		62
2,3,4-Trimethoxybenzoic acid	$C_9H_{12}O_5$	212.20		20
3,5-Dimethoxy-4-hydroxyphenylacetic acid	$C_{10}H_{12}O_5$	212.20		45

13.2. Selection of sample molecules

Sample molecules were selected based on the characteristic linkage type found in the molecules which reflect that found in the complex and diversified lignin polymeric structure (Figure 2). Five compounds were selected representing the most frequent occurring bond types in lignin molecule. These were eugenol, phthalan, diphenyl ether (DPE), benzyl phenyl ether (BPE) and diphenyl methane (DPM). Figure 35 and Table 12 show the retention time, molar mass and chemical structure of these compounds.

Lignin contains different ether bonds and C-C bonds. The most frequent ether bond is the aromatic methoxy group. Therefore, eugenol containing a methoxy group linked to the benzylic ring was chosen. Moreover it has a structural similarity to the lignin monomer substance, coniferyl alcohol. Diphenyl ether was chosen to represent aryl-aryl ethers bonds while aryl-alkyl ether bonds was represented by benzyl phenyl ether. Additionally, phthalan was chosen to represent the ether bond in the sub-units of lignin while C(aryl)-C(alkyl) bonds with a methylene bridge was represented by diphenyl methane.

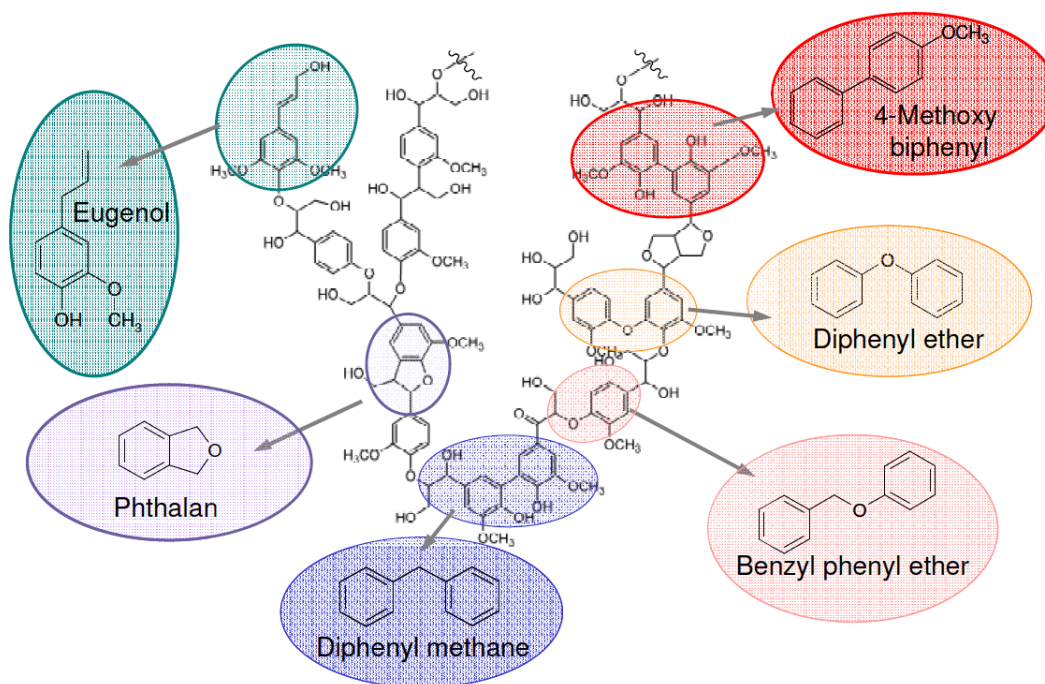
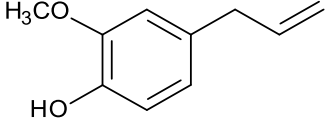
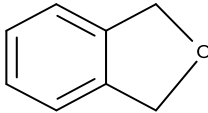
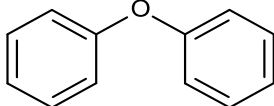
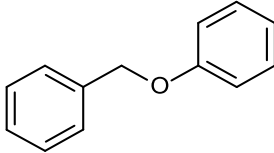
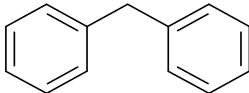


Figure 35: Selection of sample molecules

Table 12: Retention time, molar mass and chemical structure of standard compounds

Compound	Chemical formula	Molar mass [g/mol]	Chemical structure	Retention time, HPLC / min
Eugenol	C ₁₀ H ₁₂ O	164,2		37
Phthalan	C ₈ H ₈ O	120,14		18,28,46
Diphenylether(DPE)	C ₁₂ H ₁₀ O	170,21		52
Benzylphenylether (BPE)	C ₁₃ H ₁₂ O	184,23		52
Diphenylmethan (DPM)	C ₁₃ H ₁₂	168,24		52

13.2.1. Phenyl alkyl ether

In this study, benzylphenylether (BPE) was selected to represent an aryl-alkyl bond type. The ionic pathway, namely hydrolysis leads to the formation of benzyl alcohol and phenol (reaction 1 from Figure 36). Decomposition of BPE will occur by cleavage of the weakest bond in the molecule. The dissociation energy of C-O and C-C of BPE are estimated as 65 kcal mol⁻¹ and 72 kcal mol⁻¹ respectively [118]. A radical mechanism which is more expected in a photocatalytic process would cleave the ether bond in a homolytic manner generating phenoxy and a benzyl radical species. Being highly reactive these can recombine either with hydrogen to give phenol and toluene or they can recombine among themselves, with BPE or with the hydrolysis products (reaction 2 and 3 from Figure 36). In this case dimers, trimers, and higher molecular compounds can be formed. The presented products are only exemplary and many other consecutive products can be formed.

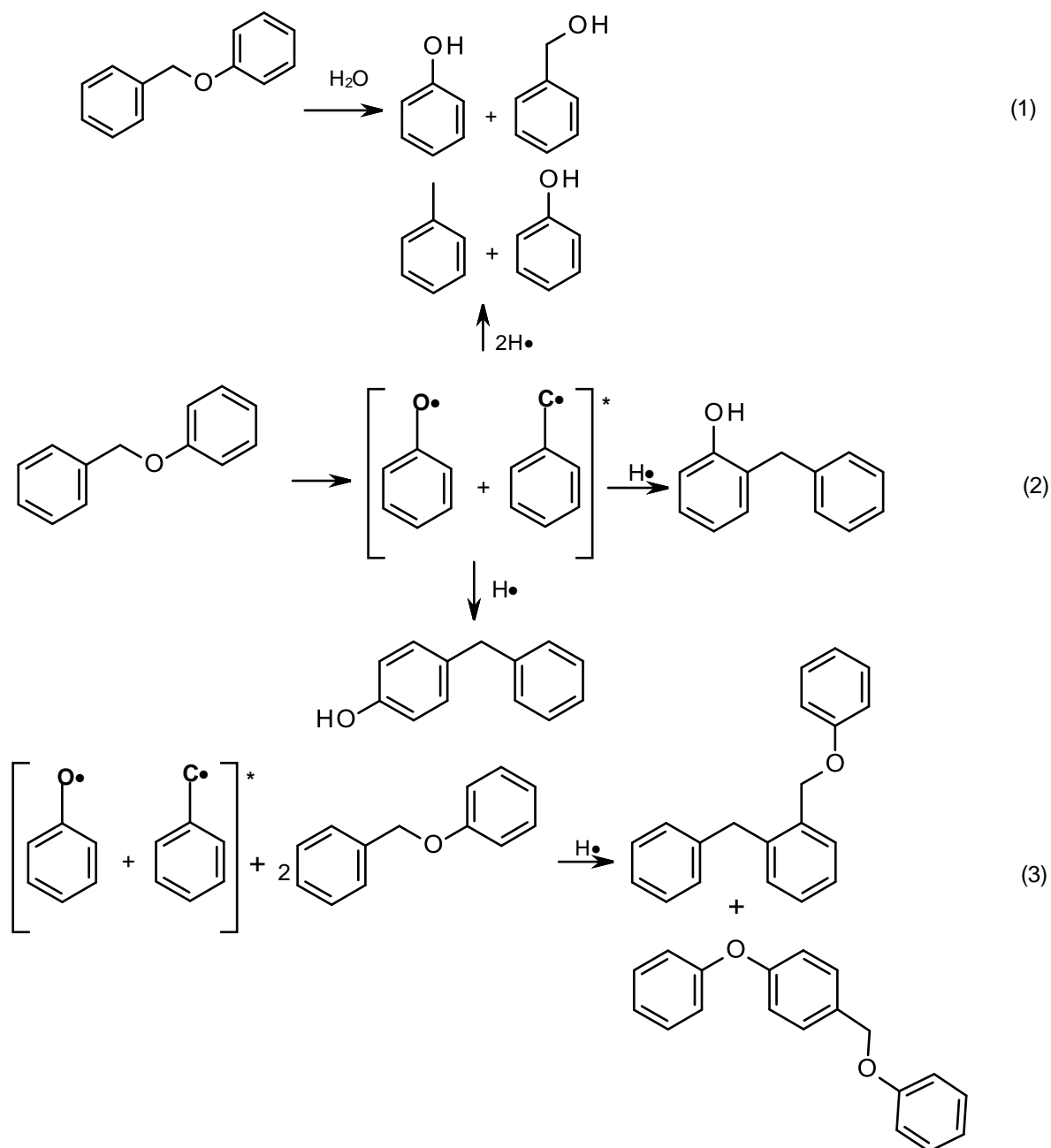


Figure 36: Radical and ionic mechanism pathway with possible recombination products [119].

13.2.2. Aryl-Aryl ether bond

The photocatalytic oxidation of DPE can proceed following two different reaction mechanisms as summarized in

Figure 37 [120; 119]. A radical mechanism, whereby the ether bond is cleaved in a homolytic manner generating phenoxy radical and phenyl radical species (reaction 2). These can recombine with hydrogen to form phenol and benzene or undergo recombination reactions with themselves leading to dimers such as 4-hydroxy biphenyl (reaction 3) or even higher

molecular compounds, e.g. phenoxy biphenyl (reaction 4). The ionic pathway, namely hydrolysis leads to the formation of 2 mol phenol for each mol of converted DPE (reaction 1) [120]. Penninger et al. [121] describe possible radical type polycondensation products such as diphenyl, phenyl diphenyl ether and phenoxy diphenyl.

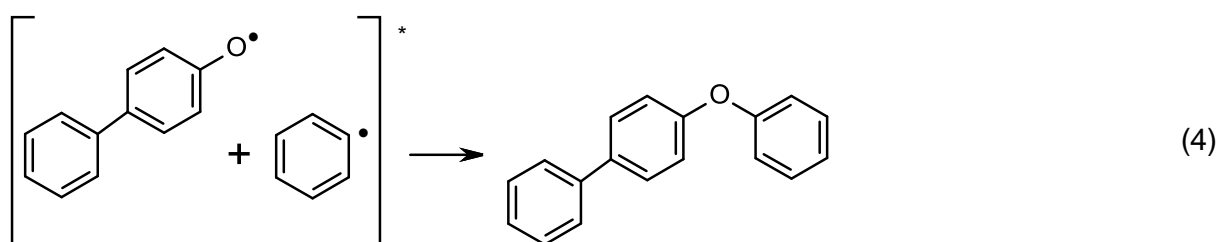
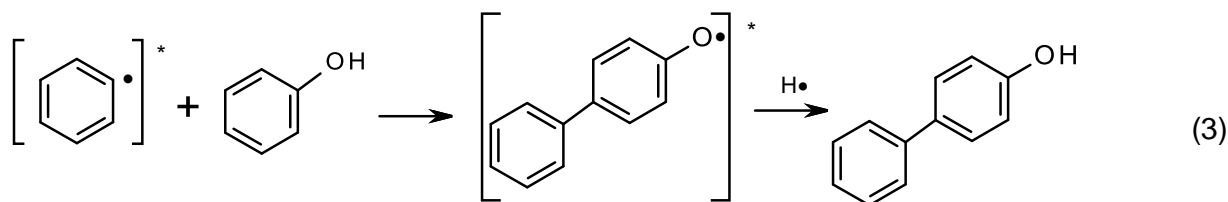
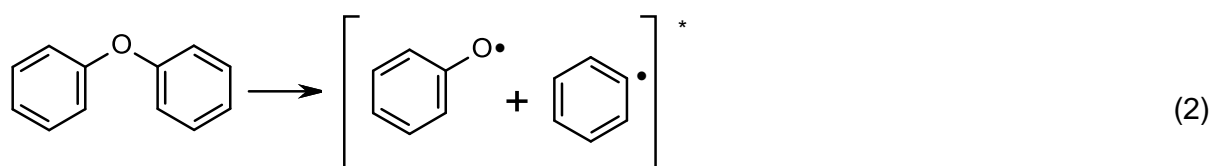
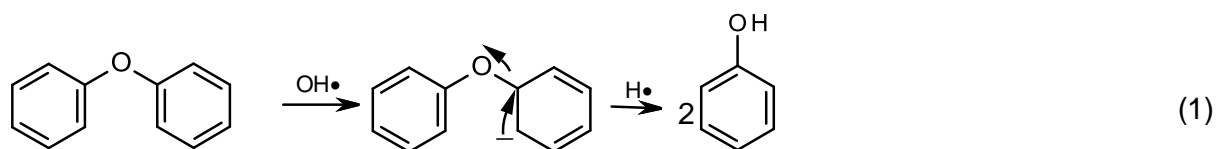


Figure 37: Radical and ionic mechanism pathway with possible recombination products.

13.3. Experimental

The experimental procedure differed depending on the sample's solubility properties. Samples which were partly or not dissolvable in water were suspended in methanol. The specifics about the solvent quantity are given in the respective sub-chapters.

The sample solution was pumped through the reactor using roller pumps in a continuous manner with a flow rate of 22,5mL/min. Figure 13 depicts the reaction setup. Samples were collected at intervals of 0h, 4h and 24h reaction time. Reactions were carried out at room temperature. The catalytic coating used for all reactions was TiO₂ prepared from sol-gel synthesis of TIOSO₄_30.6wt% as described in chapter 9.3.2. For all experiments, the standard test substance was recirculated through the reactor for 15 min before UV-light was put on. This

was to ensure uniform wettability within the packed bed and assure same starting reaction conditions for all experiments. The samples collected were analyzed by HPLC.

During HPLC analysis of samples treated with methanol, a peak at r.t. 37min was observed. This peak increased steadily in area units with reaction time. This peak resulted from the action of methanol on the packed borosilicate glass tubes. It did not matter if the sintered glass particles were coated with catalyst or not. So, this peak cannot be directly linked to a product resulting from the photocatalysis of a standard compound or lignin sulfonate.

13.3.1. Phenyl propane methoxy unit

13.3.1.1. Procedure of reaction

0,4g of eugenol (allyl-2-methoxyphenol) was dissolved in 20mL methanol (MeOH) and re-suspended in 380mL water. This gave a starting concentration of 0.5g/L considering both water and methanol as entire solvent quantity. 4x10mL of sample was pipetted at intervals; (t=0h, 1h, 4h, 20h) from the reaction mixture and analyzed via HPLC by the method described in chapter 7.2.

13.3.1.2. Results

The HPLC chromatograms resulting from the photocatalysis of eugenol are depicted in Figure 38. Following can be drawn out from the results:

- An eugenol peak at 37min. which reduced over time. The blue colored peak representing the starting concentration reduced by 34% within 1h. This peak further decreased in area and height (milli absorbance unit, mAU) over time confirming degradation Figure 39.
- A new peak at retention time (r.t.) 55min was observed (Figure 40). Though this peak was present at the beginning, a steady increase in peak area was observed over time. Its presence at the beginning could be as a result of reactions taking place in the absence of light. E.g. hydrolysis reaction during recirculation of eugenol in the dark during the first 15min prior to switching on UV-lights. A similar phenomenon was observed with the peak at r.t. 55min whereby there was a continuous increase in peak area till 4h. After 20h of reaction, this peak completely disappeared.
- Enlarging the chromatograms, many peaks particularly before r.t. 37min were observed.

- Some of the peaks (substances) produced at the beginning of the reactions are same peaks which increased in area units. In other words accumulation and selective production of substances.
- Some peaks which were present after 4h were absent after 20h photocatalysis, indicating complete degradation. This is observable at r.t. 55 min (Figure 40).Figure 40

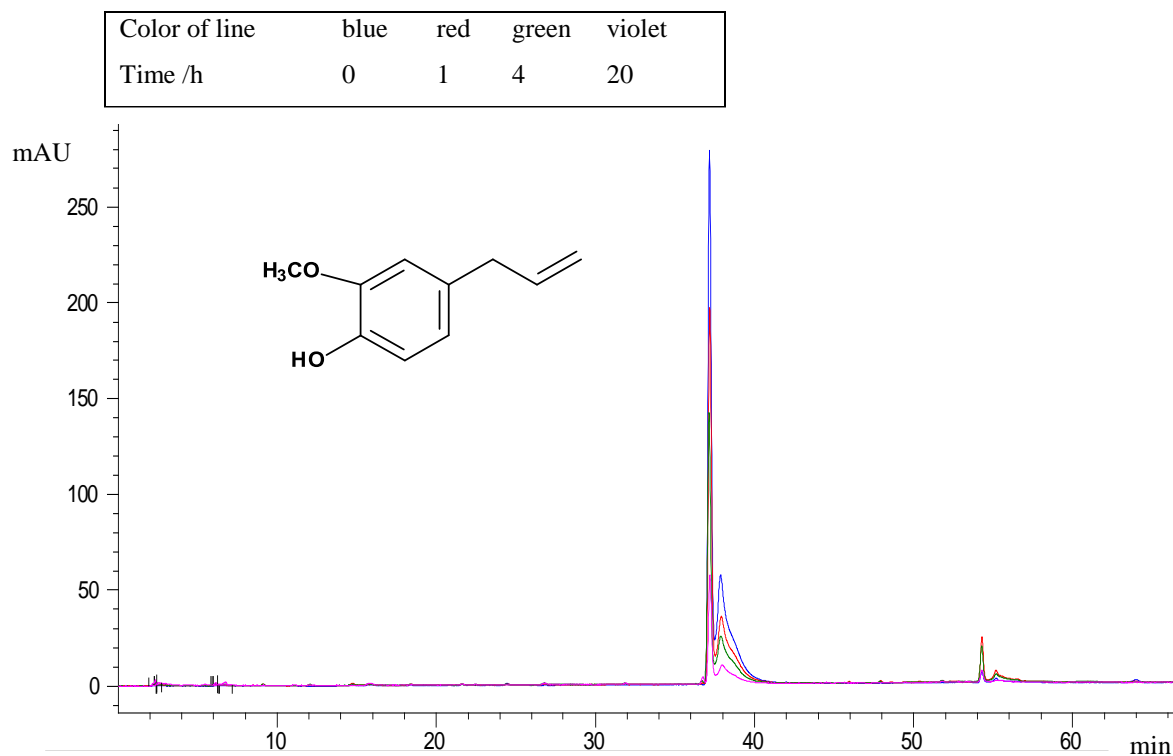


Figure 38: HPLC chromatograms of eugenol consisting of samples after (0,1,4,20)h

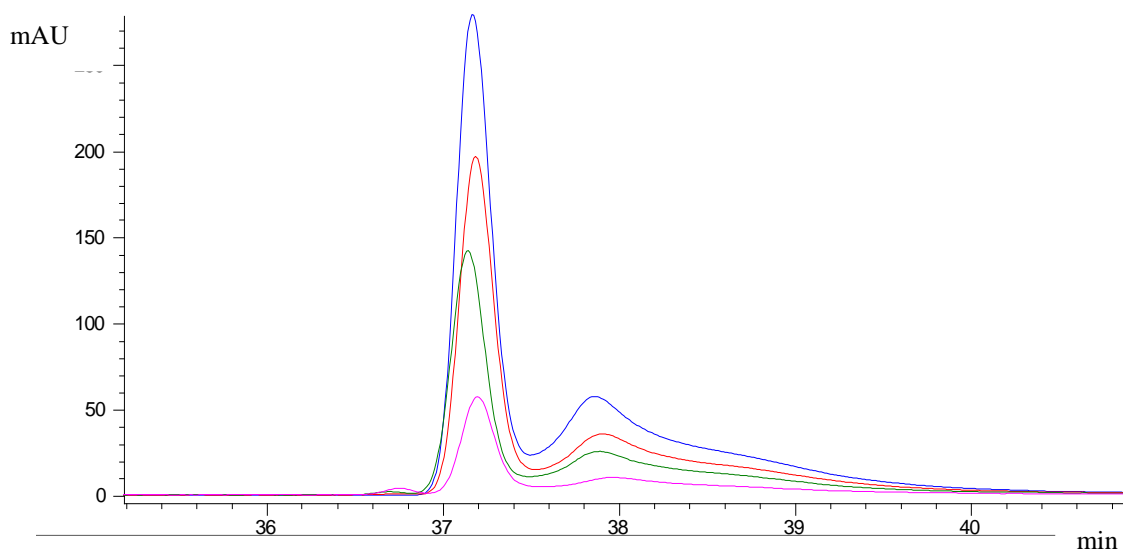


Figure 39: Enlarged chromatogram of eugenol within 35-41 min retention time.

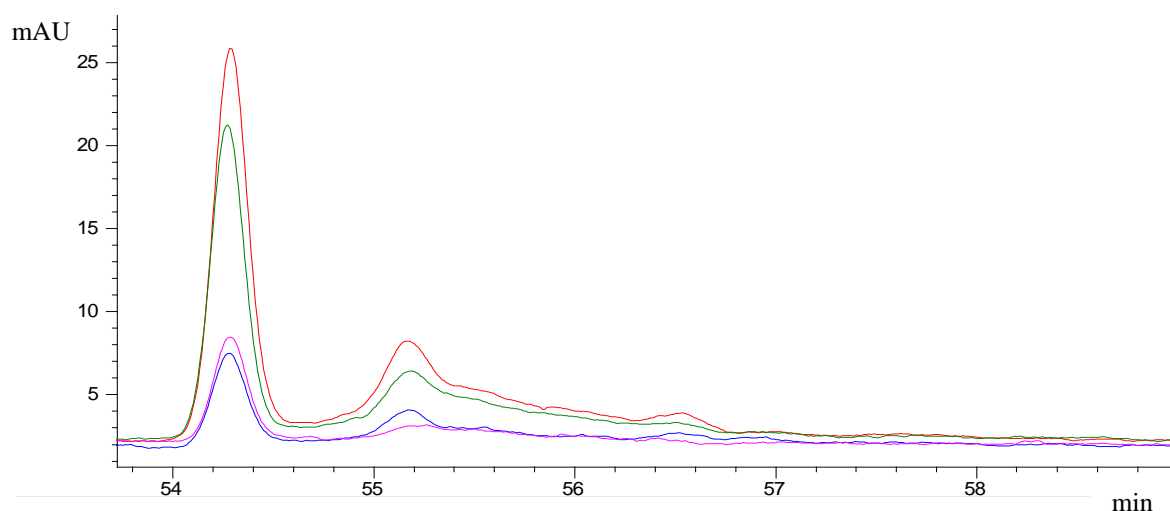


Figure 40: Enlarged chromatogram of eugenol within 53-60 min retention time.

13.3.2. C(aryl)-C(alkyl) bonds in lignin subunit

13.3.2.1. Procedure of reaction

0.5g of phthalan (2,5-Dihydro-3,4-benzofuran) was dissolved in 20mL MeOH and re-suspended in 480mL water. With the addition of water, a white precipitate was formed which was filtered. The filtrate solution was then recirculated in the photocatalytic reactor. 4x10mL of sample was pipetted at intervals; $t= 0\text{h}, 1\text{h}, 4\text{h}, 20\text{h}$ from the reaction mixture and analyzed via HPLC by the method described in chapter 7.2.

13.3.2.2. Results and discussion

The HPLC chromatograms resulting from the photocatalysis of phthalan are depicted in Figure 41 and Figure 42. Following can be drawn out from the results:

- Three Phthalan peaks at r.t., 16, 27 and 46 min results from HPLC measurements of the pure substance. This is probably because of the racemic nature of phthalan as noted by Cacamese et al.[122].
- Phthalan peaks reduced over reaction time indicating degradation.
- New peaks at r.t. 7 and 35min were observed.
- Some of the peaks (substances) produced at the beginning of the reactions were same peaks which increase in area units.
- Phthalan peak at r.t.27min showed a gradual decrease with time while that at r.t. 16 min showed considerable reduction in area after 1h. This peak area remained almost same for the next 2h. After 3h of reaction, (between 3h and 4h), an increase in peak area was noted suggesting recombination reactions.

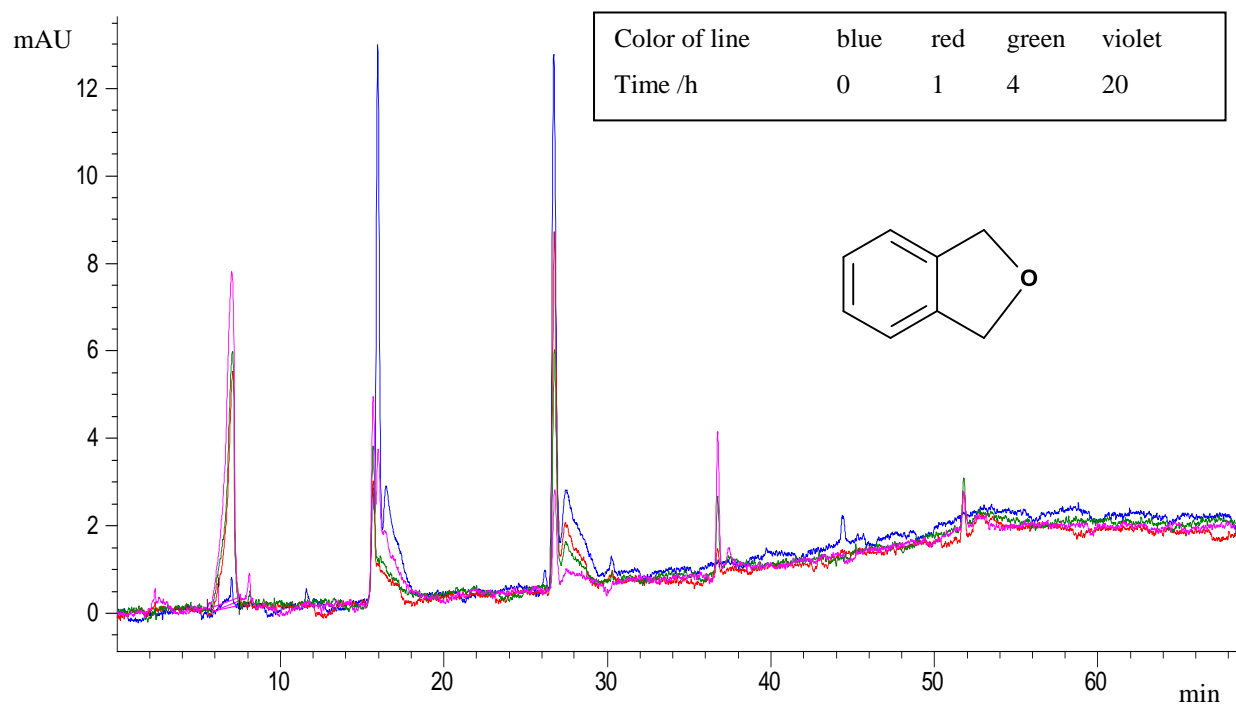


Figure 41: HPLC chromatograms of phthalan, consisting of samples after (0,1,4,20)h

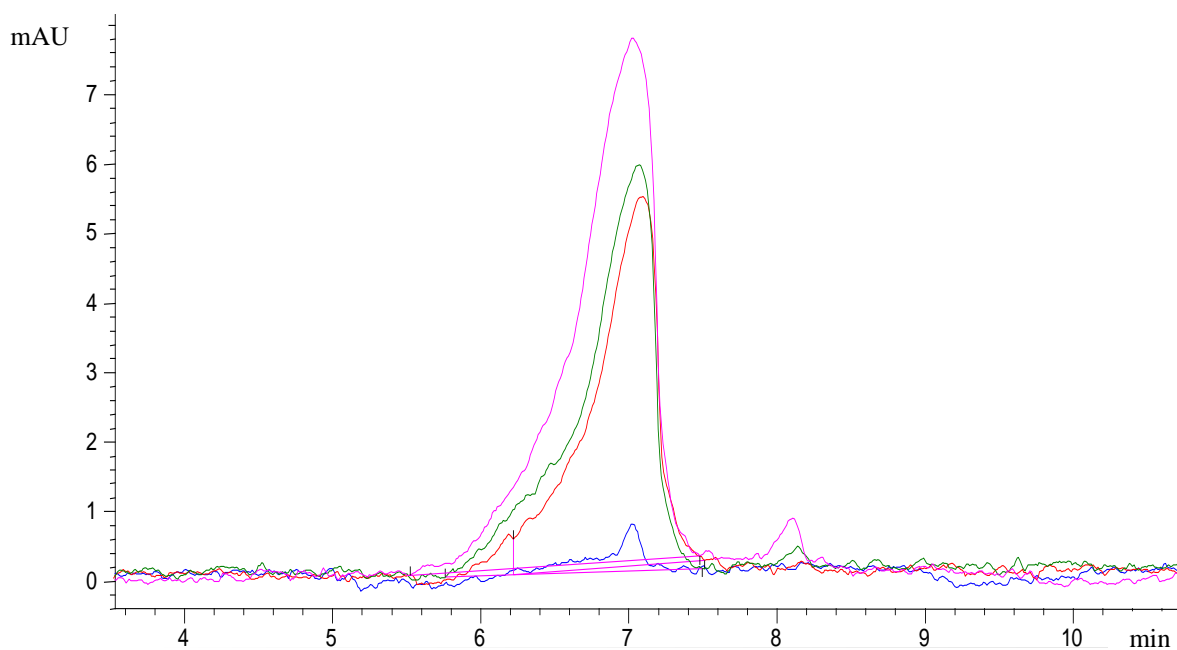


Figure 42: Enlarged chromatogram of phthalan within 0-11min retention time.

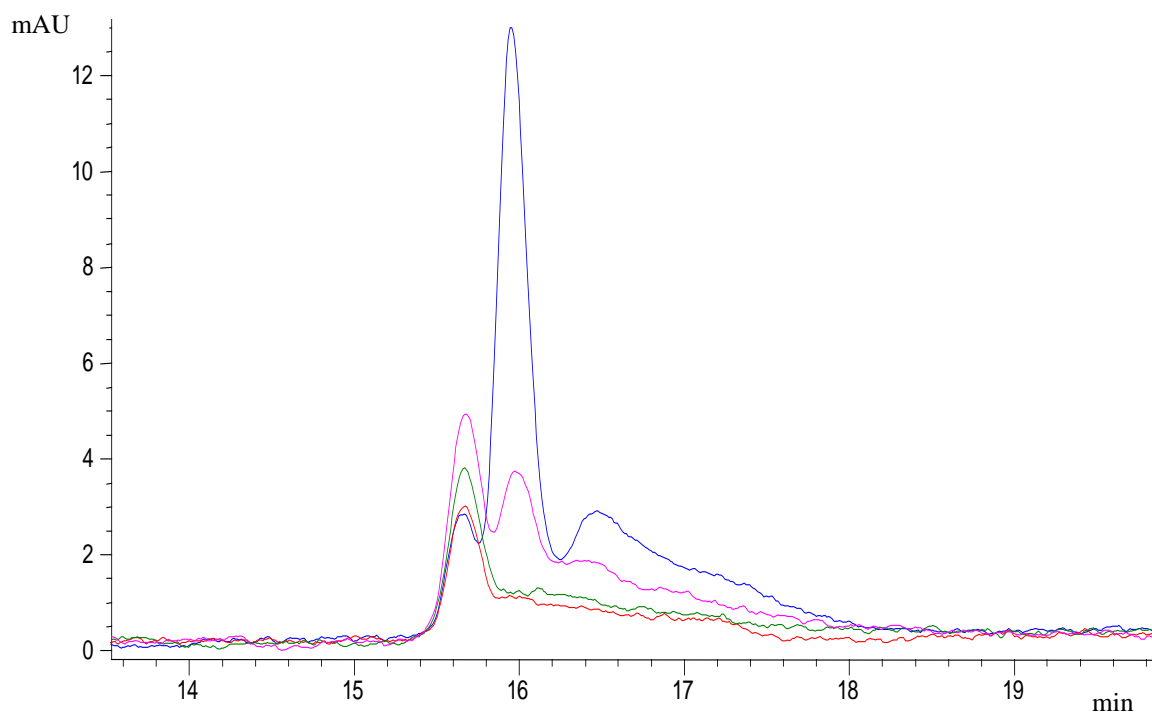


Figure 43: Enlarged chromatogram of phthalan within 13-20 min retention time

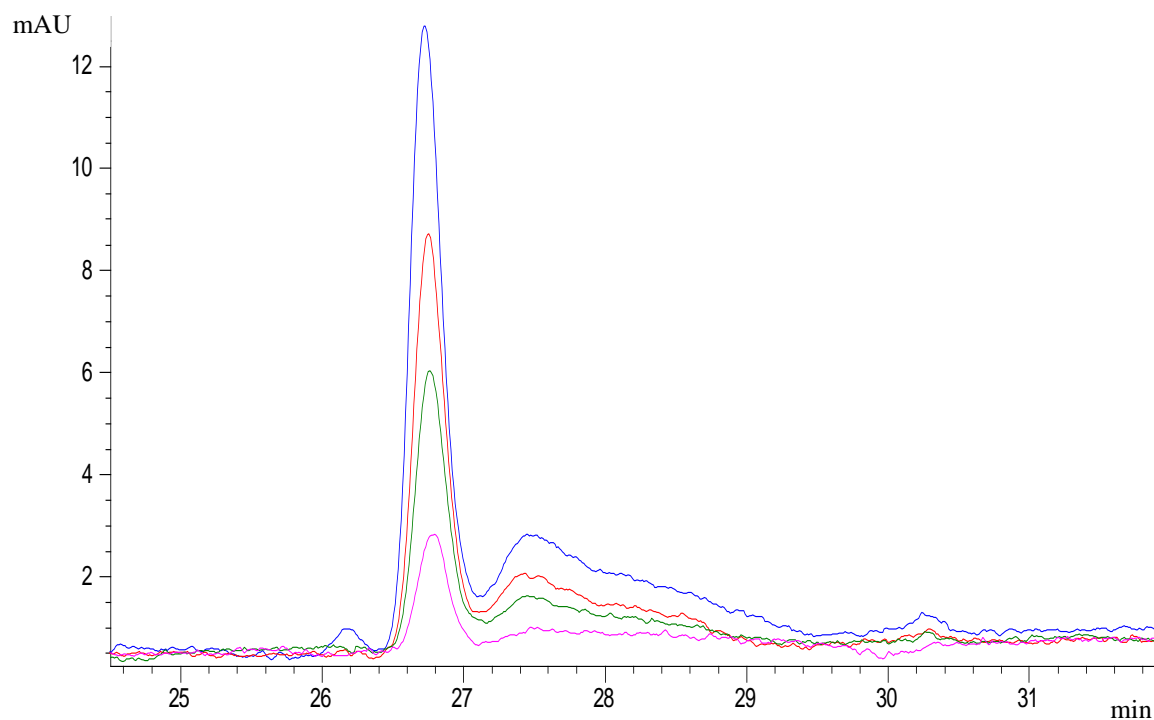


Figure 44: Enlarged chromatogram of phthalan within 25-32 min retention time

13.3.3. Aryl-aryl ether bonds

13.3.3.1. Procedure of reaction

0.5g diphenylether (DPE) was dissolved in 20mL in MeOH and re-suspended in 480mL water. Upon addition of water, a white precipitate was formed which was filtered. The filtrate solution was recirculated in the photocatalytic reactor. 4x10mL of sample was pipetted at

intervals; $t = 0\text{h}$, 1h , 4h , 20h from the reaction mixture and analyzed via HPLC by the method described in chapter 7.2.

13.3.3.2. Results

The HPLC chromatograms resulting from the photocatalysis of DPE are depicted in Figure 45 and Figure 46. The following findings can be said about the experiment:

- The r.t. of DPE is at 53 min.
- DPE peak reduced with time indicating degradation.
- The peak at r.t. 37 min cannot be directly linked DPE oxidation.

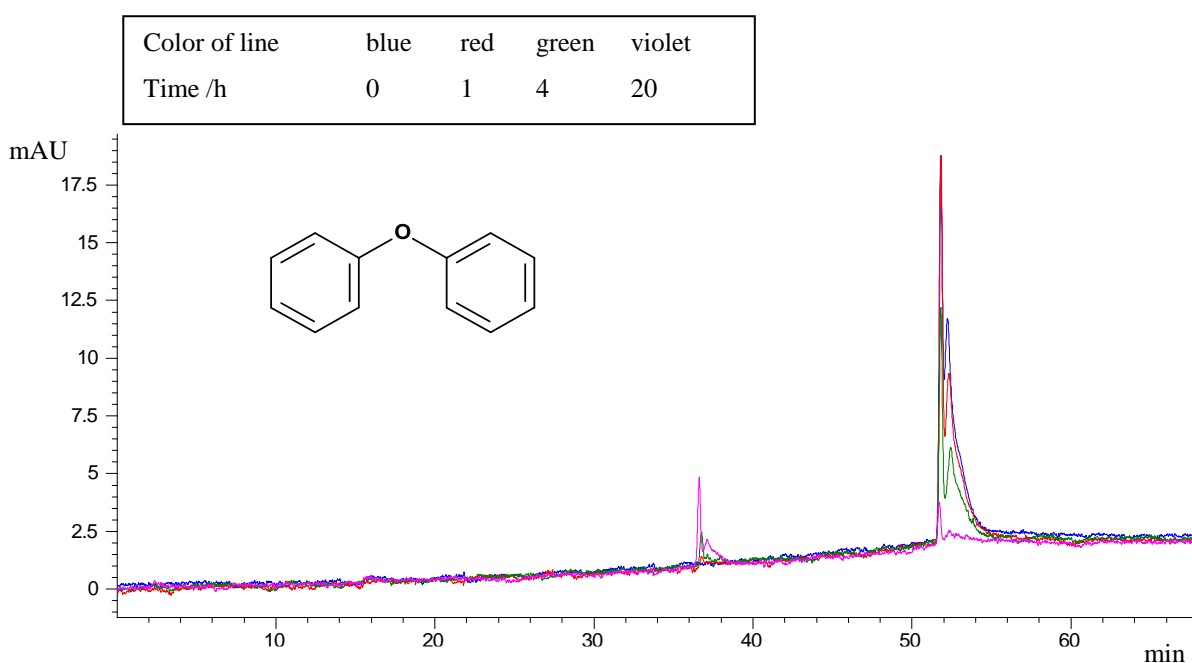


Figure 45: HPLC chromatograms of diphenylether (DPE) after (0,1,4,20)h

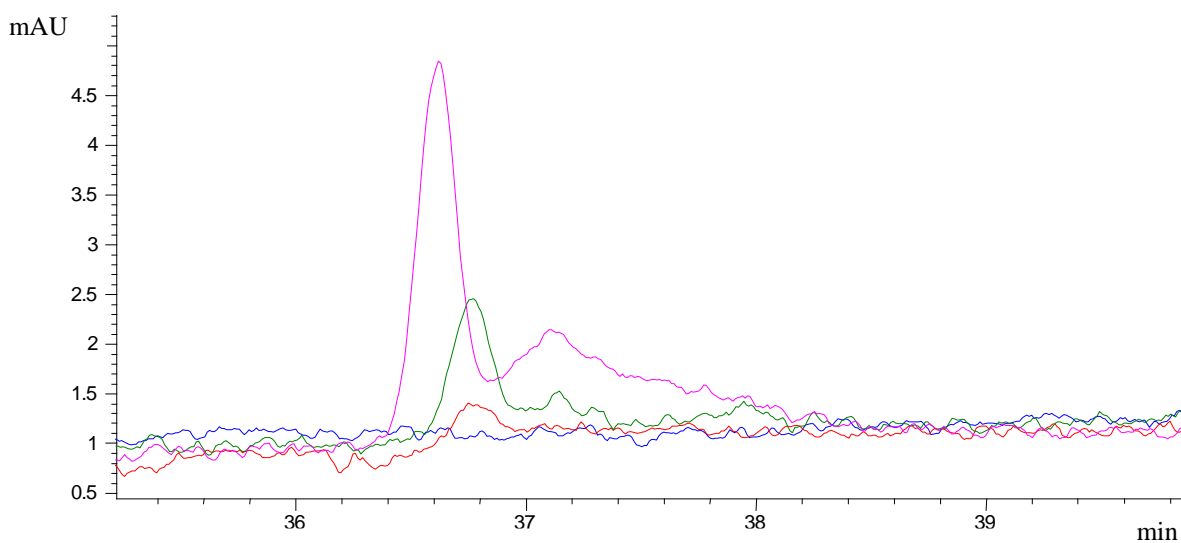


Figure 46: Enlarged chromatogram of DPE within 37-40 min retention time

13.3.4. Aryl-Alkyl ether bond

13.3.4.1. Procedure of reactions

0.5g benzylphenylether (BPE) was dissolved in 20mL in MeOH and re-suspended in 480mL water. Upon addition of water, a white precipitate was formed which was filtered. The filtrate solution was then recirculated in the photocatalytic reactor. 4x10mL of sample was pipetted at intervals; $t = 0\text{h}$, 1h, 4h, 20h from the reaction mixture and analyzed via HPLC by the method described in chapter 7.2.

13.3.4.2. Results

The HPLC chromatograms resulting from the photocatalysis of DPE are depicted in Figure 47 and Figure 48. The following findings can be said about the experiment:

- A BPE peak at r.t. ~52min which reduced with time. The small area units recorded is as result of filtration which considerably reduced the starting concentration of BPE.
- New peaks at r.t. 2, 28, 38 min were observed.
- BPE peak reduces with time while product peak increase (r.t. 2, 28).

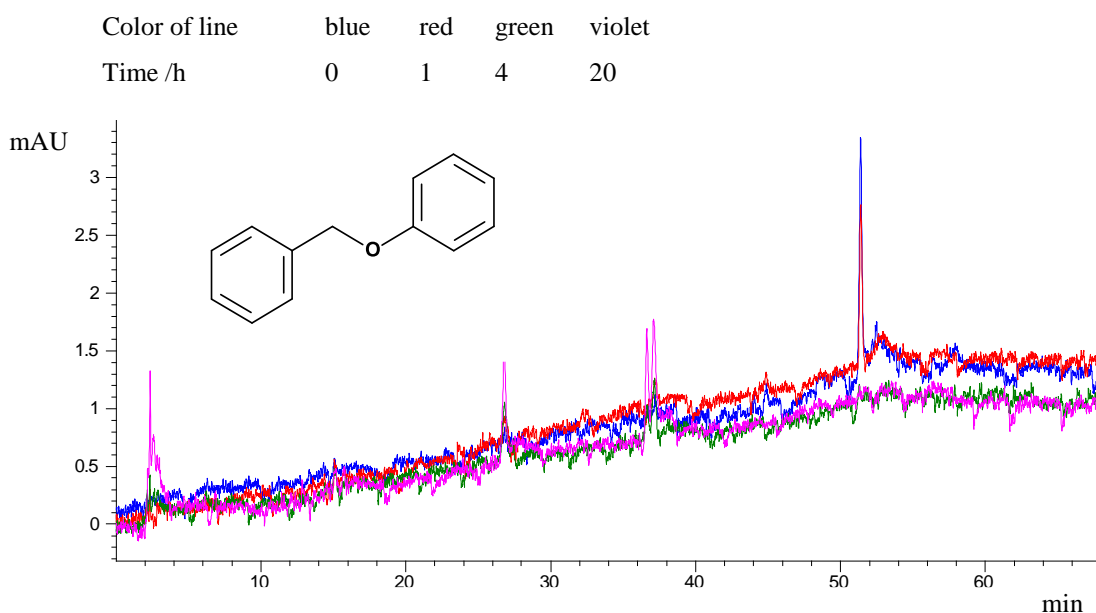


Figure 47: HPLC Chromatogram of BPE samples after (0,1,4,20)h

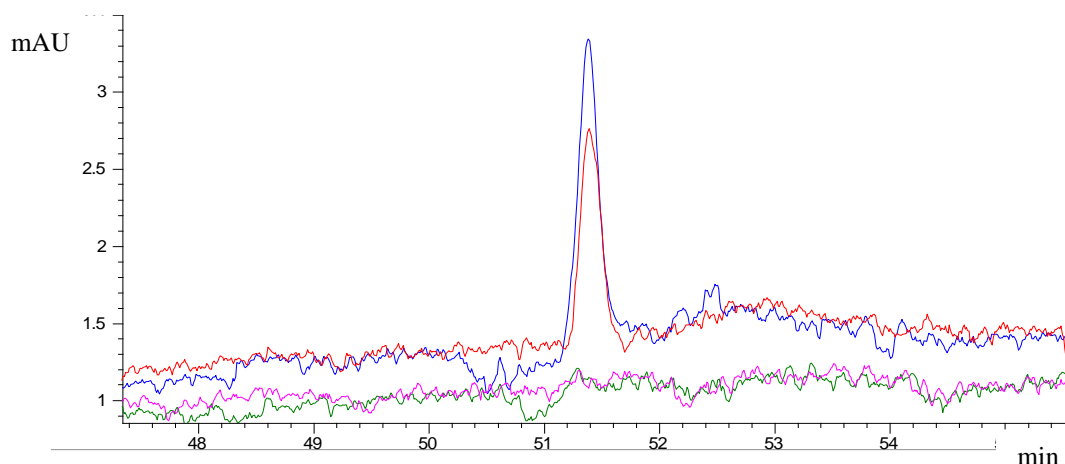


Figure 48: Enlarged chromatogram of BPE within 47-55 min retention time

13.3.5. Phenyl-phenyl bond

13.3.5.1. Procedure of reactions

0.5g diphenylmethane (DPM) was dissolved in 20mL in MeOH and re-suspended in 480mL water. Upon addition of water, a white precipitate was formed which was filtered. The filtrate solution was then recirculated in the photocatalytic reactor. 4x10mL of sample was pipetted at intervals; $t = 0\text{h}$, 1h, 4h, 20h from the reaction mixture and analyzed via HPLC by the method described in chapter 7.2.

13.3.5.2. Results

The HPLC chromatograms resulting from the photocatalysis of DPM are depicted in Figure 49. The following findings can be said about the experiment:

- A DPM peak at r.t. $\sim 55\text{min}$ which reduced with time.
- New peaks at r.t.: 2min and 38 min were observed.

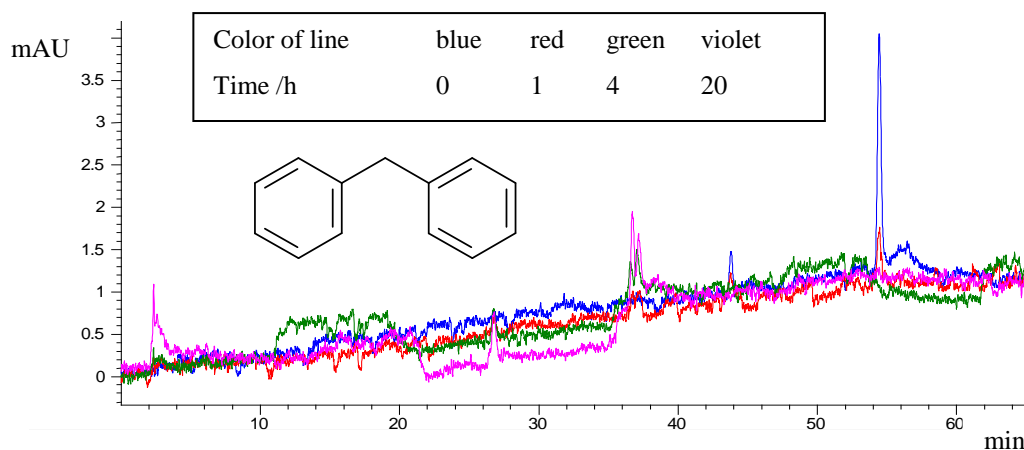


Figure 49: HPLC chromatograms of DPM samples after (0,1,4,20)h

13.4. Discussion

Most lignin standard compounds used in this study are non water soluble and thus the introduction of an organic solvent was done (methanol was used) in order to dissolve the compounds. With the use of an organic solvent, the degradation of the substrate to be studied can be compromised. This is because photocatalytic degradation shall involve both the substrate and the organic solvent. As consequence, low conversions can be attained. Additionally, due to the radical reaction pathway, side products may be formed thus complicating analysis. In this study methanol as a polar protic solvent was used and applied in minimal quantities just enough to dissolve the standard substances. Infact the HPLC chromatogram of methanol shows a peak at r.t. between 2-3min. This peak is pronounced in some chromatograms such as that of diphenyl methane. Methanol was chosen as a solvent because it is a one carbon molecule and simplest solvent with regards to possible product which may arise from its degradation and combination reactions with radical species from the standard compounds. Another reason is that, it was the mobile phase during HPLC analysis.

Due to the formation of precipitates when water was added to the reactant solution, filtration was necessary (e.g in BPE and DPM) because flow within the pores of the glass particles was impaired. As a result of filtration, the initial concentrations of the standard compounds were considerably reduced leading to small area units of peaks were recorded. Another setback during analysis was the peak at r.t.~37-38min originating from the photocatalytic reaction system. This peak was present in blank experiments whereby water was circulated in the photocatalytic reaction system under the presence of UV-light or with use methanol in the absence or presence of UV light. This peak could mask peaks originating from the photocatalytic degradation of standard compounds. For example, a substance like xylyol had a r.t. of ~ 37min (from the HPLC method used in this study: chapter 7.2). Another point to note during this study was the similarities of the r.t. of standard substances. For example, BPE and DPE both had r.t. of 52min. This means product identification from lignin sulfonate photocatalysis by simple peak superposition is not possible. In this case other analytical methods such as mass spectroscopy are imperative.

13.5. Conclusion

The photocatalysis of some standard substances gave rise to new peaks hence new products (e.g. in eugenol, BPE and DPM) while in DPE, only degradation of the original peak was observed.

14. Summarizing conclusion and outlook

14.1. Summarizing conclusion

This work was aimed to develop a photocatalytic reaction system which could effectively depolymerize lignin into value added chemicals such as phenolic derivatives or thermosets like phenolic resins thus proposing a processing concept for lignin conversion.

A description of the reaction design was done in chapter 8.2.2 and it was found out that the circulating packed bed reactor followed laminar flow conditions with Reynolds number 56.

Determining photonic efficiency through radiometric (mathematically) procedures from lignin degradation experiments poses a major challenge because of the undefined molar mass of lignin. In this work, methylene blue (MB) was chosen as test substance and its rate expression was used.

Chapter 9 treated the synthesis and characterization of catalysts which was mainly through the sol-gel hydrolysis pathway. In total, 35 different catalysts were synthesized. The advantage of sol-gel in catalyst preparation was exploited to combine catalyst to act as co-catalyst. Commercial obtainable $\text{TiO}_2\text{-P25}$ widely applied in suspension systems was effectively immobilized on sintered glass support with the aid of tetraethylortosilicate (TEOS) solution which acted as support material. The catalytic films had very good adherence on the sintered glass and the films retained a constant efficiency when re used after washing with water. The coatings were considerably well distributed all over the surface of the sintered glass. This is very promising for their potential use as immobilized catalyst in batch or flow reactors.

Prior to lignin degradation experiments, a comparative quality test of catalysts on their effectiveness and photocatalytic activity was done with methylene blue (MB) as substrate. Ten out of 35 synthesized catalytic coatings effectively degraded MB. New absorption peaks in the UV-spectrum suggested the formation of intermediate products which disappeared in course of reaction indicating destruction of MB dye and intermediate products.

A comparative assessment of the catalyst regarding the degradation rates of lignin sulfonate directly obtained from paper waste water was done with the following catalyst: $\text{TiO}_2\text{-P25-SiO}_2\text{+Pt}$, $\text{TiO}_2\text{-P25-SiO}_2$, $\text{TiOSO}_4\text{-30.6wt\%}$ and $\text{ZnO+TiO}_2\text{-P25-SiO}_2$. UV-Vis spectroscopy revealed a faster transformation of the aliphatic side chains as compared to the aromatic species. Adding Pt as metal ion to $\text{TiO}_2\text{-P25-SiO}_2$ catalyst showed a negligible effect

on degradation rates. The reaction rate of the catalytic systems was in the order $\text{TiO}_2\text{-P25-SiO}_2 + \text{Pt} \sim \text{TiO}_2\text{-P25-SiO}_2 > \text{ZnO} + \text{TiO}_2\text{-P25-SiO}_2 > \text{TiOSO}_4\text{-30.6wt\%}$.

Peaks were observed on HPLC and fluorescence chromatograms suggesting the production of new substances and fluorophores. Through simultaneous reaction-extraction pathways applying dialysis filtration and highly porous polystyrene divinylbenzene adsorbent resin (HR-P), an attempt was made to isolate smaller molecules produced from photocatalytic degradation.

Chapter 13 treated the photocatalytic study of some lignin standard compounds in order to get information about their retention time as a means to identify products arising from the photocatalytic degradation of lignin through peak superimposition. The goals of the experiments were reached; some standard substances gave rise to new peaks suggesting the formation of new products (e.g. in eugenol, BPE and DPM). Contrary to that, only the degradation of the original peak was observed in DPE which indicated transient compounds were not formed and degradation directly lead to the formation of CO_2 and H_2O theoretically.

Despite developed analytical technologies, analyzing lignin degradation products remains challenging. Proofs such as mass spectroscopy (MS), HPLC, ^{13}C or ^1H -NMR spectra from the photocatalytic degradation of lignin are not yet established. The set back to qualitatively and quantitatively analyze lignin and its degradation products starts from the native lignin polymer itself with its polymeric structure and multiple bond types. Also, the influence of different pretreatment additives and the wide variety of compounds obtainable from its degradation [123]. Moreover, lignin streams could contain proteins, inorganic salts, and other potential poisons that generally complicate catalysis [22].

It is also worth noting the challenge to identify and separate the product streams derived from the photocatalytic degradation lignin. Lignin product stream is highly functionalized and conventional techniques such as gas chromatography have the disadvantage of requiring a time consuming derivatization step. Also, because of the high boiling point of substances arising from lignin degradation, it is not easily applicable. High performance liquid chromatography (HPLC) [124] seems to be the remedy because analysis can be carried out without derivatization but the exact identification of the separated substances was difficult because of the numerous peaks arising from such a chromatogram. Unfortunately well established data bases such as that of the national institute of standard and technology (NIST) [125] cannot give information on HPLC-MS chromatograms. This is because ionization sources such as electrospray ionization (ESI) and atmospheric pressure chemical ionization (APCI) for LC-MS depends strongly on the type system used. Parameters such as cone

voltage, sample preparation, mobile phase (eluent) must be appropriately chosen. GC-MS is based on electron ionization (EI) and does not necessitate much details but the sample needs to be in the gas phase.

14.2. Outlook

Though product identification based on peak superposition gives information about a possible product, this is difficult to realize with lignin photo- degradation products because of the large number of possible products and also because some of these products may have same retention time. In order to properly identify products from lignin degradation, product isolation techniques such as column chromatography and subsequent structure research techniques such as $^1\text{H-NMR}$, $^{13}\text{C-NMR}$ spectroscopy needs to be further investigated. Alternatively, a database of model lignin compounds based on a unanimous HPLC-MS measuring procedure can be developed. This would mean much time and cost expensive investments for adequate personnel and material. However both solutions described cannot be true for all photocatalytic reaction systems because ionic species and compounds formed depends strongly on the photocatalytic system (light source, intensity, type and source of lignin used, catalyst used, etc.).

Another future concept is the coupling of photocatalysis with a consecutive catalytical process such as a biocatalysis. Photocatalyzed lignin may be an appropriate substrate for a consecutive biocatalytical process using ligninolytic enzymes such as H_2O_2 -dependent ligninolytic heme peroxidases and O_2 -dependent laccases (POX and/or Lac) as supported by experimental results of Kamwilaisak and Wright [126]. Depending on lignin treatment specification, photocatalysis can find application for complete lignin mineralization to CO_2 and H_2O (single-stage) or as an integrated technology in a multi-stage system. Combining the advantages of both catalytic processes, savings in the overall process costs will be expected in addition to elevated lignin conversion. Nonetheless, extensive research work including POX modifications are still required.

Determining the photonic efficiency of reaction systems involving lignin degradation through radiometric measurements remains a major challenge because of undefined measuring parameters. For clarity reasons, a standard method needs to be developed whereby specifications on parameters such as type and concentration of model substrate, power density of illumination are defined. This can then serve as reference to evaluate photonic efficiency.

15. References

1. **Prices, Crude Oil and Commodity.** Crude Oil and Commodity Prices. *http://www.oil-price.net*. [Online] oil-price.net, August 04, 2014. [Cited: August 04, 2014.] *http://www.oil-price.net*.
2. **Research, Directorate-General for.** *World energy, technology and climate policy outlook (WETO)*. Luxembourg : Office for Official Publications of the European Communities, 2003.
3. *http://www.polymersolutions.com/blog/green-and-natural-polymers-on-the-rise/*. [Online] [Cited: 08 08, 2014.]
4. **B. Kamm, M. Kamm, P.R. Gruber, S. Kromus.** *Biorefineries-Industrial Processes and Products Status Quo and Future Directions*. s.l. : Wiley-VCH Verlag GmbH, 2006. Vol. Volume 1. ISBN 13: 978-3-527-31027-2.
5. **R.L. Howard, E. Abotsi, E.L. Jansen van Rensburg, S. Howard.** Lignocellulose biotechnology: Issues of bioconversion and enzyme production. *African Journal of Biotechnology* 2. 2003, pp. 602-619.
6. **Stöcker, M.** Bio- und BTL-Kraftstoffe in der Bioraffinerie: Katalytische Umwandlung Lignocellulose-reicher Biomasse mit porösen Stoffen. *Angewandte Chemie* 120. 2008, pp. 9340-9351.
7. Lignocellulose conversion: An introduction to chemistry, process and economics *Bioproducts and Biorefining 1 (1)*. 39-48
8. **M. N. S. Kumar, A. K. Mohanty, L. Erickson, M. Misra.** Lignin and Its Applications with Polymers. *Journal of Biobased Materials and Bioenergy* Vol. 3, No. 1. 2009, pp. 1-24.
9. **Removal of color, COD and lignin of pulp and paper wastewater using wood ash. N. Tantemsapya, W. Wirojanagud, S. Sakolchai.** 2004, *Journal of Science and Technology* 26(Suppl. 1), pp. 1-12.
10. **Turchi, C. S. and Ollis, D. F.** Photocatalytic reactor design: An example of mass-transfer limitations with an immobilized catalyst. *Journal of Physical Chemistry*. 1998, 92, pp. 6852-6853.
11. **R. Subasri, M. Tripathi, K. Murugan, J. Revathi, G.V.N. Rao, T.N. Rao.** Investigations on the photocatalytic activity of sol-gel derived plain and Fe³⁺/Nb⁵⁺ doped titania coatings on glass substrates. *Materials Chemistry and Physics*. 2010, 124, pp. 63-68.
12. **Heller, A.** Chemistry and Applications of Photocatalytic Oxidation of Thin Organic Films. *Accounts of Chemical Research* 28. 1995, pp. 503-508.
13. **M.R. Hoffmann, S.T. Martin, W. Choi, D.W. Bahnemann.** Environmental Applications of Semiconductor Photocatalysis. *Chemical Reviews* Chem 95, vol. 1. 1995, pp. 69-96.
14. **K.V. Sarkanen, A. Islam, C.D. Anderson, in: S.Y. Lin, C.W.** *Methods in Lignin Chemistry*, P 387. Berlin : SpringerVerlag, 1992.
15. **A. Shende, R. Jaswal, D. Harder-Heinz, A. Menan, R. Shende.** Intergrated photocatalytic and microbial degradation of kraft lignin. *Cleantech*. 2012, pp. 120-123.
16. **R.J.A. Gosselink, E. de Jong, B. Guran, A. Abächerli.** Co-ordination network for lignin—standardisation, production and applications adapted to market requirements (EUROLIGNIN). *Industrial Crops and Products* 20. 2004, pp. 121-129.
17. **D. Fengel, G. Wegener.** *Wood: Chemistry, ultrastructure, reactions*. s.l. : Verlag Kessel, 1984. p. 615. ISBN 3110084813.
18. **Hill, C.** *Wood Modification. Chemical, Thermal, and Other Processes*. Chichester, U.K. : John Wiley & Sons, 2006.

19. **M. Dashtban, H. Schraft, T.A. Syed, W. Qin.** Fungal biodegradation and enzymatic modification of lignin. *International Journal of Biochemistry and Molecular Biology* 1(1). 2010, pp. 36-50.
20. **B. Saake, R. Lehnen.** *Lignin. Ullmann's Encyclopedia of Industrial Chemistry*. s.l. : Wiley-VCH Verlag GmbH & Co. KGaA, 2012.
21. **F. S Chakar, A. J. Ragauskas.** Review of current and future softwood kraft lignin process chemistry. *Industrial Crops and Product* 20. 2004, pp. 131-141.
22. **J. Zakzeski, P.C. Bruijninx, A. L. Jongerius, B. M. Weckhuysen.** The Catalytic Valorization of Lignin for the Production of Renewable Chemicals. *Chemical Review* 110. 2010, pp. 3552-3599.
23. **D.V. Evtuguin, Pascoal Neto, J. Rocha, J.D. Pedrosa de Jesus.** Oxidative delignification in the presence of molybdovanadophosphate heteropolyanions: mechanism and kinetic studies. *Applied Catalysis A* 167 (1). 1998, pp. 123-139.
24. **W.G. Glasser, H.R. Glasser.** Evaluation of lignin's chemical structure by experimental and computer simulation techniques. *Paperi ja Puu* 63. 1981, pp. 71-83.
25. **M. Erickson, S. Larsson, G.E. Miksche.** Zur Struktur des Lignins der Fichte. *Acta Chemica Scandinavica* 27, 903-914, 1973.
26. **Nimz, H.** Das Lignin der Buche - Entwurf eines Konstitutionsschemas. *Angewandte Chemie* vol 86, 336-344, 1974.
27. **Goring, D. A. I.** The physical chemistry of lignin. *Pure Applied Chemistry, Vol. 5, Issue 1-2.* 1962, pp. 233-310.
28. **M. Ek, G. Gellerstedt, G. Henriksson.** *Wood Chemistry and Biotechnology: Pulp and paper Chemistry and Technology, Vol 1.* Berlin : Walter de Gruyter GmbH & Co. KG, 2009. p. 308. ISBN: 978-3-11-021339-3.
29. **B. Neppolian, H.C. Choi, M.V. Shankar, B. Arabindoo, V. Murugesan.** Proceedings of International Symposium on Environmental Pollution Control and Waste Management (EPCOWM'2002). 2002, p. 647.
30. **Gallezot, P.** Catalytic routes from renewables to fine chemicals. *Catalysis Today* 121 (1-2). pp. 76-91.
31. **N. Busse, D. Wagner, M. Kraume, P. Czermak.** Reaction kinetics of versatile peroxidase for the degradation of lignin compounds. *American Journal of Biochemistry and Biotechnology* 9 (4). 2013, pp. 365-394.
32. **J. Rodrigues, J. Graça, H. Pereira.** Influence of tree eccentric growth on syringyl/guaiacyl ratio in Eucalyptus globulus wood lignin assessed by analytical pyrolysis. *Journal of Analytical and Applied Pyrolysis* (58-59). 2001, pp. 481-489.
33. **R. Alén, E. Kuoppala, P. Oesch.** Formation of the main degradation compound groups from wood and its components during pyrolysis. *Journal of Analytical and Applied Pyrolysis*, 36 (2). 1996, pp. 137-148.
34. **K. Pan, M.Tian, Z. H. Jiang, B. Kjartanson, A. Chen.** Electrochemical oxidation of lignin at lead dioxide nanoparticles photoelectrodeposited on TiO₂ nanotube arrays. *Electrochimica Acta* 60. 2012, pp. 147-153.
35. **D. Mantzavinos, E. Psillakis.** Enhancement of biodegradability of industrial wastewaters by chemical oxidation pre-treatment. *Journal of Chemical Technology and Biotechnology, Volume 79, Issue 5.* 2004, pp. 431-454.
36. **A. Dahm, La Lucia.** Titanium dioxide catalyzed photodegradation of lignin in industrial effluents. *Industrial and Engineering Chemistry* 43. 2004, pp. 7996-8000.
37. **Y.H. Xu, H.R. Chen, Z.X. Zeng, B. Lei.** Investigation on mechanism of photocatalytic activity enhancement of nanometer cerium-doped titania. *Applied Surface Science* 252 (24). 2006, pp. 8565-8570.

38. **Lucia Tonucci, Francesca Coccia, Mario Bressan, Nicola d'Alessandro.** Mild Photocatalysed and Catalysed Green Oxidation of Lignin: A Useful Pathway to Low-Molecular-Weight Derivatives. *Waste and Biomass Valorization* 3. 2012, pp. 165-174.
39. **A. Castellan, N. Colombo, C. Vanucci, P. Fournier de Violet, H. Bouas-Laurent.** Photodegradation of lignin. A photochemical study of an O-methylated α -carbonyl β -1 lignin model dimer: 1,2-di(3'4'-dimethoxyphenyl) ethanone (deoxyveratroyl). *Journal of Photochemistry and Photobiology A* 51. 1990, pp. 451-467.
40. **A. Fujishima, X. Zhang, D. A. Tryk.** TiO₂ photocatalysis and related surface phenomena. *Surface Science Reports* 63. 2008, pp. 515-582.
41. **A. L. Linsebigler, G. Lu, J.T. Yates, Jr.** Photocatalysis on TiO₂ Surfaces: Principles, Mechanisms, and Selected Results. *Chemical Review*. 1995, 95, pp. 735-758.
42. **Serpone, N.** Relative photonic efficiencies and quantum yields in heterogeneous photocatalysis. *Journal of Photochemistry and Photobiology A*, 104. 1997, pp. 1-12.
43. **M. Hoffman, S. Martin, W. Choi, D. Bahnemann.** Environmental applications of semiconductor photocatalysis. *Chemical Reviews* 95. 1995, pp. 69-96.
44. **C.D. Jaeger, A. Bard.** Spin trapping and electron spin resonance detection of radical intermediates in the decomposition of water at titanium dioxide particulate systems. *Journal of Physical Chemistry* 83. 1979, pp. 3146-3152.
45. **Matthews, R.W.** Hydroxylation Reactions Induced by Near-ultraviolet Photolysis of Aqueous Titanium Dioxide Suspensions. *Journal of the Chemical Society, Faraday Transactions 1(80)*. 1984, pp. 457-471.
46. **A. Machado, Am Furuyama, S.Z. Falone, R. Ruggiero, D.D. Perez, A. Castellan.** Photocatalytic degradation of lignin and lignin models, using titanium dioxide: the role of the hydroxyl radical. *Chemosphere* 40. 2000, pp. 115-124.
47. **W., Sigg L. und Stumm.** Aquatische Chemie. Stuttgart. 2 Auflage. s.l. : B.G. Teubner, 1991, p. Page 288.
48. **O. Legrini, E. Oliveros, A.M. Braun.** Photochemical processes for water treatment. *Chemical Reviews* 93. 1993, pp. 671-698.
49. **G. Rothenberger, J. Moser, M. Grätzel, N. Serpone, D. Sharma.** Charge Carrier Trapping and Recombination Dynamics in Small Semiconductor Particles Chem. Soc. (107). *Journal of America Chemical Society*, 107 (26). 1985, pp. 8054-8059.
50. **Turchi, C. und Ollis, D.** Photocatalytic degradation of organic water contaminants-Mechanisms involving hydroxyl radical attacks. *Journal of Catalysis* 122 (1). 1990, pp. 178-192.
51. **Turner, J.C.R.** An introduction to the theory of catalytic reactors. [book auth.] M. Boudart J.R. Anderson. *Catalysis Science and Technology*, vol. 1. s.l. : Springer-Verlag, Berlin, Germany, pp. 43-86. , 1981, pp. 709-711.
52. **K.J., Laidler.** Chemical Kinetics, 3rd edition, p.277. 1987 : 3rd ed., Harper & Row.
53. **D. Bahnemann, A. Henglein, J. Lilie, L. Spanhel.** Flash photolysis observation of the absorption spectra of trapped positive holes and electrons in colloidal TiO₂. *The Journal of Physical Chemistry* 88. 1983, pp. 709-711.
54. **P. Mazelier, M. Sarakha, A. Rossi, M. Bolte.** The aqueous photochemistry of 2,6-dimethylphenol. Evidence for the fragmentation of the Alpha C-C bond. *Journal of Photochemistry and Photobiology A*, 115. 1998, pp. 117-121.

55. **Y. Miyata, K. Miyazaki, M. Miura, Y. Shimotori, M. Aoyama, H. Nakatani.** Solventless Delignification of Wood Flour with TiO₂/poly(ethyleneoxide) Photocatalyst System. *Journal of Polymers and Environment* 21 (1). 2012, pp. 115-121.
56. **M. Tien, T. K. Kirk.** Lignin-degrading enzyme from phanerochaete chrysosporium: Purification, characterization, and catalytic properties of a unique H₂O₂-requiring oxygenase. *Proceedings of the National Academy of Sciences(PNAS)* 81. 1984, pp. 2280-2284.
57. **T. K. Kirk, M. Tien, P. J. Kersten, M. D. Mozuch, B. Kalyanaraman.** Ligninase of Phanerochaete chrysosporium. Mechanism of its degradation of the non-phenolic arylglycerol beta-aryl ether substructure of lignin. *Biochemical Journal* 236 (1). 1986, pp. 279-287.
58. **T. Lundell, R. Wever, R. Floris, P. Harvey, A. Hatakka.** Lignin peroxidase L3 from *Phlebia radiata*. Pre-steadystate and steady-state studies with veratryl alcohol and a non-phenolic lignin model compound 1-(3,4-dimethoxyphenyl)-2-(2-methoxyphenoxy)propane-1,3-diol. *European Journal of Biochemistry* 211. 1993b, pp. 391-402.
59. **H. E. Schoemaker, T.K. Lundell, A.I. Hatakka, K. Piontek.** The oxidation of veratryl alcohol, dimeric lignin models and lignin by lignin peroxidase: The redox cycle revisited. *FEMS Microbiology Reviews* 13. 1994b.
60. **J.M. Palmer, P.J. Harvey and H.E. Schoemaker.** The role of Peroxidases, Radical Cations and Oxygen in the Degradation of Lignin [and Discussion]. *Philosophical Transactions of the Royal Society Lond. A* 321 (1561). 1987, pp. 495-505.
61. **M. Tien, T. K. Kirk.** Lignin-degrading enzyme from Phanerochaete chrysosporium: Purification, characterization, and catalytic properties of a unique H₂O₂-requiring oxygenase. *Proceedings of the National Academy of Sciences(PNAS)* 81. 1984, pp. 2280-2284.
62. **M.E. Snook, G.A. Hamilton.** Oxidation and fragmentation of some phenyl-substituted alcohols and ethers by peroxydisulfate and Fenton's reagent. *Journal of The American Chemical Society* 96. 1974, pp. 860-869.
63. **Y. S. Ma, C. N. Chang, Y. P. Chiang, H. Fan Sung, A. C. Chao.** Photocatalytic degradation of lignin using Pt/TiO₂ as the catalyst. *Chemosphere* 71(5). 2008, pp. 998-1004.
64. **S.K. Kansal, M. Singh, D. Sud.** Studies on TiO₂/ZnO photocatalysed degradation of lignin. *Journal of Hazardous Materials* 153. 2008, pp. 412-417.
65. **K. Tanaka, R. C.R. Calanag, T. Hisanaga.** Photocatalyzed degradation of lignin on TiO₂. *Journal of Molecular Catalysis A: Chemical* 138. 1999, pp. 287-294.
66. **E. Portjanskaja, S. Preis.** Aqueous Photocatalytic Oxidation of Lignin: The Influence of Mineral Admixtures. *International Journal of Photoenergy*, article ID 73760. 2007, pp. 1-7.
67. **H. Ohnishi, M. Matsumura, H. Tsubomura, M. Iwasaki.** Bleaching of Lignin Solution by a Photocatalyzed Reaction on Semiconductor Photocatalysts. *Industrial and Engineering Chemistry Research* 28. 1989, pp. 719-724.
68. **C. A. K. Gouvêa, F. Wypycha, S. G. Moraes, N. Durán, P. Peralta-Zamora.** Semiconductor-assisted photodegradation of lignin, dye, and kraft effluent by Ag-doped ZnO. *Chemosphere* 40. 2000, pp. 427-432.
69. **M. Ksibi, S. Ben Amor, S. Cherif, E. Elaloui, A. Houas, M. Elaloui.** Photodegradation of lignin from black liquor using a UV/TiO₂ system. *Journal of photochemistry and photobiology A* 154. 2003, pp. 211-218.

70. **A. V. Vähätalo, K. Salonen, M. Salkinoja-Salonen, A. Hatakka.** Photochemical mineralization of synthetic lignin in lake water indicates enhanced turnover of aromatic organic matter under solar radiation. *Biodegradation* 10. 1999, pp. 410-420.
71. **M.Tian, J. Wen, D. MacDonald, R. M. Asmussen, A. Chen.** A novel approach for lignin modification and degradation. *Electrochemistry Communications* 12. 2010, pp. 527-530.
72. **C. Awungacha Lekelefac, P. Czermak, M. Herrenbauer.** Photocatalytic active coatings for lignin degradation in circulating packed bed reactor. *International Journal of Photoenergy*. Article ID 502326. in press.
73. **C. Awungacha Lekelefac, P. Czermak, M. Herrenbauer.** Evaluation of Photocatalytic Active Coatings on Sintered Glass Tubes by Methylene Blue. *International Journal of Photoenergy*, Article ID 614567. 2013, p. 9 pages.
74. **DeLasa, H., B. Serrano, M. Salaices.** *Photocatalytic Reaction Engineering*. s.l. : Springer US, 2005. ISBN: 978-1-4419-3627-1.
75. **K. Hashimoto, H. Irie, A. Fujishima.** TiO₂ Catalysis: A historical overview and future 44 (12). *Japanese Journal of Applied Physics*. 2005, pp. 8269-8285.
76. **M.A. Behnajady, N. Modirshahla, R. Hamzavi.** Kinetic study on photocatalytic degradation of c.i. acid yellow 23 by ZnO photocatalyst. *Journal of Hazardous Materials* 133 (1-3). 2006, pp. 226-232.
77. **M. Addamo, V. Augugliaro, A. Di Paola, E. García-López, V. Loddo, G. Marci, L. Palmisano.** Photocatalytic thin films of TiO₂ formed by a sol-gel process using titanium tetraisopropoxide as the precursor. *Solid Thin films* 516. 2008, pp. 3802-3807.
78. **N. Negishi, K. Takeuchi, T. Ibusuki.** Preparation of TiO₂ thin film photocatalyst by the dip coating process. *Journal of Sol-Gel Science and Technology* 13. 1998, pp. 691-694.
79. **L. Rideh, A. Wehrer, D. Ronze, A. Zoulalian.** Photocatalytic degradation of 2-chlorophenol in TiO₂ aqueous suspension: modeling of reaction rate. *Industrial and Engineering Chemistry Research* 36 (11). 1997, pp. 4412-4418.
80. **R.A. Doong, C.H. Chen, R.A. Maithreepala, S.M. Chang.** The influence of pH and cadmium sulfide on the photocatalytic degradation of 2-chlorophenol in titanium dioxide suspensions, *Water Res.* 35 (12) (2001). 2001.
81. **G. Gellerstedt, E.L. Lindfors.** Structural changes in lignin during kraft pulping. *Holzforschung* 38. 1984, pp. 151-158.
82. **C. Pouteau, P. Dole, B. Cathala, L. Averous, N. Boquillon.** Antioxidants properties of lignin polypropylene. *Polymer Degradation and Stability* 81. 2003, pp. 9-18.
83. **J. Hafrén, T. Fujino, T. Itoh.** Changes in cell wall architecture of differentiating tracheids of *Pinus thunbergii* during lignification. *Plant Cell Physiology* 40. 1999, pp. 532-541.
84. **T. Dizhbite, G. Telysheva, V. Jurkjane, U. Viesturs.** Characterization of the radical scavenging activity of lignins natural antioxidants. *Bioresource Technology* 95. 2004, pp. 309-317.
85. **K. Hofstadler, R. Bauer, S. Novalic, S.G. Heisier.** New reactor design for photocatalytic wastewater treatment with TiO₂ immobilized on fused-silica glass fibres: photomineralisation of 4-Chlorophenol. *Environmental Science Technology* 28 (4). 1994, pp. 670-674.
86. **J. Villasenor, H.D. Mansilla.** Effect of temperature on kraft black liquor degradation by ZnO-photoassisted catalysis. *Journal of Photochemistry and Photobiology A*, 93. 1996, pp. 205-209.

87. **B.H. Bielski, D.E. Cabelli, L.A. Ravindra, A.B. Ross.** Reactivity of HO₂/O₂⁻ Radicals in aqueous solution. *Journal of Physical Chemistry* 14. 1985, pp. 1041-1100.
88. **B.H. Bielski, A.O. Allen.** Mechanism of the disproportionation of superoxide radicals. *Journal of Physical Chemistry* 81 (11). 1977, pp. 1048-1050.
89. **B. Halliwell, J.M. Gutteridge.** The importance of free radicals and catalytic metal ions in human diseases. *Molecular Aspects of Medicine* 8. 1985, pp. 89-193.
90. **J. M. Palmer, P. J. Harvey and H. E. Schoemaker.** The role of Peroxidases, Radical Cations and Oxygen in the Degradation of Lignin [and Discussion]. *Philosophical Transaction of the Royal Society A*. 321 (1561). 1987, pp. 495-505.
91. **S.Y. Yin, C.W. Dense.** *Methods in Lignin chemistry*. s.l. : Springer Verlag, 1992. ISBN: 978-3-642-74067-1 (Print) 978-3-642-74065-7 (Online).
92. **P. Kumar, S. Kumar and N. K. Bhardwaj.** Photocatalytic oxidation of elemental chlorine free bleaching effluent with UV/TiO₂. *2nd International Conference on Environmental Science and Technology, IPCBEE vol.6*. 2011.
93. **K. Kobayakawa, Y. Sato, S. Nakamura, A. Fujishima.** Photodecomposition of kraft lignin catalized by titanium dioxide. *Bulletin of the Chemical Society of Japan* 62. 1989, pp. 3433-3436.
94. **Kinstre, R.B.** An overview of strategies for reducing the environmental impact of bleach-plant effluents. *Tappi Journal* 76, (5). 1993, pp. 105-113.
95. **A. Castellan, H. Choudhury, R.S. Davidson, S. Grelier.** Comparative study of stone-ground wood pulp and native wood 3. Application of fluorescence spectroscopy to a study of the weathering of stone-ground pulp and native wood. *Journal of Photochemistry and Photobiology A* (81). 1994, p. 123.
96. **B. Albinsson, S. Li, K. Lundquist, R. Stomberg.** The origin of lignin fluorescence. *Journal of Molecular Structure* 508. 1999, pp. 19-27.
97. **A. Houas, H. Lachheb, M. Ksibi, E. Elaloui, C. Guillard, J. M. Herrmann.** Photocatalytic degradation pathway of methylene blue in water. *Applied Catalysis B: Environmental* 31. 2001, pp. 145-157.
98. **V. Vuppala, M. G. Motappa, S. S. Venkata, P.H. Sadashivaiah.** Photocatalytic degradation of methylene blue using a zinc oxide-cerium oxide catalyst. *European Journal of Chemistry* 3(2). 2012, pp. 191-195.
99. **Rhodes, M.** *Introduction to Particle Technology*. s.l. : Wiley, 1989. ISBN 0-471-98482-5.
100. **F. Benyahia, K. E. O'Neill.** Enhanced Voidage Correlations for Packed Beds of Various Particle Shapes and Sizes. *Particulate Science and Technology* 23. 2005, pp. 169-177.
101. **P. Reeves, R. Ohlhausen, D. Sloan, K. Pamplin, T. Scoggins, C. Clark, B. Hutchinson, D. Green.** Photocatalytic destruction of organic dyes in aqueous TiO₂ suspensions using concentrated simulated and natural solar energy. *Solar Energy* 48 (6). 1992, pp. 413-420.
102. **Matthews, R. W.** Photooxidative degradation of coloured organics in water using supported catalysts. TiO₂ on sand. *Water Resource* 25 (10). 1991, pp. 1169-1176.
103. **M.C. Hidalgo, D. Bahnemann.** Highly photoactive supported TiO₂ prepared by thermal hydrolysis of TiOSO₄: Optimisation of the method and comparison with other synthetic routes. *Applied Catalysis B: Environmental* 61 (3-4). 2005, pp. 259-266.
104. **M.C. Hidalgo, S. Sakthivel, D. Bahnemann.** Highly photoactive and stable TiO₂ coatings on sintered glass. *Applied Catalysis A-General*. 2004, 277, pp. 183-189.
105. **Murry, John Mc.** *Organic chemistry, 7th edition*. 2008.

106. **PSA Ciemat, Plataforma Solar de Almeria.** Solar Photocatalysis.
http://www.psa.es/webesp/areas/tsa/docs/solar_photocatalysis.pdf. [Online]
107. **S.R. Yoganarasinhan, C.N.R Rao.** Mechanism of crystal structure transformations. Part 3. Factors affecting the anatase-rutile transformation. *Transactions of the Faraday Society* 52. 1962, pp. 1579-1589.
108. **Y. Hu, H.L. Tsai, C. L Huang.** Phase transformation of precipitated TiO₂ nanoparticles. *Materials Science and Engineering A*, 344 (1-2). 2003, pp. 209–214.
109. **P.B. Dejohn, R.A. Hutchins.** Treatment of dye wasters with granular activated carbon. *Tex. Chem. Color.* 8. 1976, p. 69.
110. **Y.M. Slokar, A.M. Le Marechal.** Methods of decoloration of textile wastewaters. *Dyes and Pigments* 37. 1998, pp. 335-356.
111. **S.S. Patil, V.M. Shinde.** Biogegradation studies of anilin and nitrobenzene in aniline plant wastewater ny Gas Chromatography. *Environmental Science Technology* 22(10). 1988, pp. 1160-1165.
112. **M. Kerzhentsev, C. Guillard, J.M. Herrmann.** Photocatalytic pollutant removal in water at room temperature: Case study of the total degradation of the insecticide fenitrothion (phosphorothioic acid OO-dimethyl-O(3-methyl-4-nitro-phenyl) ester). *Catalysis Today* 27. 1996, pp. 215-220.
113. **J. Bennani, R. Dilert, T. M. Gesing, D. Bahnemann.** Physical properties, stability and photocatalytic activity of transparent TiO₂/ SiO₂ films. *Separation and Purification Technology* 67. 2009, pp. 173-179.
114. **R. Fretwell, P. Douglas.** An active, robust and transparent nanocrystalline anatase TiO₂ thin film. Preparation, characterisation and the kinetics of photodegradation of model pollutants. 2001, pp. 229-240.
115. **Mahmoodi, N.M.** Photocatalytic Degradation of Dyes Using Carbon Nanotube and Titania Nanoparticle. 2013, p. 224.
116. **I.K. Konstantinou, T.A. Albanis.** TiO₂ assisted photocatalytic degradation of azo dyes in aqueous solutions: kiinetic mechanistic investigations-a review. 2004.
117. **Teruhisa Ohno, Koji Sarukawa, Kojiro Tokieda, Michio Matsumura.** Morphology of a TiO₂ Photocatalyst (Degussa, P-25) Consisting of Anatase and Rutile Crystalline Phases. *Journal of Catalysis, Volume* 203, Issue 1. 2001, pp. 82-86.
118. **P.F. Britt, A.C. Buchanan, A. C., E.A. Malcolm.** Thermolysis of Phenethyl Phenyl Ether: A Model for Ether Linkages in Lignin and Low Rank Coal. *Journal of Organic chemistry* 60 (20). 1995, pp. 6523–6536.
119. **C. Yokoyama, K. Nishi, A. Nakajima, K. Seino.** Thermolysis of Organosolv Lignin in Supercritical Water and Supercritical Methanol. *Journal of the Japan Petroleum Institute* 41. 1998, pp. 243-250.
120. **A. R. Katritzky, R.A. Barcock, M. Balasubramanian, J.V. Greenhill, M. siskin, W. N. Olmstead.** Aqueous high-temperature chemistry of carbo- and heterocycles. 20. Reactions of some benzenoid hydrocarbons and oxygen-containing derivatives in supercritical water at 460°C. *Energy and Fuels* 8. 1994, pp. 487-497.
121. **J.M.L. Penninger, R.J.A. Kersten, H.C.L. Baur.** Reactions of diphenylether in supercritical water-mechanism and kinetics. *Journal of Supercritical Fluids* 16. 1999, pp. 119-132.
122. **S. Caccamese, R. Chillemi, F. M. Perna, S. Florio.** Resolution of phthalans obtained by ortho-litiathion of aryloxiranes by enantioselective high-performance liquid chromatography: Performances of various chiral stationary phases. *Journal of Chromatography A*, vol. 1216, Issue 15. 2009, pp. 3048–3053.
123. **S. Baumberger, A. Abaecherli, M. Fasching, G. Gellerstedt, R. Gosselink, B. Hortling, J. Li, B.Saake, E. De Jong.** Molar mass determination of lignins by size-exclusion chromatography: towards standardisation of the method. *Holzforschung* 61, 459-468, 2007.

-
124. **R. Pecina, P. Burtscher, G. Bonn, O. Bobleter.** GC-MS and HPLC analyses of lignin degradation products in biomass hydrolyzates. *Fresenius Zeitschrift für Analytische Chemie* (325). 1986, pp. 461-465.
125. **(NIST), The National Institute of Standards and Technology.** NIST Standard Reference Database. <http://www.nist.gov/srd/nist1a.cfm>. [Online] 02 2014. [Cited: 02 15, 2014.] <http://www.nist.gov/srd/nist1a.cfm>.
126. **K. Kamwilaisak, P.C. Wright.** Investigating Laccase and Titanium Dioxide for Lignin Degradation. *Energy & Fuels* 26 (4). 2012, pp. 2400-2406.

16. Acknowledgement

I shall start by thanking Michael (Prof. Dr. Ing. Herrenbauer) and Peter (Prof. Dr.-Ing. Czermak) for the opportunity to research on this interesting topic. I am grateful for their guidance and support throughout my PhD. This work was done at the University of Applied Sciences Mittelhessen (THM), in the laboratories of material science, surface interface and system design and at the institute of bioprocess engineering and pharmaceutical technology,(IBPT). I also thank Prof. Alter, Mrs. Donnerwert, and Mrs. Fröhlich for their laboratory equipment and space allocated to me especially at the beginning of my research work. This greatly contributed for a quick start in laboratory experiments. My appreciation also goes to Mr. Steffen Kerker for assisting me with his HPLC apparatus.

Many thanks to the entire lignin team (Johannes Hild, Christoph Steiner, Nadine Busse) and the many students who carried out project work during the execution of this thesis. Tuesday discussions definitely played a significant role for the preparation and accomplishment of this thesis. I thank the department of membrane filtration of the IBPT headed by M.Sc. Mehrdad Ebrahimi for lignin provision and its treatment.

I gratefully thank the Federal Ministry of Education and Research (BMBF) for funding (FKZ17N0310) this cooperation project between IBPT (Prof. Czermak) and the laboratories of material science, surface interface and system design (Prof. Herrenbauer). Many thanks to Sappi-Ehingen AG, Robu Filterglas GmbH, Hattert and Evonik industries for providing materials used in this work.

Last but not the least; my appreciation goes to my loving family; Louis, Noah, Danuta, Pastor Lange, my parents (Prodencia & Peter Kunju), and siblings (Achianga, Atemkeng, Ankhakem, Nchumbonga, Emengu, Atemzi, Tanyi) for their fullest support during this research period.

Porevolumes and Inner Surface

of the different Poresize-Classifications

Porosity Classification	Pore Volume (% void)	Inner Surface (BET)
Por. 00	~ 30%	~ 0,015 m ² /gr
Por. 0	~ 33%	~ 0,020 m ² /gr
Por. 1	~ 34%	~ 0,085 m ² /gr
Por. 2	~ 36%	~ 0,130 m ² /gr
Por. 3	~ 41%	~ 0,350 m ² /gr
Por. 4 / Por. M	~ 42%	~ 0,500 m ² /gr
Por. F	~ 45%	~ 1,200 m ² /gr
Por. 5 / Por. UF	~ 48%	~ 1,750 m ² /gr

Die angegebenen Werte können in Abhängigkeit von produkt- und einsetzspezifischen Merkmalen schwanken. Sie sind als annähernd zu verstehen und dienen lediglich der Orientierung.

The values given may change depending on application- and material specific properties. They are only of approximate value. Deviations from these orientation value are possible.



ROBU Glasfilter-Geräte GmbH
Schützenstrasse 13
D - 57644 Hattert
Germany

Tel. : .. 49 - (0)2662 - 8004-0
Fax : .. 49 - (0)2662 - 8004-40
Email : info@robuglas.com
Web : <http://www.robuglas.com>



Figure 50: Porevolumes and inner surface of Vitrapor® sinterfilter borosilicate glass 3.3

17. List of figures

Figure 1: Monomer structures of lignin [21].	5
Figure 2: Structure of a softwood lignin fragment showing the prominent linkage types, reprinted with permission from Zakzeski et al.[22] and Evtuguin et al.[23].	6
Figure 3: Lignocellulosic biorefinery scheme with particular emphasis on the lignin stream, reprinted with permission from Zakzeski et al. [22]. Copyright (2010). American Chemical Society.	8
Figure 4: Photocatalysis principle, adapted from Linsebigler et al. [41].	10
Figure 5: Formation of singlet oxygen, hydroxyl and superoxide radicals as principal reactive species in a photocatalytic process [42; 43].	11
Figure 6: Adsorption –diffusion reaction pathway in photocatalysis. Adapted from Turner [51].	12
Figure 7: Formation of phenoxyl radicals by intermolecular abstraction of phenolic hydrogen by carbonyl groups [54].	13
Figure 8: Supposed lignin degradation scheme by autooxidation induced by TiO ₂ / poly (ethylene oxide) [55].	13
Figure 9: Proposed radical reaction scheme initiated by enzyme (lignolytic heme peroxidase) for the conversion of adlerol possessing Cβ-O-4 bonds into smaller units, summarized by Busse et al. [31], abstracted from Tien and Kirk [56], Kirk et al.[57], Lundell et al.[58], Schoemaker et al.[59] and Palmer et al.[60].	14
Figure 10: Time dependent UV-Vis absorption spectra of aqueous lignin solution from waste paper water irradiated with UV light (280-420nm) for different time intervals. The spectra are obtained for sol-gel derived TiO ₂ nanocrystalline coating (TiO ₂ -P25-SiO ₂) [72].	27
Figure 11: Gradual change from the characteristic yellow lignin sulfonate to a colorless liquid after a period of 20h. Catalyst: TiO ₂ -P25 (Degussa)+TEOS, UV-light, room temperature (25°C), lignin concentration: 0.5g/L [72].	28
Figure 12: Variation of DC with time of aqueous lignin sulfonate solution from paper waste paper water irradiated with UV light (280-420nm) for different time intervals. The spectra are obtained for sol-gel derived TiO ₂ nanocrystalline coatings (TiO ₂ -P25-SiO ₂ +Pt, TiO ₂ -P25-SiO ₂ , TiOSO ₄ _30.6wt%, ZnO+TiO ₂ -P25-SiO ₂) [72].	29
Figure 13: Experimental setup for the photocatalytic degradation of lignin sulfonate.	37
Figure 14: Photocatalytic cycle process with integrated solid phase extraction and dialysis membrane	38
Figure 15: Photocatalytic reactor	39
Figure 16: Catalyst coating on sintered glass via pumping of gel in a circulatory manner through borosilicate glass tube.	48
Figure 17: SEM images for uncoated borosilicate sintered glass ((a) and (b)), TiO ₂ (TiOSO ₄ _30.6wt%) coating on borosilicate glass ((c)and (d)), TiO ₂ -P25-SiO ₂ ((e) and (f)), ZnO+TiO ₂ -P25-SiO ₂ ((g) and (h)).	49
Figure 18: The chemical structure of methylene blue (drawn with symyx draw).	52
Figure 19: Typical time dependent UV-Vis absorption spectra of aqueous MB solution irradiated with UV light (280-420nm) for different time intervals. The spectrum is obtained for sol-gel derived TiO ₂ from titanyloxysulphate	54
Figure 20: Absorption-time diagram, uncoated glass and no lights	55
Figure 21: Absorption-time diagram, coated glass and no lights	55
Figure 22: MB decolorization with TiOSO ₄ 30.6wt% + TiO ₂ -P25 catalyst.	56

Figure 23: Change in concentration of MB with time. MB initial concentration: 14mg/L, UV radiation $\lambda > 280\text{nm}-420\text{nm}$, recirculating reactor open to air, absorption at 665nm and immobilized catalysts.	57
Figure 24: Degradation kinetic of MB using diverse immobilized catalyst under UV light. MB initial concentration: 14mg/L, UV radiation $\lambda > 280\text{nm}-420\text{nm}$, recirculating reactor open to air, absorption at 665nm and immobilized catalysts.	57
Figure 25: Reaction rates of the photocatalytic degradation of MB(14mg/L) under UV light on immobilized catalysts.....	58
Figure 26: Photocatalytic reaction setup. Lignin sulfonate is pumped through the reactor using roller pumps in a continuous manner.	62
Figure 27: Time dependent UV-Vis absorption spectra of aqueous lignin sulfonate solution. Concentration: 0.5g/L in 200mL, reaction time: 20h, catalyst: sol-gel derived $\text{TiO}_2\text{-P25-SiO}_2$, reaction at room temperature, UV radiation (280-420nm).	63
Figure 28: Effect of different catalyst on percentage degradation of lignin sulfonate under UV light at wavelength 203nm (lignin sulfonate concentration: 0.5g/L in 200mL, reaction time: 20h, reaction at room temperature, UV radiation (280-420nm)).	64
Figure 29: Effect of different catalyst on percentage degradation of lignin sulfonate under UV light at wavelength 280nm (lignin sulfonate concentration: 0.5g/L in 200mL, reaction time: 20h, reaction at room temperature, UV radiation (280-420nm)).	65
Figure 30: Removal of dissolved carbon in lignin sulfonate. Concentration: 0.5g/L in 200mL, reaction time: 20h, reaction at room temperature, UV radiation (280-420nm).	66
Figure 31: Reaction rates of the photocatalytic degradation of lignin sulfonate (500mg/L) under UV light on immobilized catalysts. Concentration: 0.5g/L in 200mL, reaction time: 20h, reaction at room temperature, UV radiation (280-420nm).	67
Figure 32: 2 g/L lignin through reactor before illumination. Catalyst: $\text{TiO}_2\text{-P25-SiO}_2$, reaction at room temperature, absence of UV radiation, absence of dialysis filter and SPE with HP-R.....	69
Figure 33: HPLC chromatogram and fluorescence peaks of lignin sulfonate solution. Reaction volume: 200mL, Concentration of lignin sulfonate: 0.5g/L, reaction time: 4h, catalyst: $\text{TiO}_2\text{-P25-SiO}_2$, reaction at room temperature, presence of UV radiation, simultaneous reaction, dialysis filter and SPE with HP-R cartridge during reaction.....	70
Figure 34: Fluorescence chromatogram of lignin sulfonate degradation product. Emission spectrum, λ_{em} : 240nm, λ_{ex} : 330nm, concentration: 100mL 0.5g/L, reaction time: 20h, catalyst: $\text{TiOSO}_4\text{-30.6wt\%}$, reaction at room temperature.	72
Figure 35: Selection of sample molecules.....	77
Figure 36: Radical and ionic mechanism pathway with possible recombination products [119].	79
Figure 37: Radical and ionic mechanism pathway with possible recombination products.	80
Figure 38: HPLC chromatograms of eugenol consisting of samples after (0,1,4,20)h	82
Figure 39: Enlarged chromatogram of eugenol within 35-41 min retention time.	82
Figure 40: Enlarged chromatogram of eugenol within 53-60 min retention time.	83
Figure 41: HPLC chromatograms of phthalan, consisting of samples after (0,1,4,20)h	84
Figure 42: Enlarged chromatogram of phthalan within 0-11 min retention time.	84
Figure 43: Enlarged chromatogram of phthalan within 13-20 min retention time	85

Figure 44: Enlarged chromatogram of phthalan within 25-32 min retention time	85
Figure 45: HPLC chromatograms of diphenylether (DPE)after (0,1,4,20)h	86
Figure 46: Enlarged chromatogram of DPE within 37-40 min retention time	86
Figure 47: HPLC Chromatogram of BPE saples after (0,1,4,20)h	87
Figure 48: Enlarged chromatogram of BPE within 47-55 min retention time	88
Figure 49: HPLC chromatograms of DPM saples after (0,1,4,20)h	88
Figure 50: Porevolumes and inner surface of Vitrapor® sinterfilter borosilicate glass 3.3	102

18. List of tables

Table 1: Overview of most frequent bond types found in lignin.....	6
Table 2: Summary of starting conditions for the photocatalytic degradation of lignin derivatives.....	16
Table 3: Parameters, analytical methods and results from different work groups.	18
Table 4: Laboratory equipment.....	30
Table 5: Table of materials used.....	31
Table 6: Table of chemicals used.....	32
Table 7: Parameters for flow characterization in the photocatalytic reactor.	40
Table 8: Data obtained for the calculation of photonic efficiency (rate of degradation to incident photonic flux) of the different catalyst with MB as substrate.	41
Table 9: Catalytic coatings divided into categories.....	45
Table 10: Peaks at particular retention in relation to catalyst tested.....	71
Table 11: Retention time, molar mass and chemical structure of standard compounds.....	75
Table 12: Retention time, molar mass and chemical structure of standard compounds.....	78

Curriculum Vitae

Personal details

Name: Colin Awungacha Lekelefac

Email: colin.awungacha@udo.edu

Education

12.2010 - Date University of Applied Sciences Mittelhessen – Giessen. Doctorate:
Development of a photochemical reaction system for the conversion of Lignin derivatives.

10.2001 - 09.2007 TU Dortmund, Chemistry studies, specialization: Chemical technology.
Theses: *Water-soluble transition metal complexes for butadiene/glycerol telomerization.*

09.1996 - 06.1998 Government bilingual high school Yaounde, GCE - A levels

Professional career and internships

12.2010 –08.2014 Scientific worker, Institute of Bioprocess Engineering and Pharmaceutical Technology, University of Applied Sciences Mittelhessen, Giessen, Germany.
Development of a photochemical reaction system for the conversion of Lignin.

03.2009 - 12.2010 Technical University (TU) of Chemnitz, Technical Chemistry, Scientific staff
Innovative strategies for the hydroformylation of diisopropenylbenzene.

09.2008 - 02.2009 FM Insurance Company Ltd – Frankfurt a. M, Risk Engineer

09.2004 - 12.2006 TU Dortmund, physical Chemistry II, Scientific worker

- Contribution in research projects in the field of colloid and interfacial chemistry.

08.2006 - 10.2006 Max Planck Institute for Coal Research, Muelheim – Germany. *Reactive deposition of conformational Palladium and titan films from supercritical carbon dioxide and ethane solutions.*

Complete lists of publications

- C. Awungacha Lekelefac, Nadine Busse, M. Herrenbauer, P. Czermak, *Photocatalytic based degradation processes of lignin derivatives*. Accepted for publication in International Journal of Photoenergy, Article ID 137634, 2014, 18 pages, <http://www.hindawi.com/journals/ijp/aa/137634/>.
- C. Awungacha Lekelefac, J. Hild, P. czermak, M. Herrenbauer. *Photocatalytic active coatings for lignin degradation in circulating packed bed reactor*. International Journal of Photoenergy, Article ID 502326. 2014, p. 10 pages, <http://dx.doi.org/10.1155/2014/502326>.
- C. Awungacha Lekelefac, P. Czermak, M. Herrenbauer. *Evaluation of Photocatalytic Active Coatings on Sintered Glass Tubes by Methylene Blue*. International Journal of Photoenergy, Volume 2013, Article ID 614567. 2013, 9 pages, <http://dx.doi.org/10.1155/2013/614567>.
- Arno Behr, Guido Henze, Leif Johnen, Colin Awungacha. *Advances in thermomorphic liquid/liquid recycling of homogeneous transition metal catalyst*. Journal of Molecular Catalysis A, Volume 285, Issues 1-2, 18 April 2008, P. 20-28, DOI: 10.1016/j.molcata.2008.01.021.
- A.Behr, J. Leschinski, C. Awungacha, S. Simic, T. Knoth. *Telomerization von Butadiene mit Glycerol: Reaction Control through Process Engineering, Solvents, and Additives*” ChemSusChem, volume 2 Issue 1, 18 Dec. 2008, P. 71-76, DOI: 10.1002/cssc.200800197.

Conference contributions

- Poster: Deutscher Katalytiker Tagung-Weimar 2013, *Photocatalytic reaction system for the degradation of paper waste water lignin derivative*.
- Presentation: Sustainability in the chemical synthesis conference: Kaiserslautern 2012 *Photocatalytic reaction system for the Degradation of paper waste water lignin*.
- Poster: Deutscher Katalytiker Tagung-Weimar 2011, *Photocatalytic reaction system for the degradation of paper waste water lignin derivative*.
- Presentation of results: Cognis GmbH – Düsseldorf. Additives and promoters: *Butadiene/Glycerol-Telomerization in multiple phase reaction systems*. Sept.2007.